Understanding the role of polyglutamylation in the mitotic spindle

Ivan Zadra

TESI DOCTORAL UNIVERSITAT POMPEU FABRA / 2021 /

Department of Experimental and Health Sciences

Thesis supervisor:

Dra. Isabelle Vernos

Cell and Developmental Biology

Centre for Genomic Regulation

A mia nonna Fiorella,
inconforme con i suoi tempi,
non gli é mai mancato il sorriso
e me l'ha inevitabilmente contagiato.

Acknowledgement

It was the 31st of December 2016 when I did my first interview with Isabelle, I think around 10 am. After that, I came for another interview in Barcelona on the 21st of January 2017. On my way to the airport, I got an email offering me the position in the DivIDE ITN network. I still remember how pleasant the way back was. I was almost a PhD student.

After about 5 years since then I am here, submitting the thesis, and my first thought goes to my parents, Elsa and Gianni. Unicamente grazie a loro deposito questa tesi di dottorato della quale sono molto orgoglioso. Senza il loro sostegno e grandi sacrifici non avrei mai potuto arrivare a questo punto. So che crescermi non é stato facile, peró credo che ne sia valsa la pena. E se son ci a scriver ste rige l'é ancia per tut chel che m'eu ensegná, chel no el me lo tirerá via mai enzun. Za che gi sen, vuei ringraziar ancia me fradel, che ne sen semper volesti ben e aidadi pero no 'n el sen mai diti. Infine voglio ricordare mia nonna Fiorella che é venuta a mancare durante il mio dottorato, che mi ha insegnato che l'umiltá é tutt'altra cosa che porgere l'altra guancia. Me sarues plasest che fustus ancor ci, sarostus stada ancor pu orgogliosa de chel che za eres de to neo. Ringrazi el Bonvi, el Morris, el Gianna, la Giorgia, el Pallino e ancia el Mastro, che l'é da l'autra man del mondo, ogni bota che ve vedi me par che el temp no el pasia mai. Quiero agradecer, dentro de esta parte dedicada a mi familia y mis amigos, a Ana mi inseparable pareja desde hace ya mas que 3 años. Amiga y novia al mismo tiempo, mente dinámica y curiosa, intolerante a las injusticias lo cual le han creado unos problemas, no te preocupes estaré a tu lado.

Quiero agradecer también a todos mis amigos de "Princess of Climbing", Nico, Paul, Greg, Fra, José, Toni, Ian y Sergi que han hecho estos años aquí especiales. Hemos compartidos muchas aventuras, risas y cervezas y seguiremos compartiendo. Vuestra alegría, ganas de hacer y espontaneidad me ha contagiado y no puedo estar mas contento que haber encontrado estas personas, que inevitablemente se han vuelto amigos.

A todos mis compañeros de laboratorio va una mención especial. El ambiente siempre ha sido muy colaborativo, alegre y inclusivo. En particular quiero agradecer a Nuria para escucharme sin descanso todas las veces que necesitaba desahogarme o simplemente hacer mas ligero el día, eres el alma de este laboratorio. Gracias a Georgina, que con su infinita paciencia y calma siempre está disponible a ayudar. Gracias a Jacopo por sus charlas especulativas infinitas. Gracias a Alejandra, la mejor compañera de doctorado que se pueda desear. Nunca de la misma opinión creando discusiones infinitas, que puntualmente se acababan cuando ya no podía mas de mi. Agradezco también toda la ayuda burocrática. Gracias a Aitor también para acompañarme en este doctorado. Gracias a Mónica que al principio del doctorado pacientemente me ha enseñado técnicas y ayudado a desarrollar ideas. Y gracias a Nuria, la nueva doctoranda, digna substituta de Alejandra, la diferencia es que no me deja ganar los debates. Agradezco vuestra capacidad que aguantar mis charlas infinitas durante las comidas, pero en el fondo se que un poco os hace gracia.

I want to acknowledge Isabelle. Her way to mentor increased my critical skills, my communication skills and, above all, my self-confidence. She always had one hour more to explain me how to improve an experimental design or how to enhance the quality of a presentation, and in general to teach you to be a great scientist. Before starting the PhD, someone told me that to carry out a successful PhD, you have to find a great mentor before a great project. I think I have found both, and now I feel I am a scientist.

I acknowledge the doctoral thesis board that agreed to discuss my thesis work: Mónica Bettencourt Dias, Thomas Surrey, Patrick Meraldi.

And Finally, thanks to the DivIDE network, to all the students, the PIs and Natalia for all the scientific and personal moments we shared that allow me to grow as a scientist.

Abstract

To ensure faithful segregation of the genetic material, cells build the mitotic spindle, a machinery made of dynamic microtubules (MTs) and MT associated proteins (MAPs). Chromosome bi-orientation is achieved through the attachment of the kinetochore pairs to MTs emanating from the two opposite spindle poles. Kinetochore-MT (KMT) dynamics are finely tuned within a narrow range to support the error correction mechanism and accomplish error-free anaphases.

This work shows that mitotic spindle MT polyglutamylation triggered by the TTLL11 enzyme ensures chromosome segregation fidelity in HeLa cells and zebrafish embryos. Consistently, bioinformatics analysis reveals TTLL11 downregulation in human cancer, and a negative correlation of its expression with aneuploidy. MT polyglutamylation imbalance in HeLa cells leads to an enhanced MT stability without affecting mitotic progression and the functionality of the spindle assembly checkpoint (SAC). Altogether, these results suggest that MT polyglutamylation provides a novel SAC-independent mechanism that ensures chromosome segregation fidelity.

Resumen

Per tal d'assegurar una segregació fidel del material genètic, les cèl·lules construeixen el fus mitòtic, una maquinària feta de microtúbuls (MTs) dinàmics i proteïnes associades als MTs. La orientació bipolar dels cromosomes s'aconsegueix a través de la unió dels dos parells de cinetocors amb els MTs que sorgeixen dels dos pols oposats del fus mitòtic. Les dinàmiques cinetocor-MT estan controlades finament en un petit rang per tal de permetre el mecanisme de correcció d'errors i aconseguir anafases sense defectes.

Aquest estudi mostra que la poliglutamilació dels MT del fus mitòtic mitjançada per l'enzim TTLL11 assegura una segregació fidel dels cromosomes en cèl·lules HeLa i embrions de peix zebra. De la mateixa manera, un anàlisi bioinformàtic revela l'existència d'una regulació a la baixa de TTLL11 en mostres humanes de càncer, i una correlació negativa de la seva expressió amb aneuploïdia. El desequilibri de poliglutamilació dels MTs en cèl·lules HeLa condueix a un augment de l'estabilitat dels MTs, sense afectar la progressió mitòtica i la funcionalitat del punt de control de l'acoblament del fus mitòtic (SAC). En conjunt, aquests resultats suggereixen que la poliglutamilació dels MTs constitueix un nou mecanisme independent del SAC que assegura la segregació fidel dels cromosomes en la divisió cel·lular.

Table of Contents

Introduction

1. Introduction

Cell division is one of the most critical cell processes. It is essential for many physiological events, from forming the gametes and the organism development to the tissue homeostasis maintenance. The final goal of cell division is to generate two daughter cells containing the same genetic material during mitosis, or to generate two gametes with a perfect chromosome balance during meiosis. Errors in chromosomes segregation generate aneuploidy (an imbalance of chromosome number) which may jeopardize the survival and development of the whole organism.

The mitotic spindle is a complex machinery structurally and functionally sustained by different populations of microtubule (MT) arrays with specialized properties. Three different populations of MTs are present in the mitotic spindle: astral MTs, running from the pole to the cell cortex; interpolar MTs, emanating from the pole toward the midzone; and the k-fibres, bundles of several MTs that attach the sister kinetochores of each mitotic chromosome to the opposite spindle poles, exerting mechanical forces to align and segregate the chromosomes between the two daughter cells. The goal of this complex MT network called mitotic spindle is to achieve the faithful segregation of the chromosomes. The primary surveillance mechanism ensuring chromosome segregation accuracy is the Spindle Assembly Checkpoint (SAC), a biochemically compounded safety device that monitors that all the kinetochores are appropriately attached to the corresponding K-fibre. If it is not the case, the SAC will stop mitosis until the error is corrected. An Aurora-B dependent pathway provides a mechanism for correction of these erroneous attachments. Such an error-correction mechanism is relatively inefficient, and it strongly relies on correct K-fibre dynamics. One class of erroneous KMT attachments are not sensed by the SAC and may result in aneuploidy of the daughter cells.

The spatial and temporal remodelling of the MT networks in different cell types as well as during mitosis, need a fine control of MT dynamics and functions. The functions of MTs are mediated by a highly complex and diverse set of

interacting proteins. Moreover, alpha and beta-tubulin, the building blocks of MTs, present a vast subset of isotypes in most multicellular organisms. Besides the incorporation of different tubulin isotypes in the MT lattice, MTs present a wide range of post-translational modifications (PTMs) that, alone or in combination, can generate distinct chemical differences among MTs that could intrinsically tune their dynamics, organization and function. The mitotic spindle is particularly rich in these MT PTMs; one of them, polyglutamylation is specifically enriched in the spindle MTs. In the chapters of this thesis, I will first introduce the basis of MT dynamics and function in-vitro and, in its physiological context, I will then revise the state of the art of our current understanding of the nature, role and regulation of MT PTMs, the basis of mitotic spindle assembly and the mechanisms of chromosomes segregation. I will then focus on my PhD project work aiming at the the characterization of the spindle MT polyglutamylation and its role in chromosome segregation.

Two years after the rediscovery of the Mendel theory in 1900, Theodor Boveri a German embryologist, formulated the Chromosome Theory; the Mendel's alleles dwell on the chromosomes. He took the idea from his experiments with sea urchins. He, indeed, fertilized sea urchin eggs with multiple sperm, producing spindles with three poles, showed that this led to dramatic errors in chromosome segregation in meiosis, and suggested that similar errors caused cancer. He published these findings in its manuscript "

Zur Frage der Entstehung maligner Tumoren" (1915)

1.1. A historical perspective

After the discovery of the cell by Robert Hooke in his *Monographia, or some Physiological Description of Minute Bodies made by Magnifying glasses*, German-Polish embryologist, Robert Remak, almost two centuries later, described for the first time that these cells divide. For him "*it begins with the division of the nucleolus, is continued by simple constriction and division of the nucleus, and is completed by division of the cell body and membrane* " (Remark, 1852). In the following years, cell division was better described, thanks to Walther Flemming, we used the word mitosis to refer to the cell division occurring in all eukaryotes. His drawings depicting the cell division steps with filamentous structures apparently guiding chromosome movements are indeed famous (Flemming, 1882) (Fig. 1A). For descriptive purposes, mitosis was divided into four main subsequent phases and separated by not-well defined limit phases still in current use: i) *Prophase*; or preparatory changes; ii) *Metaphase*; which involves the essential step in the division of the nucleus; iii) *Anaphase*, in

A

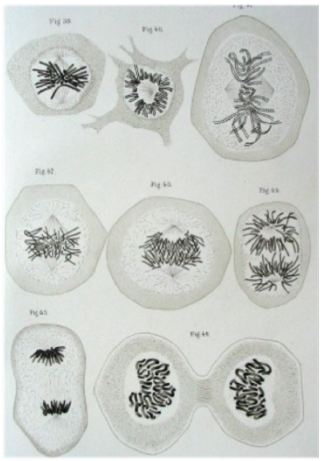

B

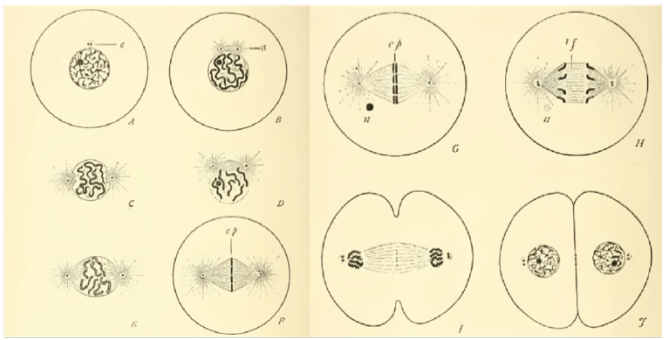

C

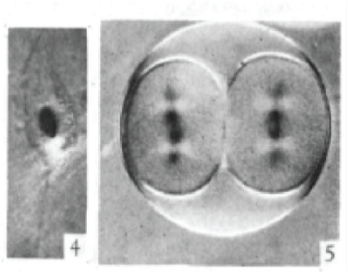

D

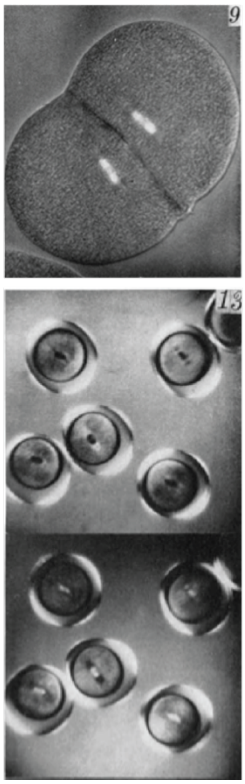

E

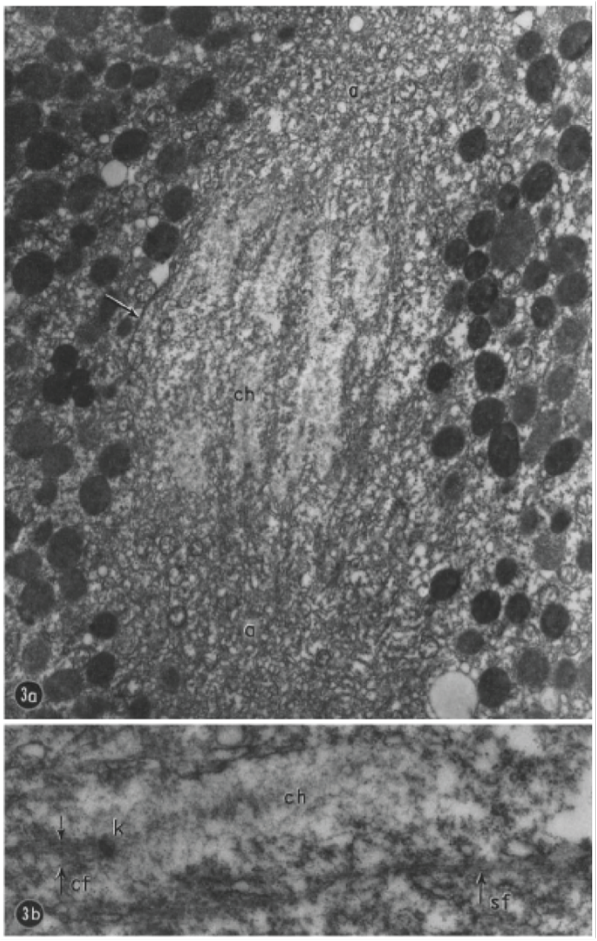

Figure 1 l Drawings and first visualization of mitotic/meiotic spindles. A) Flemming's drawing of chromosome movements during mitosis. B) Wilson's drawing of different mitotic phases from interphase through the different mitosis steps to the formation of the daughter cells. C) Swann paper's image back to 1948 showing sea-urchin egg, two-cells stage spindles visible thanks to the polarized light; x 350. D) Inoué paper's image of positively birefringent spindles of sea-urchin egg. E) "a. Chromosomes (ch) at an early stage of motion toward their respective poles." […] "b. Enlarged portion of a, showing kinetochore (k) with chromosomal fibers (cf, arrows) extending in the direction of the aster. Continuous spindle fibers (sf, arrow) which appear to run from pole to pole can be seen between the chromosomes. X 31,000." Legend adapted from the original legend in Harris, 1961.

which the nuclear material is distributed; iv) *Telophase*, in which the entire cell divides (Fig. 1B) (Wilson, 1896). What Flemming's filamentous structures were, had been debated for decades. In the comprehensive monography *The Cell in Development and Heredity (Wilson, 1925)*, Wilson states that the filamentous fibres are artefacts due to the chemical reaction of fixative within cells. The advent of polarized light helped to shed light on the nature of these filamentous structures. This "cytoplasmic mass" started to be called birefringence fibres due to the polarised light reactivity. The scientific community started accepting that a mitotic spindle formed by proteins may provide contractile forces for chromosome segregation. Moreover, the first spindle characteristics as orientation, surface thickness and dynamic start being described (Fig. 1C) (Hughes et al., 1948). With this technology, in 1951, Inoue first described time-dependent fluctuations in spindle birefringence and was able to use cinematography to capture all the mitotic processes in living cells (Inouéa et al., 1951). This technical innovation led to a general acceptance that spindle fibres were real (Fig. 1D). We have to wait one decade more with the advent of electron microscopy to directly visualize single spindle fibres reaching up the chromosomes (Harris, 1961). In 1963 the term MT was first coined by Slautterback, Ledbetter and Porter (Porter, 1963; Slautterback, 1963). In the same year, electron microscope observations revealed the exact nature of the filaments composing the flagellum and the mitotic spindle (Harris, 1961; Pease, 1963). Flemming's filamentous structures first described in the XIX century, finally got their name (Fig. 1E). Later experiments (Harris, 1961) with sea urchin mitotic spindles identified a protein binding to the drug colchicine (Borisy et al.,

1967); the following year, this protein was named as tubulin (Mohri, 1968). The building blocks of the mitotic spindle were set and MTs established as the essential element. From there on, many advances on spindle physiology and cell division knowledge have been made. Pioneering works on the spindle and MTs dynamics and kinetics, cell division and chromosomes segregation have been shedding light on many aspects of cell division, generating many theories sometimes lasting only a few years while some others lasting, almost intact for decades. However, the field has plenty of new and old intriguing questions that have yet to be answered.

""I begged to do this as a thesis project," says Borisy. "He said no, no, no, it's too risky. But I begged to do it." Others told him, " You'll have nonspecific binding and it'll be a mess.' But what did I know—I was a student." […] The results," concluded the authors, "are consistent with the hypothesis that the binding site is the subunit protein of microtubules. […] But soon enough Mohri (1968) "gave it the obvious name—the name we considered and rejected." The term "tubulin" was now official, although "spactin," "flactin," and "tektin" stuck around as alternative monikers for a little while"

William A. Wells (2005) The discovery of tubulin. J Cell Biol

1.2. Microtubule properties

Microtubules (MTs) are the largest filamentous components in the eukaryotic cytoskeleton. In most cells, cytosolic MTs are involved in intracellular transport, organelle positioning, cell shape and cell motility. MTs control differentiation processes involving intracellular rearrangements and changes in morphology. In neurons, MTs give rise to an impressive network in the axons and dendrites essential for cargo transport and for other physiological functions. Cilia and flagella are sensory and beating organelles composed of circular series of two overlapping MTs called axoneme that serves as a scaffold for intraciliary/intraflagellar transport, signal transduction and motility. In dividing cells, MTs form two essential structures: the mitotic spindle and the midbody. To manage all these different functions, MT must have a versatile nature that allows them to modulate their dynamics upon need.

a) Basis of MT physiology

MTs are hollow tubes composed of 13 protofilaments in mammalian cells with an external diameter of 25 nm. The MT building blocks are the alpha and beta-tubulin heterodimers linearly interacting in a non-covalent way. Each dimer polymerizes end-to-end, forming protofilaments that interact laterally to form a single hollow tube; this inner space of the MT is referred to as the lumen. Lateral protofilament interactions are always α-tubulin with α-tubulin and β-tubulin with β-tubulin. However, there is a lateral protofilament interaction called "seam", where the interaction is alpha-beta (Nogales, 2000). MT ends are defined as plus-end, the one exposing β-tubulin and, the opposite end, the minus-end, exposing an α-tubulin. This polarized MT orientation also involves the presence of guanosine-5'-triphosphate (GTP) on the β-tubulin subunits of the heterodimer only toward the plus-end (Figure 2A) (Berry et al., 1972; Weingarten et al., 1975). To form MTs, the tubulin heterodimer polymerizes only when in the GTP-bound state. β-tubulin has a GTPase activity which is stimulated upon polymerization. However, beta-tubulin alone does not have all the residues to carry out a successful GTP hydrolysis. These residues are donated by the α -subunit of the heterodimer when it docks at the end of the MT lattice (T. J. Mitchison, 1992; Nogales et al., 1991). When tubulin heterodimers are GTP-bound and polymerize to the MT plus-end, they confer stability to the whole MT, forming a sort of “GTP-cap”. This stable "cap" permits the MT to avoid easy depolymerization due to the unstable conformation of the GDP-tubulin form in the MT body (Caplow et al., 1996; Drechsel et al., 1994; Nogales et al., 1991) (Figure 2B). As the GTP-cap stabilizes MTs, its loss, for any reason, leads to the fast depolymerization of the MT; this event is called "catastrophe". On the other hand, when a new GTP-cap forms by association of new tubulin dimers to the depolymerizing MT, it is first stabilized, and then it starts to polymerize again in a phenomenon called "rescue" (T. Mitchison et al., 1984a; T. J. Mitchison, 2014) (Figure 2B). These characteristics led to a description of MT dynamic instability by the four parameters listed above: the rate of polymerisation and depolymerisation and the frequency of catastrophe and rescue (T. Mitchison & Kirshner, 1984a; T.

Mitchison et al., 1984b). MT dynamic instability indeed refers to the property of MTs to continuously alternate between growth and shrinking phases. Even if it is well-known that in-vitro, the polymerisation rate is tightly bound to the level of tubulin concentration, and catastrophe frequency proportionally decreases, the relationship between these two events is still not completely understood. The interplay between growth and shrinkage and catastrophe and rescue seems stochastic, resulting in MTs never stopping at a precise length. However, the average MT length is determined by the intrinsic dynamic instability parameters and the free tubulin concentration in the solution (Desai et al., 1997).

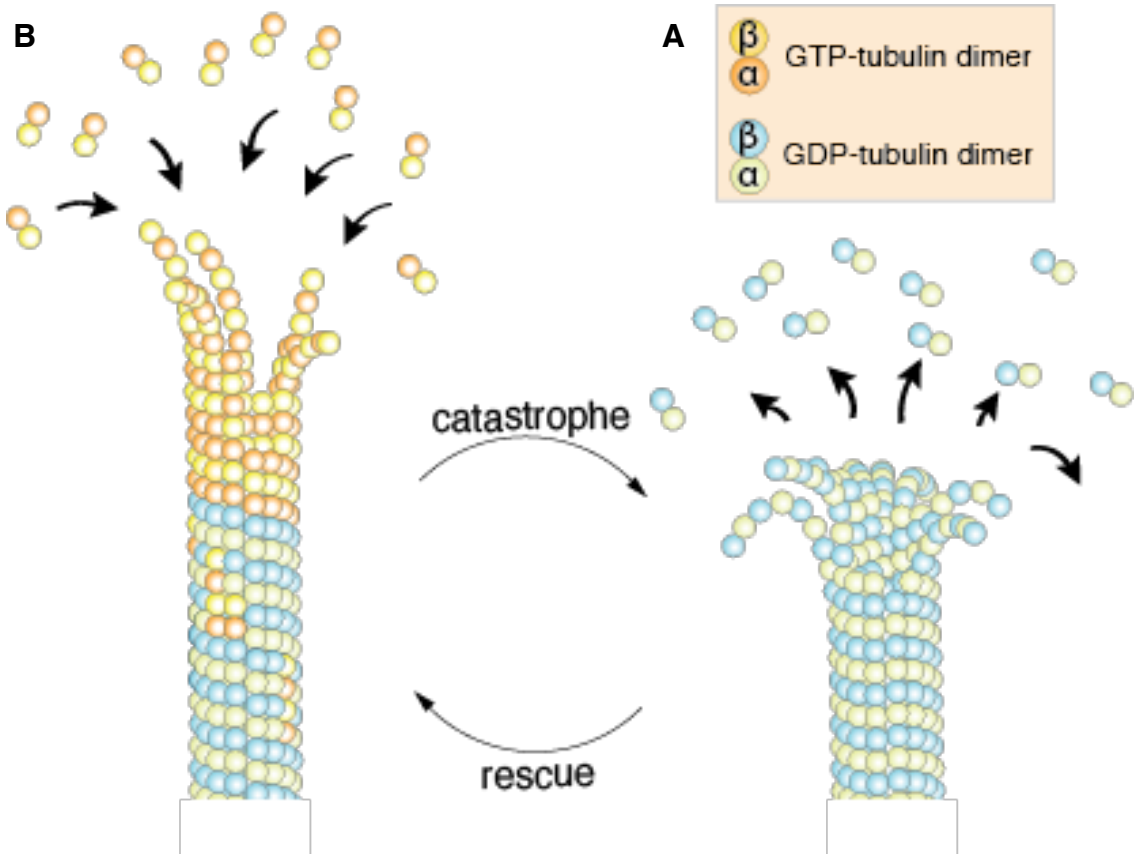

Figure 2 I Plus-end MT dynamics, the rescue and the catastrophe. A) α- and β-tubulin interact non-covalently to form tubulin heterodimers of 8 nm in length. Tubulin dimers can be present under 2 conditions with GTP or GDP bound to β-tubulin. B) MTs polymerize by incorporation of GTP-tubulin dimers at the plus-end. After incorporation of the GTP-tubulin dimers in the MT lattice the GTP molecule gets hydrolysed to GDP, this leads to a destabilization of the lattice. The plus-end is protected by the GTP-cap avoiding MT depolymerization. *In-vitro* MT plus-end dynamics is driven by stochastics events, loss of the GTP-cap leads to immediate MT depolymerization which still stochastically can be rescued and the same MT starts polymerising again. This is a reaction equilibrium which can be moved toward either MT polymerization or depolymerization, by increasing or decreasing the concentration of free tubulin in solution.

The critical tubulin concentration is defined as the concentration required for spontaneous MT assembly. In cells, this concentration is kept well below this cut-off value at around 25 μM (Gard et al., 1987). In vivo, indeed, to improve MT assembly capability, the cells provide seeds for MT nucleation. This seed is a protein complex called the γ-tubulin ring complex (γ-TuRC). It works as a scaffold providing a template to sustain MT nucleation in the cell (Moritz et al., 1995; Teixido -Travesa et al., 2012). Besides γ-TuRC the cell presents an incredible number of MT associated proteins (MAPs) favouring MT assembly or disassembly, polymerisation, GTP-cap stability and overall MT dynamic properties. Motor proteins drive the organisation of MT networks and transport different types of cargoes contributing to the specific functions. Recently, MT PTMs have emerged has important regulators, controlling MT properties in cis (intrinsic properties) and trans (tuning MAPs binding and functions).

"In his seminal review of the mitotic cycle, Daniel Mazia boldly stated: "Nothing we have learned about mitosis since it was discovered a century ago is as dazzling as the discovery itself" (1987) This statement reflected Mazia's (and the whole field's) frustration with the lack of mechanistic understanding of cell division. Although voluminous phenomenological data had been gathered on the mitotic apparatus (spindle), the principles governing its assembly remained elusive. Interestingly, Mazia's opus major was published merely a year after the original formulation of the "search and capture" (S&C) hypothesis. If Mazia had read that paper (it was not cited in his 1987 review), he might have changed his stance. Indeed, S&C offered the first plausible mechanism to drive spindle assembly in animal cells and signified the transition from descriptions to molecular investigations of the process."

R. Heald and A. Khodjakov (2015) "Thirty years of search and capture: The complex simplicity of mitotic spindle assembly". J Cell Biol

,

1.3. The self-assembly of the mitotic spindle

The transition between interphase and mitosis leads to a complete rearrangement of the cell structures and compartments, being the nuclear structure and the cytoskeleton, the major players affected.

When cyclin B-Cdk1 levels reach an activation threshold, the cell formally enters into mitosis. The first detectable events are chromosome condensation, MT disassembly, centrosome separation, Golgi and endoplasmic reticulum fragmentation and nuclear envelope breakdown (NEB). Then starts prophase, and mitosis will be continuously evolving until the end of telophase. All the phases (as described in chapter 1.1) are arbitrarily set according to phenotypic changes, except the metaphase anaphase transition which account with a biochemical mechanism. The spindle assembly checkpoint (SAC) stops the mitotic progression between metaphase and anaphase until all kinetochore pairs present

on each chromosome are correctly attached to MTs emanating from the two spindle poles.

Different MT nucleation pathways are activated in mitosis. Moreover, many proteins participate in defining the dynamics and organization of the mitotic MT network to give rise to different MT populations and cope with correct chromosome segregation into the two daughter cells. In 1986, Kirschner and Mitchison described for the first time MT dynamic instability and based on this they proposed a model to explain how MTs catch kinetochores and spindles assemble. They called it the "search and capture" (S&C) model (Kirschner et al., 1986). They laid the basis for a mechanism that drives spindle assembly that nowadays is still considered although with some modifications. The increase in MT dynamic instability when cells enter mitosis transform the longer, more stable interphase MTs into two dynamic radial arrays nucleated by the duplicated centrosomes that stochastically grow and shrink until they get captured by a kinetochore. This connection stabilizes the MTs, leading to the attachment of the chromosomes to the spindle poles. Progressively MTs occupy all the kinetochores forming stable connections generating the bipolar spindle apparatus. In 1990, the visualization of MT capture by a kinetochore strengthened this model (Hayden et al., 1990; Rieder et al., 1990). However, modelling approaches later suggested that spindle assembly only based on the S&C model would be several times longer than canonical mitosis (Wollman et al., 2005). New findings also showed that additional MT nucleation and regulation pathways play a fundamental role in spindle self-assembly. Hence a combined theory could explain how the spindle assemble. In this section, I will extensively review the function and regulation of MTs that give rise to a functional mitotic spindle.

a) MT assembly pathway in mitosis

In mitosis, MT nucleation is controlled by three pathways: centrosomal, RanGTP and MT-amplification (S. Meunier et al., 2016). γ-TuRC is the common nucleation scaffold for all the MT nucleation pathways in and outside of mitosis (Teixido -

Travesa et al., 2012) (Figure 3A). In mitosis, Nedd1 is recruited with γ-TuRC complexes to the three different pathways. Phosphorylation cascades regulate Nedd1 functions, allowing control of MT nucleation spatially and temporally

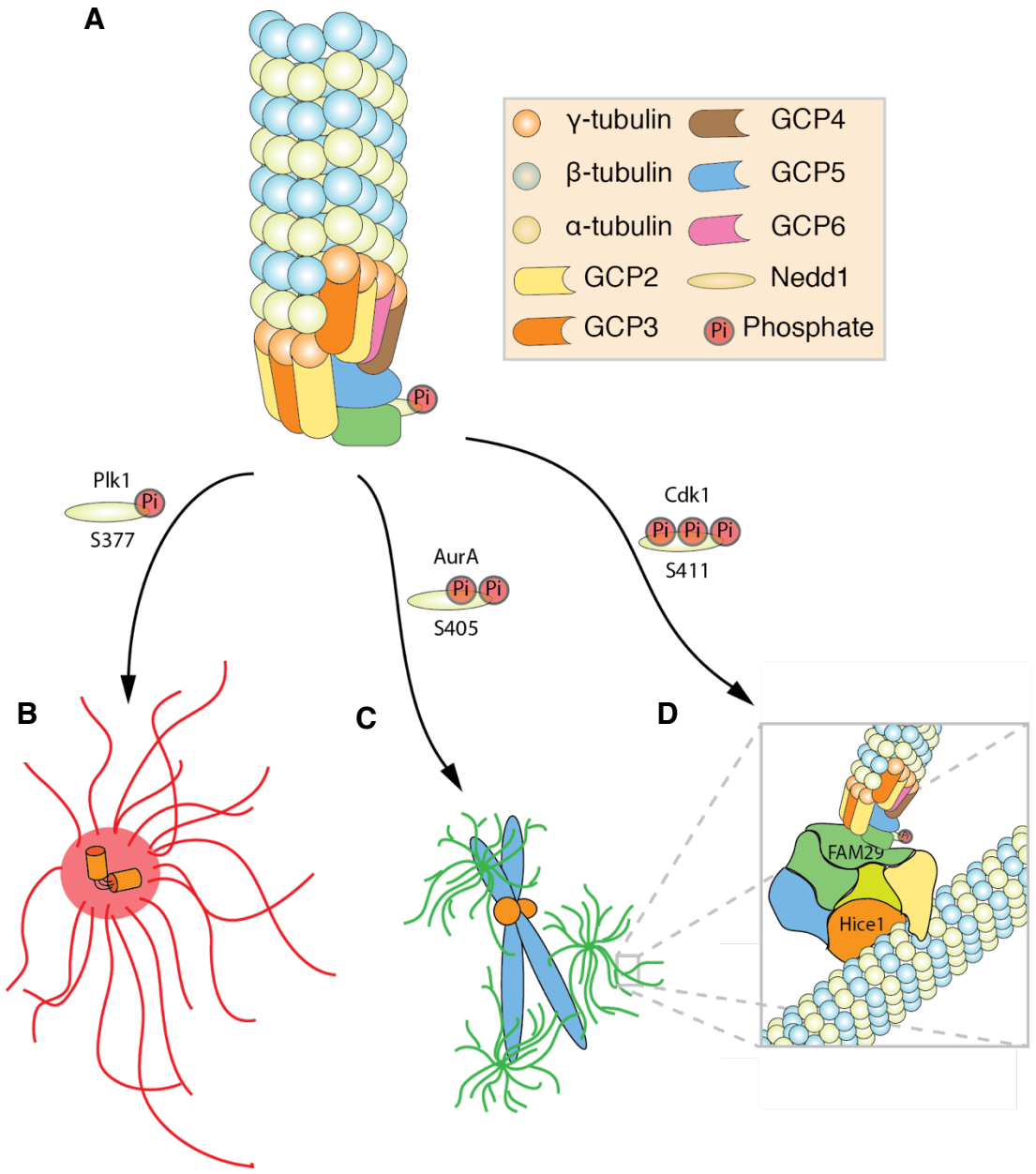

Figure 3 I MT nucleation pathway. A) γ-TuRC complex depicting the GCPs/γ-tubulin dimers and other scaffold proteins nucleating a MT. B) Plk1 phosphorylates Nedd1 on serine 377 to promote γ-TuRC recruitment to the PCM and MT nucleation at the centrosome in cells entering mitosis. C) Aurora-A phosphorylates Nedd1 on serine 405, promoting MT nucleation through the chromosome pathway. D) Cdk1 phosphorylates NEDD1 on serine 411 and promotes augmin dependent MT nucleation on a prexisting MT. A zoom-in square represents how the Augmin complex binds to the MT lattice. Hice1 has a MT binding domain and FAM29 recruits the γ-TuRC on the Augmin complex.

through the different pathways (Lüders et al., 2006; Pinyol et al., 2013; Sdelci et al., 2012).

b) Centrosomal pathway

Centrosomes have been considered for a long time as the only source of MT nucleation in mitosis. The centrosome is a large organelle consisting of a pair of barrel-shaped centrioles surrounded by amorphous pericentriolar material (PCM) where nucleation takes place, generating polarized MT arrays with their plus ends extending outward. A major component of the PCM is the specialized tubulin called γ-tubulin, which assembles into a multi-subunit γ-tubulin ring complex (γ-TURC). In dividing cells, centrosomes duplication occurs coordinately with chromosome replication. Procentrioles starts growing out from the mother centrioles in S phase to complete replication in G2/M. The resulting daughter centrosomes mature and start segregating apart upon mitosis entry (Bettencourt-Dias et al., 2007). During maturation, centrosomes recruit and incorporate various components to the PCM and increase their MT nucleation activity. These components include Cep120, Cep192, Cep152, Cdk5RAP2, AKAP9, NEDD1 and the y-TuRC among many others. One key regulatory event is the phosphorylation the y-TuRC associated protein Nedd1 at S377 by the NIMA kinase Nek9 (Sdelci et al., 2012) (Figure 3B). We will see in the following sections that Nedd1 phosphorylation on different residues by different kinases is essential for the sequential activation of the different MT nucleation pathways in mitosis. Centrosome separation and their increased MT nucleation activity results in the formation of 2 asters of dynamic MTs that explore the mixed nucleoplasmic/cytoplasmic environment and establish contacts with the kinetochores, the cell cortex and other MTs in an antiparallel fashion giving rise to the mitotic spindle. For decades these highly dynamic centrosomal MTs were considered the unique players for spindle assembly and central in the "search and capture" hypothesis explained in the previous chapter. However, the assembly of bipolar spindles in acentrosomal meiosis (Severson et al., 2020) and the development of full organisms with minor defects in the absence of

centrosomes (Vérollet et al., 2006) suggested that centrosomes are dispensable for spindle assembly. Nowadays, we know that other MT nucleation pathways are necessary and even indispensable for spindle assembly.

c) RanGTP pathway

It took some decades from the first observation of MT nucleation close to the chromatin until the wide acceptance of the existence of a MT nucleation pathway triggered by the chromosomes (Karsenti et al., 2001a; McGill et al., 1975).

The underlying mechanism controlling MT nucleation in the chromosome proximity is under RanGTP control. RanGTP with the karyopherins receptors mediate the shuttling between the nucleus and cytoplasm. Karyopherins receptors are divided into importins that bind to proteins with nuclear localization signal (NLS) and import them into the nucleus and exportins that bind to proteins with nuclear export signals (NES) and export them from the nucleus to the

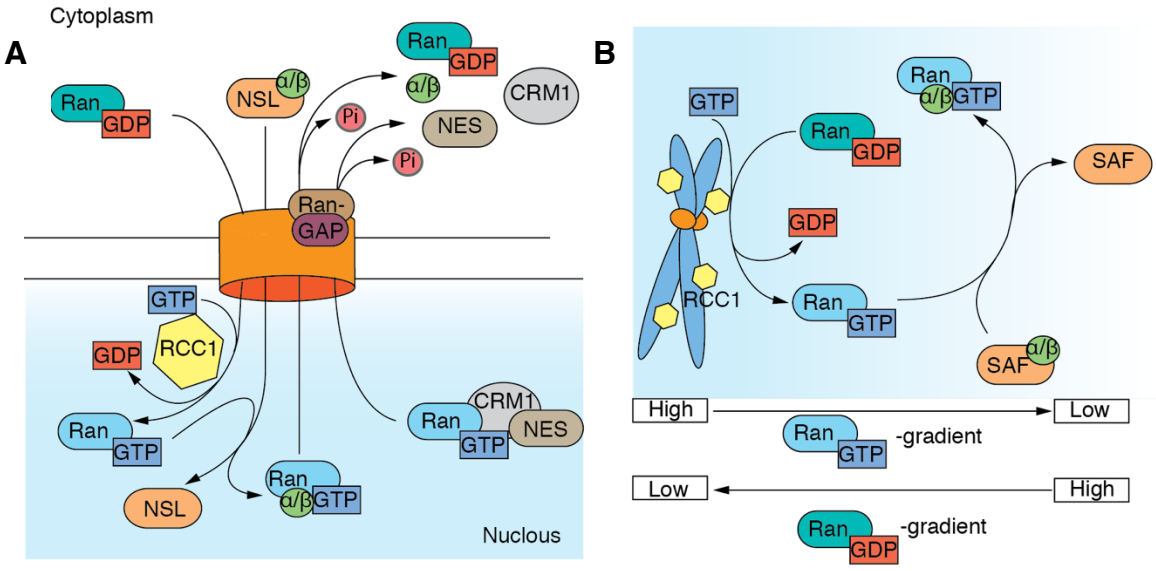

Figure 4 I The RanGTP pathway in interphase and mitosis. A) Schematic representation of the nucleo-cytoplasmic transport regulated by RanGTP. By NLS and NES I indicate the subset of proteins that bear either an NLS or a NES (however both signals can be present on the same protein and the interaction be regulated through the cell cycle and other events). B) Ran pathway in mitosis. SAF indicate the protein involved in the spindle assembly and regulation that bear a NLS regulating the interaction with the importins. In mitosis there is no physical barrier between nuclear and cytoplasmic environments, so that, RanGTP generate a gradient that is high close to the chromosomes and fades out while getting farther from the chromosomes.

cytoplasm. In interphase, RanGTP binds the importins that release their cargo into the nucleus, actively transporting back the importin from the nucleus to the cytoplasm through the NPC. There the low GTPase activity of Ran is stimulated by additonal factors such as RanGAP converting RanGTP into RanGDP, releasing the importin in the cytoplasm and maintaining the importins population outside the nucleus. This cycle closes when RanGDP gets back into the nucleus, and the guanine nucleotide exchange factor, RCC1, associated with the chromatin, exchanges GDP by GTP on Ran. It is clear that with this mechanism, the cell can maintain the directionality of the transport by keeping high RanGTP levels in the nucleus and high RanGDP in the cytoplasm. On the other hand, the export is mediated by the exportin CRM1 that binds to the NES of proteins, subsequently bound to RanGTP exporting and releasing the complex in the cytoplasm once hydrolyzed by RanGAP (Kuersten et al., 2001) (Figure 4A). In mitosis, the nuclear envelope providing the physical barrier between the nucleus and the cytoplasm disassembles and the nucleoplasm and the cytoplasm mix while RCC1 remains associated with the condensed chromosomes. This generates a RanGTP gradient peaking around the chromosomes (Carazo-Salas et al., 1999; Kalab et al., 2002). RanGTP then releases proteins from importins, allowing them to exert their function in the proximity of the chromosomes; these proteins were generally grouped as spindle assembly factors (SAFs) (Figure 4B) (Karsenti et al., 2001b). The first SAF identified TPX2 (Targeting Protein for Xklp2), is essential for MT nucleation through the RanGTP pathway (Wittmann et al., 2000). TPX2 exerts a critical function: it oligomerizes and activates Aurora-A kinase (AurA), which in turn phosphorylates Nedd1 at S405 (Scrofani et al., 2015), thus, promoting the formation of a complex including Nedd1, RHAMM, TPX2 and γ-TuRC hence promoting MT nucleation via RanGTP pathway (Pinyol et al., 2013) (Figure 3C). Several SAFs have been identified so far (Cavazza et al., 2016); they provide specific activities regulating MT dynamics and organization beyond MT nucleation. MCRS1is a SAFs identified in the lab as a KMT minus end dynamic regulator (S. Meunier et al., 2015; S. Meunier et al., 2011) ; NuMA, pole formation and interacting with motor dynein.

From this chapter, it becomes clear that considering only the centrosomal MTs is not sufficient to understand spindle assembly (S. Meunier & Vernos, 2016). The RanGTP pathway is essential to increase the cell capacity to nucleate MTs in mitosis and finely regulate their function, creating an environment completely different from the cytoplasmic one. However, another MT nucleation pathway relying on Augmin is also essential.

d) MT- amplification pathway (Augmin)

The Augmin pathway was discovered more recently (Goshima et al., 2008).The Augmin complex, aka HAUS complex in human cells, mediates the recruitment of y-TuRC on pre-existing MTs. The complex consists in eight proteins. FAM29A bonds to y-TuRC through NEDD1(Sánchez-Huertas et al., 2015), establishing the interface between the complex and the new nucleating MT. HICE1 targets the lattice of a pre-existing MT(S. Meunier & Vernos, 2016), functioning as an anchoring point for the complex. This complex generates MT grooving with a narrow angle (30º-20º) respect to the MT it targets. This is very convenient as the new MT preserve the polarity of the pre-existing MT, likely helping k-fibre assembly (Petry, 2016). The phosphorylation of Nedd1 at the S411 residue by Cdk1 is fundamental for the interaction of the Augmin complex with y-TuRC via Nedd1 (Lüders et al., 2006) (Figure 3D).. Finally, these MTs can be transported toward the pole by dynein directed transport (Lecland et al., 2014). In the the absence of the augmin complex spindle MT density is low and chromosome segregation defects occur (Goshima et al., 2008; Zhu et al., 2008). It has been proposed RanGTP pathway also controls the augmin pathway. However, this is still not entirely clear because the putative role of TPX2 (downstream effector of RanGTP) in the MT branching process is not well understood yet (Petry et al., 2013; Tariq et al., 2020; Verma et al., 2019).

e) The regulation of mitotic MTs

Microtubules completely reorganise during mitosis, providing a dramatic example of the importance of their dynamic instability. Indeed, interphase MTs have long half-lives usually up to 9-10 minutes depending on the cell line being analysed; for example in neurons MT can last hours (Baas et al., 2016). On the other end, the transition toward mitosis comes with changes in MT dynamics, and their half-life drops down to half a minute for some classes of mitotic MT (Zhai et al.) (Figure

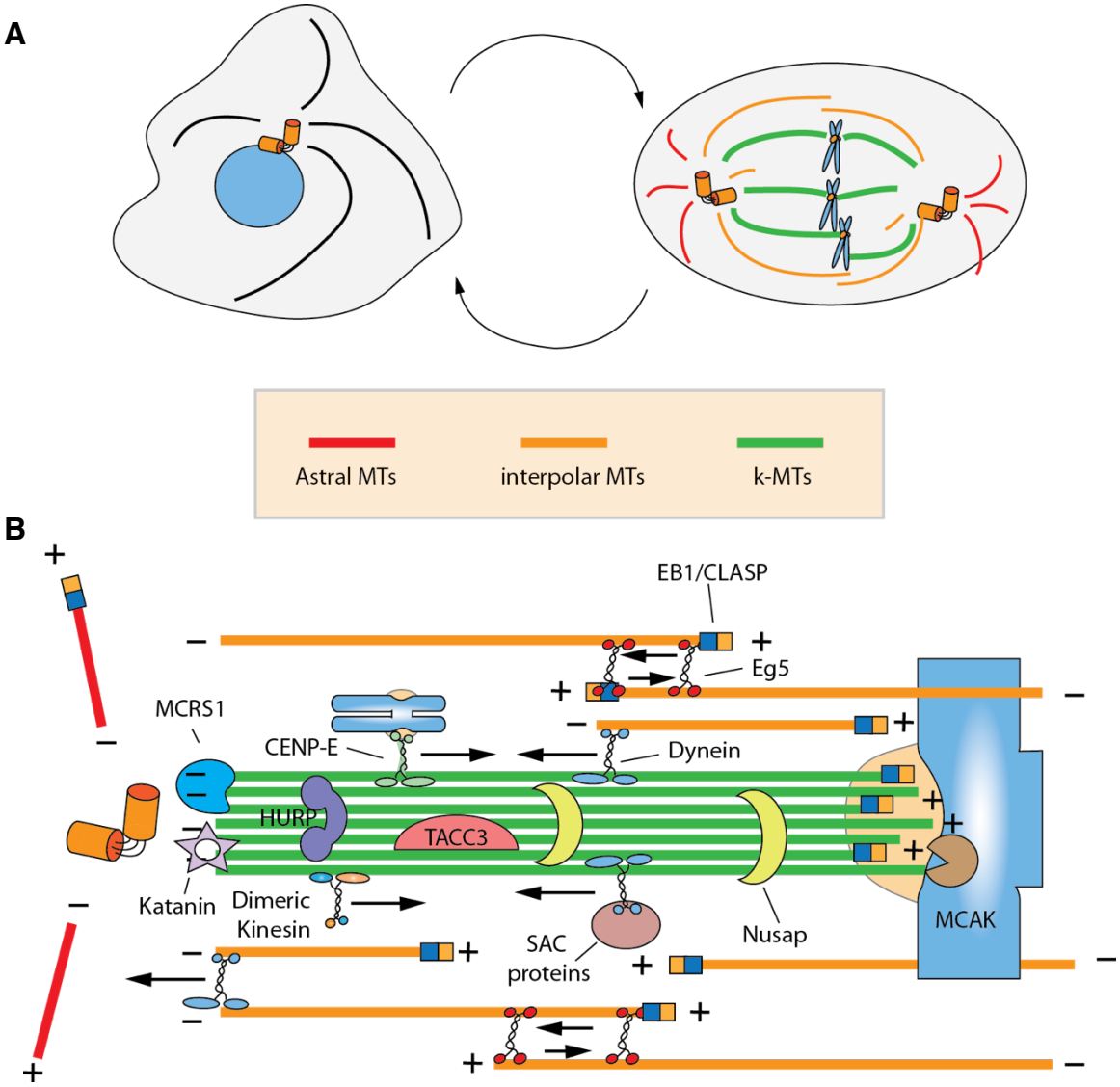

Figure 5 I Mitotic spindle regulation. A) Simple schematic representation of MT network rearrangement during cell cycle between interphase(left) and mitosis (right). B) Perspective view of a portion of the mitotic spindle showing all the three MT classes. Arrows indicate either the motor's direction of motion or, in the case of Eg5 the resulting forces. Some MT interacting protein are depicted in their actual localization.

5A). Besides dynamics, mitotic MTs change functions within the spindle mash. To sustain these differences, mitotic MTs undergo tight temporal and spatial regulation. The cells achieve and maintain these high MT dynamics by activating/recruiting/re-localising a vast cohort of proteins, specifically upon mitosis (S. Meunier et al., 2012).. Several proteins regulate the plus- and minus-end balancing spindle's inner forces and controlling MT-kinetochore interactions. For example, MCRS1 regulates the MT minus-end dynamics in mitosis (S. Meunier & Vernos, 2011); HURP, TACC3 and NUSAP1 stabilise MTs; XMAP215 is an MT polymerase; Katanin, a severing enzyme, increase its activity at the minus-end; finally, PRC1 is essential for spindle assembly, bundling MTs at the spindle midzone (S. Meunier & Vernos, 2012). At both ends, we find MCAK, aka Kif2c, which destabilizes MT ends (Maney et al., 2001; Wordeman et al., 1995), CLASP and EB1 proteins are also essential to regulate the dynamics (Figure 5B). Another basic set of proteins in mitosis are the molecular motors. Molecular motors confer organisation to the mitotic spindle and generate forces. The cells deploy kinesins, plus-end directed motors and dyneins, minus-end directed motors to organise the mitotic spindle (Figure 5B). The organisation of the spindle by means of molecular motors consumes energy in the form of ATP, hydrolysing it to step forward on the MT. Dynein is involved in the pole focusing on mitosis. Indeed, dyneins stably bind a MT while walking on another MT toward the minus-end. On the other hand, Eg5, a plus-end directed kinesin motor, binds two antiparallel MT simultaneously, therefore walking toward the plus-ends, slides the MT apart, generating forces to extrude the two poles giving the so-called bipolar structure to the spindle (Surrey et al., 2001). The inhibition of Eg5 leads to monopolar spindle formation in cells which ultimately fail to divide. Chromosomes congression also makes use of molecular motors. Kinetochores bind motor that walk on MTs and generate forces to influence chromosome position and MT dynamics. Probably all kinetochores bind minus end-directed motors (Musacchio et al., 2007a). Kinetochores also bind at least one plus end-directed motor. Kinesin-13, a catalyst of MT depolymerization that lacks motility, is also present on the kinetochore contacting the MTs. CENP-E is an MT plus-end-directed

kinetochore motor that has the chromosome as cargo, and its motor activity is guided by MT tyrosination to fulfil chromosome segregation (Barisic et al., 2015; Yu et al., 2019). Impairment in its activity leads to mitotic arrest via SAC signalling. In summary, motors are fundamental for two mitotic functions, spindle assembly and organization and correct chromosome segregation.

f) MT populations in the mitotic spindle (a focus on the k-fibre)

The aforementioned MT nucleation pathways contribute to building the complex machinery known as the mitotic spindle. Centrosomes, RanGTP and augmin pathways together increase the cell MT nucleation capability and MT dynamics dramatically. The mixing of the cytoplasm with the nucleoplasm creates a new environment, to a certain extent, regulated by RanGTP. In addition, MT nucleation and dynamics keep changing through the mitotic phases. We may think that mitosis is a process divided into discrete, compartmentalised series of events starting with prophase and going through prometaphase, metaphase, anaphase and telophase. However, mitosis is a biphasic process. There is a continued evolution of the MT dynamics and network complexity, and the only natural constriction at the metaphase/anaphase transition is controlled by the SAC. Mitosis starts with the NEBD, and centrosomes massively nucleate MTs, entering in contact with the nucleoplasm and the chromosomes and expanding radially in the cell volume until the bipolar spindle forms.

In the mitotic apparatus, MT can be classified into three different population: astral MTs, interpolar MTs and k-fibres. Astral MTs, non-kinetochore MTs that emanate from the MTOC located at the spindle pole, usually the centrosomes, running toward the cell cortex. Dynein and adaptor complexes contact the cortex, anchoring the molecular motor to the cell membrane, exerting pulling forces directed toward the centre, essential to position and orient the spindle poles (Lu et al., 2013; S. Meunier & Vernos, 2012). Interpolar MTs are another class of non-kinetochore MTs. As astral MTs, they are mainly a structural MT class. They emanate from the spindle poles but grow toward the midzone,

where they meet interpolar MTs emanating from the opposite pole (S. Meunier & Vernos, 2012). A fundamental plus-end motor protein called Eg5 crosslinks the antiparallel interpolar MT, sliding them apart generating pulling forces directed toward the cell cortex separating the centrosomes (Walczak et al., 1998). Hklp2 is another plus-end motor protein essential for maintenance, and in some cases, generation of bipolar structure (Vanneste et al., 2009). Spindle bipolarity also involves dynein-mediated minus end-directed transport of MTs and MT clustering to generate the spindle poles (Heald et al., 1997). Non-kinetochore MTs are very dynamic with a half-life of around 1 minute in human cells, meaning that half of the non-kinetochore MT is either renewed or disassembled every minute (Zhai et al., 1995).

The last class of MT in the mitotic spindle are the k-fibres formed by spatially organized bundles of KMT. The number of MTs forming the k-fibres varies throughout species and can span from 1 single MT in *S. cerevisiae* (Winey et al., 1995) to 2-4 in *S. pombe* (Ding et al., 1993), 4-6 in *D. melanogaster* (Maiato et al., 2006) and up to 15-25 MTs in human cells (McEwen et al., 2010). Studies performed in Hela cells showed how k-fibre bundles are kept together by the

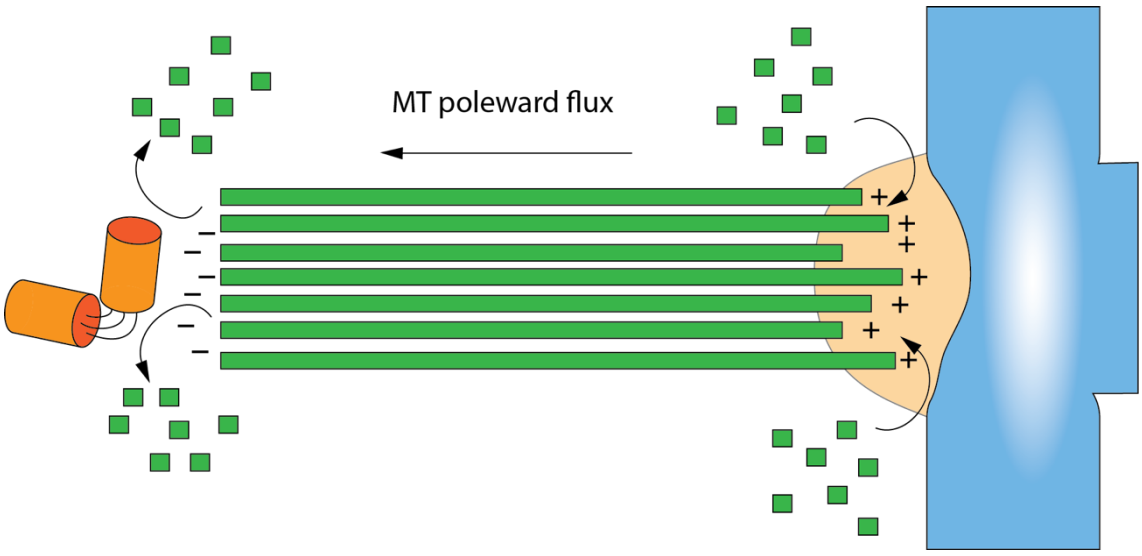

Figure 6 I MT poleward flux. The MT poleward flux is driven by two activities: net polymerization at the plus-end and depolymerization at the minus-ends. The equilibrium between plus-end polymerization and minus-end depolymerization can vary depending on the mitotic stage.

TACC3–ch-TOG–clathrin complex mediated by AuroraA phosphorylation of TACC3 S588. The complex makes multiple contacts with MTs forming a network of MT connectors called "the mesh"(Nixon et al., 2015). This provides structural stability to the k-fibre, with a lower turnover rate (as mentioned above). They are more resistant to cold and drug induced depolymerization than the other spindle MTs (Brinkley et al., 1975). The k-fibres are the main effectors of chromosome movements, alignment and segregation and the only ones responsible for SAC satisfaction. K-fibres form upon an end-on attachment of MTs to the kinetochore and go through a process of maturation with new MTs attaching and detaching from the kinetochore (Kalantzaki et al., 2015). The process can have two endings: either a robust k-fibre-kinetochore attachment via the KMN network arising from the outer kinetochore is formed, or the MT-kinetochore interface collapses. This KMT attachment/detachment process is regulated by MT dynamics and by an Aurora B dependent pathway with MCAK as one of the downstream effectors (Andrews et al., 2004) and through Ncd80 complex phosphorylation. Both mechanisms can independently interplay to guarantee error-free k-fibre attachment to the chromosomes.

Spindle MTs undergo a phenomenon called MT poleward flux. In 2020 the Barisic's group has reported an accurate vision of the MT poleward flux. In prometaphase the flux is predominantly driven by CENP-E at the kinetochore level. During late prometapase and metaphase the MT flux is driven by a coordination of the prometaphase activities with Eg5 and hKlp2 (Steblyanko et al., 2020). The poleward flux seems to be prominent in the k-fibre, it is plausible that interpolar MTs contribution, if any, has to be negligible due to their fast turnover compared to the one of K-fibre. Indeed, the predominant hypothesis is that the MT poleward flux is driven by forces transmitted from the non-KMTs to the KMTs. This does not exclude that MT poleward flux is also driven by MT depolymerisation at the minus-end and MT polymerisation at the plus-end. Indeed, at the plus-end, EB1 recruits CLASP proteins promoting the incorporation of tubulin dimers. On the other side, the minus-end depolymerisation is controlled by MCAK and Kif2a (Figure 6) (T. Mitchison et al., 1986; A. Musacchio & E.D.

Salmon, 2007a), while motor proteins can slide KMTs toward the pole generating a steady-state scenario contolling the spindle morphology (Barisic et al., 2021). Even if tubulin poleward flux physiological meaning has been under debate, it is clear that it can generate forces and can be a readout of k-fibre dynamics (Girão et al., 2020). Tubulin poleward flux also can control the interkinetochore distance by accounting for a certain level of stretching between the two sister chromatid kinetochores. Interkinetochore stretching generates upon tension. For decades, interkinetochore tension was unequivocally associated with SAC satisfaction. Lately, this idea has been debated, showing that SAC satisfaction is rather associated KMT dynamics and kinetochore-MT occupancy (Amaro et al., 2010; Dudka et al., 2018b).

In the next chapter, I will review the structures and the pathways involved in SAC satisfaction, the importance of KMT, and the consequences of chromosomes segregation errors.

"In 1969, Nicklas and Koch showed that insect spermatocytes could correct chromosome alignment errors. They produced the errors by micromanipulating the paternal and maternal copies of a chromosome so that they were attached to the same pole of the meiotic spindle. Cells detect the error […] giving it (the chromosome/chromatid) a chance of achieving the correct orientation. Nicklas wondered whether the cell might wait to make sure that the errors had been corrected, but he decided that his data weren't strong enough to answer this question."

Andrew W. Murray (2011), "A brief history of error". Nat Cell Biol

1.4. Chromosome segregation and SAC

Chromosome segregation occurs during anaphase once k-fibres have successfully attached all chromosomes to the two spindle poles. Anaphase consists of two phases, anaphase A and B. During anaphase A, the chromosomes move to the poles achieved by k-fibre MT shortening; during anaphase B, the spindle poles move apart as interpolar MTs elongate and slide apart forming the central spindle. Subsequently the spindle apparatus starts breaking down in telophase (the following phase) while the nuclear envelope forms around the decondensing chromosomes and an actin ring generate forces to constrict the central spindle and separate the two diploid daughter cells containing the same genetic material. Chromosome segregation defects result in detrimental consequences for the viability of the daughter cells or the organism. For example, in humans, Down syndrome occurs when a meiotic error generates an organism with cells carrying an extra copy of chromosome 21. Cells with an

altered ploidy can be also harmful for somatic cells and characteristic of most human solid tumours. Aneuploidy is the irreversible consequence of chromosome missegregation events. The persistent errors in chromosome segregation generate chromosomal instability (CIN), also often found in tumours. CIN produces continuous changes in gene expression patterns, giving the cell chances of tumoral transformation and, in the case of an eventual transformation: advantages and adaptation strategies.

Chromosome segregation fidelity is the endpoint of mitosis; faithful chromosome segregation is achieved despite large stochasticity and variability in many parameters: number and size of the chromosomes, their initial locations, and the stochastic behaviour of the spindle MTs that are captured by kinetochores from almost any angle (R.B. Nicklas, 1997). At the beginning of mitosis (prophase), chromosomes are scattered in the cito/nucleoplasmic environment, and centrosomes are sometimes not yet positioned at opposite sides forming the spindle poles. This means that kinetochores do not have a defined poleward orientation, and spindle geometry is under defining conditions, increasing the probability of erroneous kinetochore-MT interactions that could last up to anaphase. Indeed, erroneous KMT attachments are extremely common in prophase. So, how does it work? How does the cell ensure chromosome segregation fidelity? If the whole system would rely only on random interactions, the probability faithful mitosis in human dividing cells would dwell at around 10^{-10} (M.A. Lampson et al., 2017).However, in normal dividing cells, the frequency of missegregation lies between 10^{-2}-10^{-3}. In culture immortalised cell lines, this factor increases approximately ten times (S.L. Thompson et al., 2008). These numbers are impressively low compared to random chances, making then undoubtable that robust self-organisation machinery/ies sustain chromosome segregation to avoid or resolve kinetochore attachment errors. We know that the SAC provides a robust mechanism to monitor the correct attachment of the chromosomes to the spindle poles and that it can delay mitosis progression to allow error correction. However, it does not interfere with the kinetochore-MT

interface; it only senses it. So other mechanisms may enhance fidelity of chromosome segregation.

I will briefly review in the next section the structure and function of the kinetochore, the SAC, how and why wrong KMT attachments occur, and the error correction mechanisms.

a) The kinetochore

Kinetochores are central players for chromosome segregation. They consist of a non-passive scaffold structure contacting the DNA in a precise locus called the centromere, and, on the other side, they catch MTs regulating their dynamics and kinetics. The kinetochore is a self-assembled machinery counting more than 100 protein components impressively conserved throughout the eukaryotic kingdom (Cheeseman et al., 2008). Indeed, the kinetochore and its regulatory components are highly homologous in budding yeast – model organism for studying the kinetochore - and humans despite some differences in mitosis in these two organisms (Kitagawa et al., 2001). In humans, the kinetochore structure is divided into two main modules, the inner and the outer kinetochore. I will briefly review, structurally and functionally, the inner and outer kinetochore modules.

i) The inner kinetochore module

The inner kinetochore is responsible for interacting with the centromeric chromatin. The first step towards kinetochore assembly is the recognition of the centromere area that must be unique for every chromatid. Centromeric protein A (CENP-A) is the protein that epigenetically localises the the centromere. It is, indeed, a homologue of histone H3. CENP-A replaces one or both H3 in the nucleosome on the portion of the chromosome that will be the centromere (Palmer et al., 1985; Shelby et al., 1997). This epigenetic mark is the starting point for kinetochore assembly. CENP-C and CENP-N directly recognise CENP-A and interact with other nucleosome subunits; however, the discriminant

interaction is CENP-A (Kato et al., 2013) (Figure 7A and 8A). Other CENP proteins constitute complexes that interact with each other in the inner kinetochore module, forming what is referred to as Constitutive Centromere Associated Network (CCAN). Surprisingly and interestingly, the inner kinetochore is built by evolutionally conserved CCAN and CENP-A interactions (extensively reviewed in (Musacchio et al., 2017).

ii) The outer kinetochore module

The outer kinetochore module is responsible for the MT end-on attachment and the force transduction generated by the depolymerising KMT. The kinetochore-MT interface must be robust enough to transduce forces to drive chromosome motility while also coupling the intrinsic dynamic instability of bound KMT to chromosome movement. Its core structure accounts for three different complexes, the Knl1, Mis12 and Ndc80 complex, forming the KMN network (Musacchio & Desai, 2017). The Ncd80 complex consisting of Spc24, Spc25, Nuf2 and Ncd80 is the primary MT receptor at the kinetochore. The complex has a rod-shaped structure with a globular region composed of Spc24 and Spc25 at one end (Wei et al., 2006), and the globular domain of Nuf2 and Ncd80 that stretch and localises at the surface of the kinetochore (Wei et al., 2005). Spc24 and Spc25 interact with CENP-T within the CCAN network at the inner kinetochore; the interaction is mediated by CDK phosphorylation of CENP-T (Figure 7A and 8A) (Pekgoz Altunkaya, 2016; Veld et al., 2016). The globula domains of Ncd80 and Nuf2 are responsible for the interaction with the MTs (Guimaraes et al., 2008; Joglekar et al., 2006; Zaytsev et al., 2015). The Ndc80 complex alone has weak MT binding affinity, that is synergistically increased when it associates with the Mis12 and Knl1 complex, with Knl1 contacting directly the MT lattice (Cheeseman et al., 2006). This could allow a dynamic attachment without losing all the MTs from the kinetochore, balancing the need to capture MTs at the kinetochores while allowing erroneous kinetochore-MT attachments

correction (Cheeseman & Desai, 2008). Other proteins function in parallel to Knl1 and Ndc80 complexes to interact with MTs.

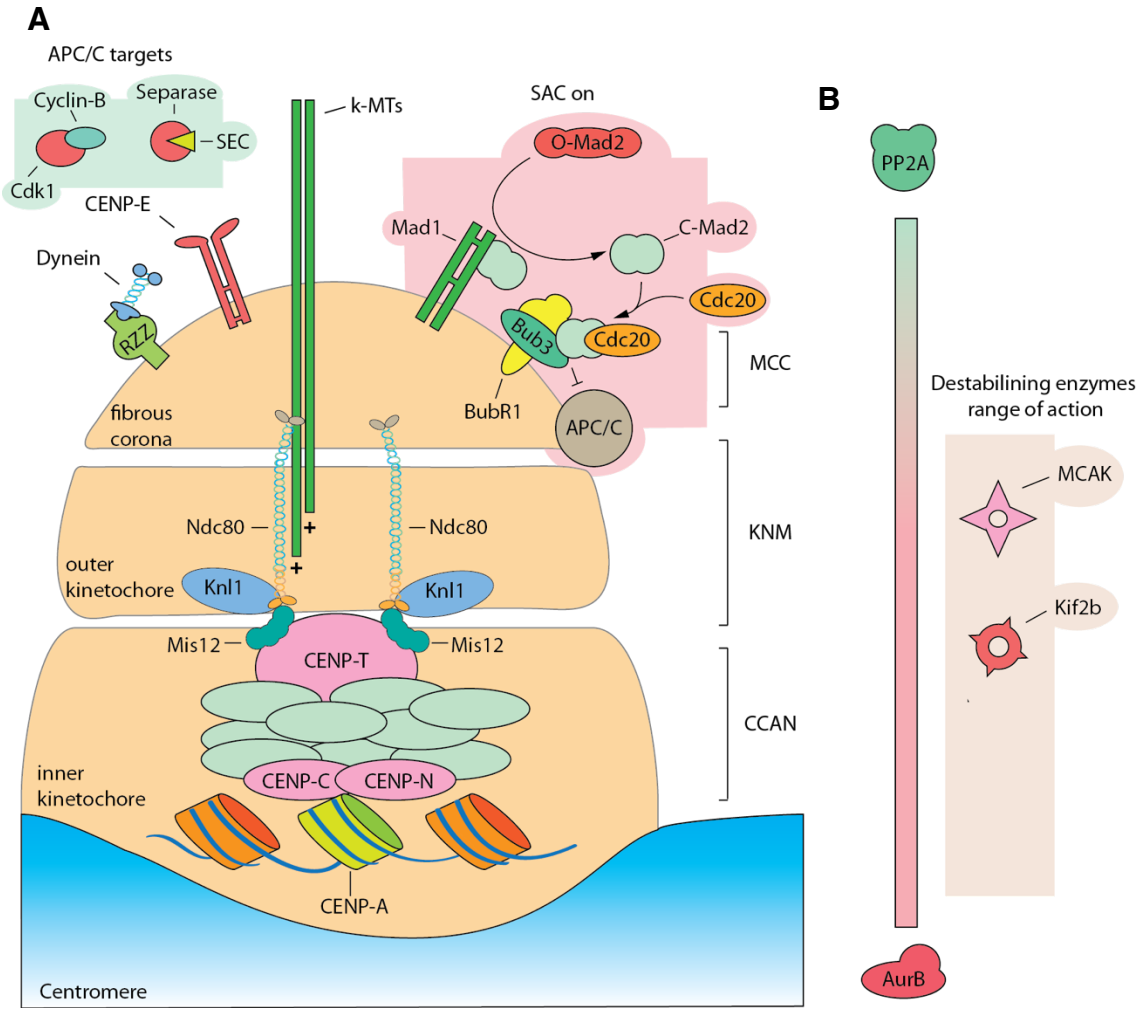

Figure 7 I Physiognomy of an unattached kinetochore. A) Schematic representation of the kinetochore. Inner kinetochore structure starts by the recognition of CENP-A by CENP-C and CENP-N and subsequent assembly of the CCAN complex involving many other CENP proteins organized in modules. The outer kinetochore module is formed by the KNM complex that anchors on the CENP-T protein of the CCAN. The KNM complex is responsible to intercept the KMT at the kinetochore through the Ndc80 complex. However, the interaction kinetics is regulated by the balance of Aurora-B phosphorylation and PP2A phosphatase activities. In this scenario an unoccupied kinetochore is depicted, therefore not subjected to tension and so KMT interaction with Ndc80 and KMT stability itself are subsequently destabilized by Aurora-B phosphorylation and the Kif2b activity. The MCC assembly is shown at the surface of fibrous corona inhibiting APC/C, SAC partial feedback loop is undelight in red. On the left part the principal motor proteins involved in kinetochore interaction, chromosome congression and SAC regulation are represented with RZZ sequestering Dynein, impairing SAC proteins stripping. Green highlight represents the inactivated CDK1 and Separase, the final effector of anaphase entry. B) Aurora-B and PP2A work with counteracting gradients. When the kinetochores are not under tension the kinetochore-MT interface is closer to Aurora-B and the Kif2b destabilizing enzymes, which is more active than MCAK. Leading to fast turnover of KMT.

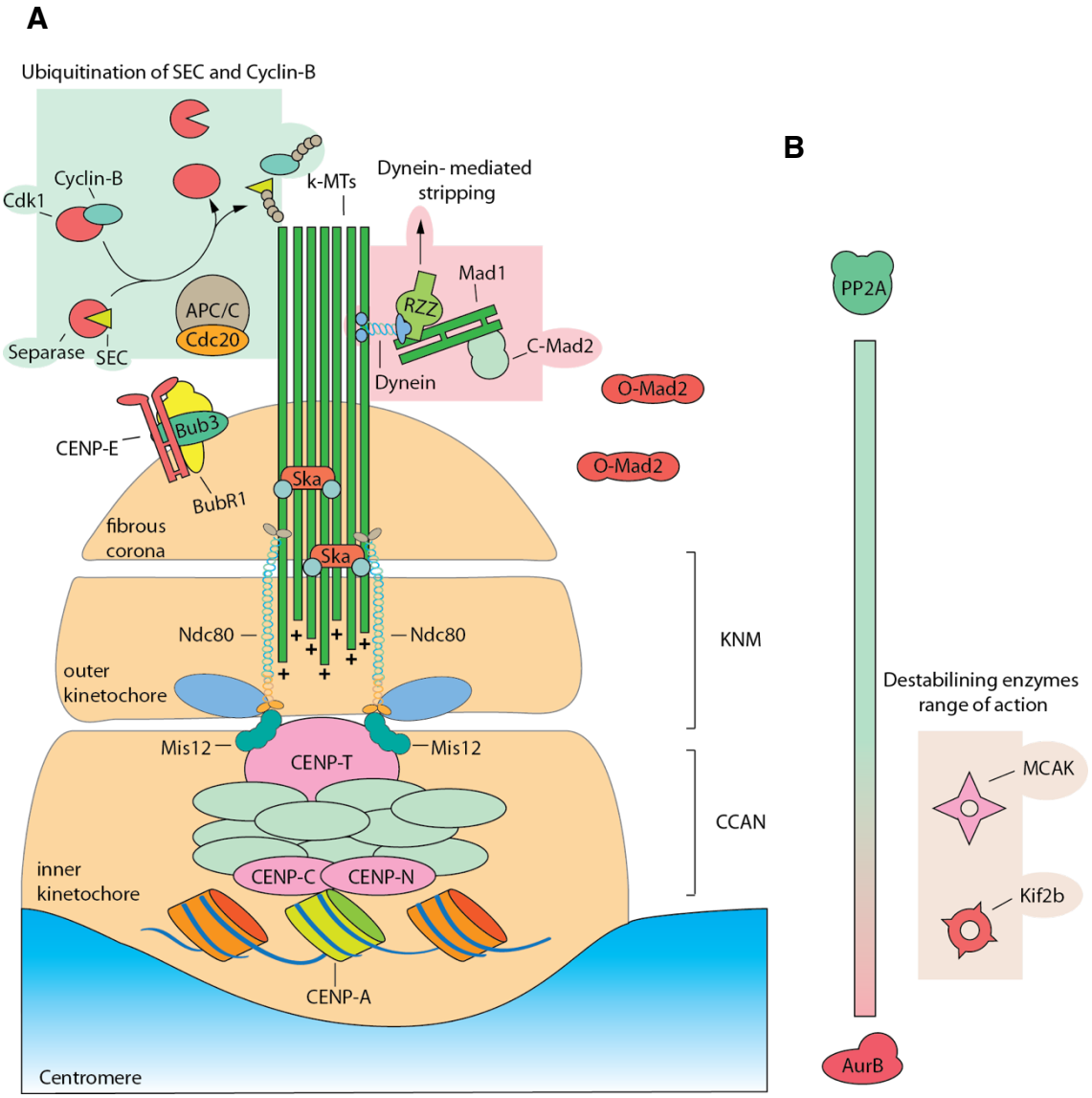

Figure 8 I Physiognomy of an attached kinetochore. A) As in Fig. 12A-B, but here representing a fully occupied kinetochore being under tension. Rearrangement of SAC proteins leads to its silencing, dynein-mediated stripping brings the SAC component from the kinetochore to the spindle poles. SAC silencing is achieved also by CENP-E-mediated sequestering of the BuR1-Bub3 complex. So, APC/C is free to bind Cdc20 and ubiquitinylates SEC and Cyclin-B allowing Cdk1 phosphorylation cascade and the separation of sister chromatids. B) KMTs are more stable in this configuration. The kinetochore is more stretched and therefore the outer kinetochore module feels less the Aurora-B destabilizing gradient. Ndc80, critical for kinetochore-MT stabilization binds more effectively the KMTs and only MCAK is kept in the vicinity to fulfill with the error correction mechanism. Kif2B, more active than MCAK, will find the KMT out of its range of action.

Dynein and CENP-E are the two main motor proteins that work in parallel with the abovementioned complexes. Dynein associates with the kinetochore through the adaptor proteins dynactin and spindly (Griffis et al., 2007). The spindly-dynein-dynactin complex binds then to the RZZ complex in the fibrous corona, the outer part of the outer kinetochore module (Karess, 2005). Here, dynein plays a double role. First, before chromosome alignment, it moves chromosomes poleward to an area with high MT concentration increasing the chances of MT end-on attachment at the kinetochore (Yang et al., 2007). Second, once bi-orientation is achieved, dynein is accountable for the disassembly of the fibrous corona and the removal of SAC proteins from the kinetochore which is essential to promote correct metaphase/anaphase transition (Figure 8A) (Howell et al., 2001). CENP-E, a plus-end directed kinesin, is fundamental for chromosome congression. Like dynein it localises to the fibrous corona in the outer kinetochore (Figure 7A and 8A) (Kapoor et al., 2006; Yao et al., 1997). It opposes the dynein-mediated chromosome minus-end directed movement to start chromosome congression. The two opposite directed motor proteins dynein and CENP-E interplay to reach proper metaphase chromosome congression is still under debate and other proteins could also regulate these movements. Interestingly, recent data showed that a specific MT PTM confers a navigation code for CENP-E role in chromosome congression (Barisic et al., 2015).

b) Kinetochore-MT interface dynamics and beyond

Drawings and images in university textbooks could suggest that k-fibres are stable, rigid polymers that generate forces during anaphase. It could not be more wrong. K-fibres are highly dynamic MT bundles. Although even in live imaging of mitotic cells a k-fibre appears as stable as it does not disappear over time and its length is kept quite constant in metaphase, it is in fact constantly turning over.

The k-fibres undergo MT poleward flux which accounts on KMTs sliding toward the pole and the treadmilling mechanism of plus-end polymerization and minus-end depolymerization. As already mentioned in a previous chapter, MT

plus-end incorporation of tubulin subunit is mediated by the recruitment of CLASP by EB1 at the MT tip. At the poles, MT depolymerisation is controlled by Kif2a and MCAK (Ganem et al., 2006). The k-fibre poleward sliding is then controlled by four different kinesins (Steblyanko et al., 2020). In. metaphase, k-fibre plus-ends exhibit net tubulin incorporation but the individual KMT can show contrasting behaviours (VandenBeldt et al., 2006) and this independence could be at the basis of the error correction mechanism. The role of spindle flux in generating chromosome segregation forces in anaphase A is largely unclear. Indeed, its contribution impressively varies across the eukaryotic kingdom. In human cells, spindle MT flux accounts for one-third of the poleward chromosome movement, the remaining two-thirds of which is due to plus-end disassembly (Ganem et al., 2005). There is apparently no flux in budding or fission yeast, so anaphase A in these cells is probably explained entirely by plus-end disassembly (Maddox et al., 2000). In contrast, flux appears to be solely responsible for anaphase A in plant cells (Dhonukshe et al., 2006).

Apart from Ncd80, many other proteins are necessary for maintaining a dynamic but, at the same time, stable kinetochore-MT interface to allow both error correction and proper chromosome congression and segregation. The SKA complex is recruited by Ncd80 at the fibrous corona once MTs are captured and plays a fundamental role in MT coupling at the kinetochore. It can track polymerising and depolymerising KMTs allowing thereby a stable association with dynamic MTs (Monda et al., 2017; Schmidt et al., 2012). In a simplified molecular model, SKA together with CENP-E remains stably attached to MTs and can move bi-directionally, permitting the transduction of the MT depolymerising flow into a poleward-directed force for chromosome segregation (Gudimchuk et al., 2013; Yu et al., 2019).

Chromosome congression, bi-orientation and segregation depend on precise regulation of the stability and dynamics of the MTs in the mitotic spindle. This balance is achieved through the combined actions of numerous proteins that positively and negatively regulate KMT dynamics and stability in space and time. KMT dynamics regulator at the kinetochore-MT interface includes MCAK, a MT

depolymerase that localizes to the kinetochore (Wordeman & Mitchison, 1995). Its function enhances the likelihood of chromosome bi-orientation and it is essential for the correction of erroneous kinetochore-MT attachments. Other activities such as ch-TOG, CLIP-170, and CLASP counterbalance MCAK activity (Dujardin et al., 1998; Gergely et al., 2003). The kinesin-like protein KIF18A suppresses MT dynamics and must be inhibited to reach a proper anaphase configuration. Another essential component for the stability of the kinetochore-MT interface is the Aurora-B kinase that forms a phosphorylation gradient at the centromeres (A. Musacchio & E.D. Salmon, 2007a). Its activity is coupled to the chromosomal passenger complex (CPC) and mediates the phosphorylation of many kinetochore-MT interface proteins regulating the KMT plasticity (Carmena et al., 2012). One of its targets is MCAK. Indeed, Aurora-B is the upstream effector KMT detachment regulation, and it participates in the SAC silencing (D. Liu et al., 2009). The Aurora-B phosphorylation activity is counteracted by the phosphates PP2A. In the next chapter, I will discuss the process of error detection, correction and the SAC mechanism.

c) SAC and error correction mechanisms

The SAC components are conserved in all eukaryotes. The SAC is turned on in the presence of unattached kinetochores where the Mad1/C-Mad2 complex actively recruits and converts cytosolic O-Mad2 into C-Mad2 (O- and C-Mad2 stand for the Open and Close conformation of Mad2), which together with Bub3 and BubR1 constitute the mitotic checkpoint complex (MCC). The MCC sequesters Cdc20, a co-factor of the ubiquitin ligase APC/C, inhibiting its activity and arresting the cell in mitosis (Sudakin et al., 2001). The inhibition of APC/C prevents the ubiquitinylation of cyclin-B and securin, hence their targeting to the proteasome. Cyclin-B and securin act by inactivating Cdk1 kinase and separase, respectively. Cdk1 promotes mitotic exit, whereas separase cleaves the cohesin complex holding together the two sister chromatids (Figure 9) (Peters, 2006). The

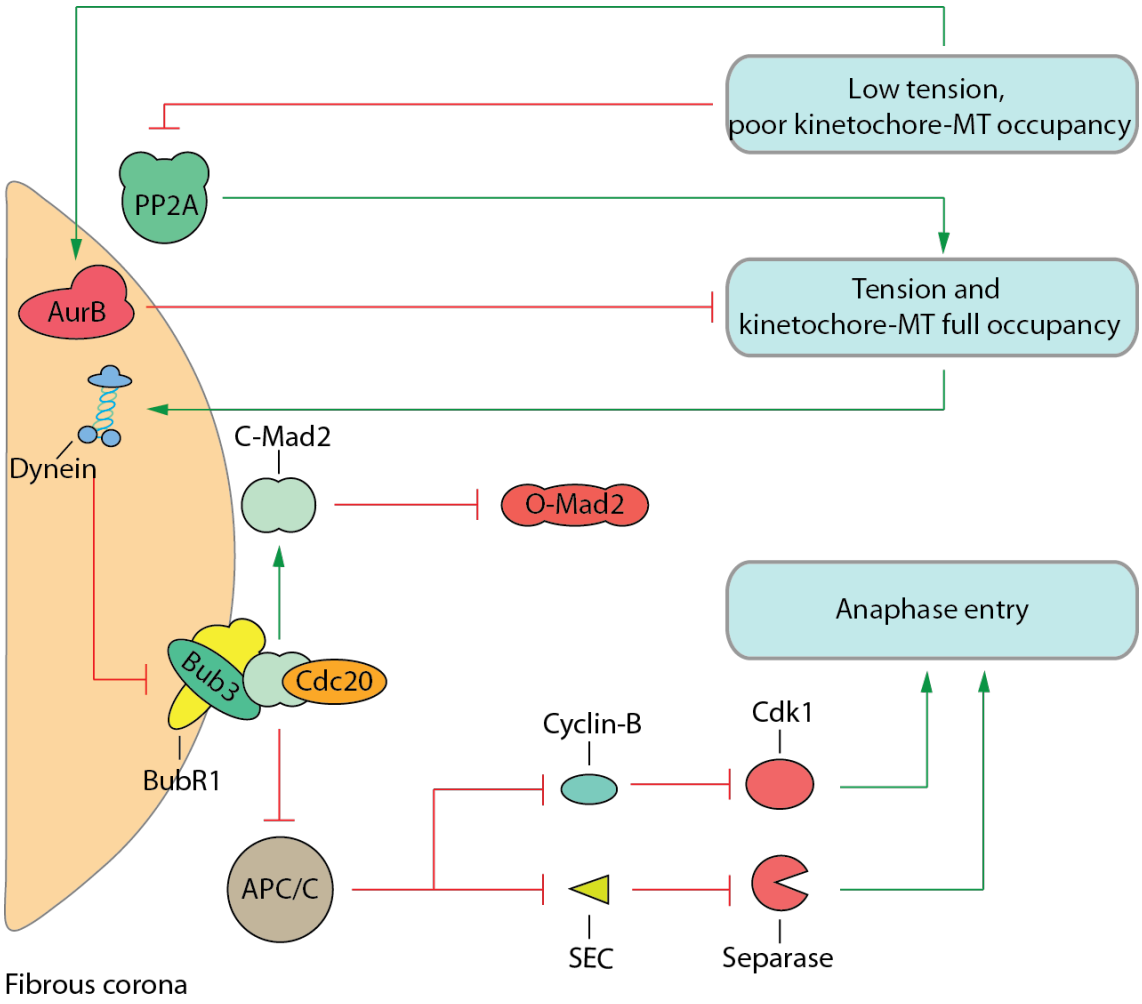

Figure 9 I Simplified feedback loop of the SAC. The SAC network is complex, here I present a minimized version of it. In the absence of KMTs in prometaphase, several biochemical activities point toward the creation of the MCC, which is an APC/C inhibitor. Green segments mean activation/promotion, whereas the red segments indicate inhibition.

SAC prevents this chain of events, prolonging prometaphase until all chromosomes have become bi-oriented on the metaphase plate. Chromosome bi-orientation and subsequent kinetochore MT occupancy finally extinguishes the checkpoint, relieving the mitotic arrest and allowing anaphase to proceed. Bub1, Mps1 and Aurora-B promote the recruitment of all the SAC components to the fibrous corona of unattached kinetochore (A. Musacchio & E.D. Salmon, 2007a). Once the kinetochores are correctly attached to the MTs, SAC proteins are transported poleward by dynein, and as a consequence, the SAC is silenced, and the cell can enter anaphase (Figure 7 and 8) (Howell et al., 2001; Wojcik et al., 2001). It has been calculated that only one unattached kinetochore could

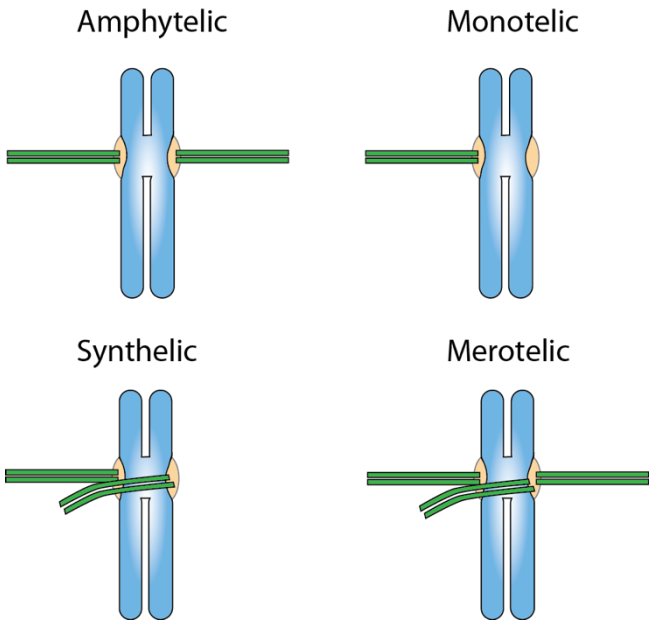

generate enough signal to stop mitosis progress, underscoring the high importance of faithful chromosome segregation (Rieder et al., 1995). However, SAC does not work as a binary code being on when a kinetochore has no attached KMT and off when kinetochores have all attached KMTs. Depending on the nature of the

Figure 10 I KMTs attachment categories. Amphitelic attachment is the correct kinetochore-MTs configuration. The two sister kinetochores are correctly attached and the SAC is switched off. Monotelic attachment refers to chromosomes with only one kinetochore attached to one pole. The unoccupied kinetochore will keep the SAC on. Syntelic attachments occur when both sister kinetochores are attached to MTs coming from the same pole. The loss of inter-kinetochore tension prevents the silencing of the SAC. Merotelic attachments occur when both sister kinetochores are bioriented but one sister is attached to both spindle poles. This configuration generates tension and since both sister kinetochores are attached to MTs the SAC is silenced and the cell enters anaphase. If the merotelic attachment persist, this could lead to generation of aneuploidy for both daughter cells.

kinetochore-MT interface that can be inadequately occupied or generate poor interface stability and forces, the SAC can persist (R.B. Nicklas et al., 1995).

There are four possible kinetochore-MT configurations: amphitelic, monotelic, syntelyc and merotelic (Figure 10). Amphitelic attachment is reached when MTs from opposite spindle poles attach one of the two sister chromatids. This is the correct configuration. The mitotic error correction mechanism aims to establish amphitelic attachments in all chromosomes before progressing toward anaphase. However, during prophase, it is normal that many attachment errors occur. At prophase, almost all kinetochores are either unattached or poorly occupied by MTs. Therefore, SAC proteins start accumulating on the fibrous corona of mature kinetochores. At this point, the topological distribution of chromosomes is almost random, and kinetochore-MT attachment stochastically occurs (Cimini et al., 2003). Mechanisms involving dynein and CENP-E enhance

the level of kinetochore-MT capture (Yang et al., 2007). MT attachments to only one of the sister kinetochores are called monotelic attachment. They are the most frequent configuration in prophase. It is intuitive that the first attachment events on chromosomes are prone to involve only one of the two kinetochores. Indeed, chromosomes at this stage are likely to be found close to either one or the other pole, and geometric constraints could favour monotelicity. This configuration starts silencing the SAC signal coming from one kinetochore while on the other, the SAC is kept on (Tanaka, 2008). Syntelic attachments refer to the attachment of sister kinetochores to MTs emanating from the same spindle pole. Also, this kind of attachment is frequent in prophase due to localisation of the chromosomes in the proximity of one of the poles exposing both kinetochores to MT emanating from the same pole. In this case, both kinetochores are occupied by MTs. However, the kinetochore-MT interface is intrinsically unstable, and the SAC can sense it (M.A. Lampson & Grishchuk, 2017). Due to geometric constraints, this conformation can lead to poor kinetochore-MT occupancy of one or both kinetochores (Rieder et al., 2004). Moreover, sister kinetochores would not be under tension. It has been studied that tension between kinetochores is essential to stabilise the interface that otherwise would encounter a fast turnover, and the kinetochore would release the KMTs (M.A. Lampson & Grishchuk, 2017; R.B. Nicklas et al., 1969; Skibbens et al., 1997). The proposed mechano-sensation mechanism transducing tension forces is still elusive. Aurora-B mediated error correction may be involved in destabilising syntelic attachments. Aurora-B forms a phosphorylation gradient in the kinetochore that fades towards the outer part of the kinetochore. When kinetochores are under tension, the Aurora-B gradient is low at the interface, whereas in the absence of tension, the kinetochore-MT interface is within the Aurora-B range of action. So, the poor occupancy and the fast turnover keep the SAC active in these kinetochores (Funabiki, 2019; M. A. Lampson et al., 2004; Tanaka et al., 2002). At the onset of anaphase, all the sister kinetochores should present an amphitelic configuration that silences all the sources of SAC-mediated mitotic arrest.

One type of erroneous kinetochore MT attachments is however not sensed by the SAC. These attachments called merotelic, occur when one sister kinetochore attaches simultaneously to MT emanating from the two spindle poles while the other one is correctly bi-oriented. This aberrant configuration is not detected by the SAC. Merotelic attachments can be corrected through the Aurora-B depending mechanism (Knowlton et al., 2006). However, the error correction mechanisms may be less efficient because MT occupancy at the kinetochore is achieved and sister kinetochores can be partially under tension stabilising the interface. Since anaphase can proceed in the presence of merotelics , these could result in one or more lagging chromosomes that may segregate into the wrong cell generating aneuploidy (Cimini et al., 2002). Nowadays, it is clear that merotelicity is a predominant cause of aneuploidy and it can also promote chromosome instability (CIN), both characteristics of many cancer cells (Bakhoum et al., 2014; Bakhoum, Thompson, et al., 2009; Cimini, 2008; Cimini et al., 2001b).

d) Merotelic attachment correction: KMT dynamics match the mitotic clock

Merotelic attachments are a predominant cause of aneuploidy and CIN and may promote transformation (Bakhoum et al., 2014; Bakhoum, Thompson, et al., 2009; Cimini, 2008; Cimini et al., 2001b). The correction of erroneous MT-kinetochore attachments involves the specific parameters of KMT turnover as well as the restrictive kinetochore geometry. Indeed, there is a bias of kinetochores to capture MTs that emanate from the spindle pole they face (R.B. Nicklas et al., 1994). This together with the unbiased turnover of the KMTs at the kinetochore-MT interface, kinetochores will by occupied only by correct-sided incoming KMTs as mitosis progresses. So, cells have no need to develop mechanisms that precisely target mal-oriented KMTs, geometric constraints and KMT turnover would be enough to correct this over a normal mitotic timing (Bakhoum, Thompson, et al., 2009; M.A. Lampson & Grishchuk, 2017).

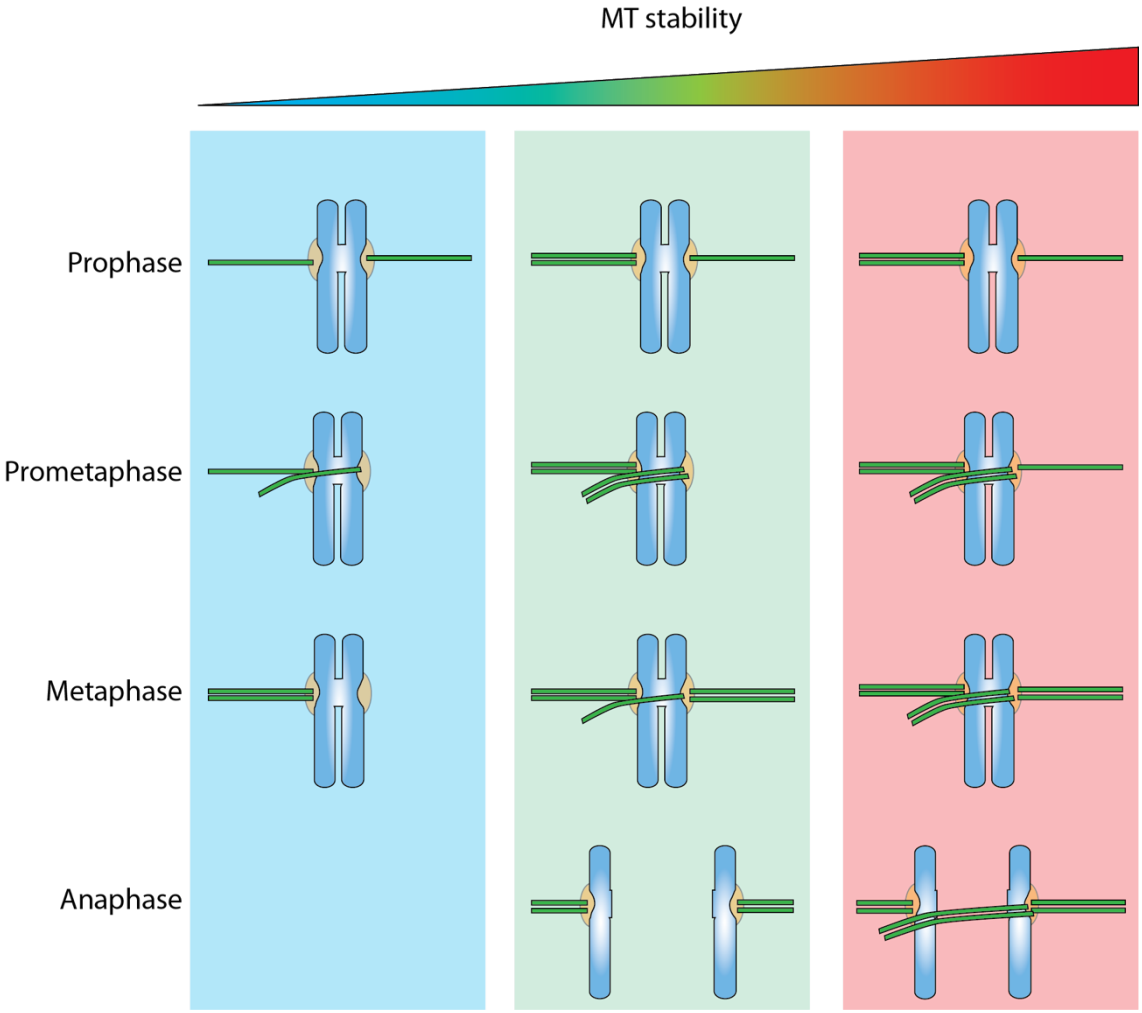

Figure 11 I Representation of anaphase outcome according to KMT stability. The light blue background shows the kinetics of kinetochore-MT interface of KMT poorly stable. We can see how in this scenario kinetochores cannot reach full occupancy and as an outcome there will be a failure in entering anaphase. The light red box represents the case in which KMTs are highly stable. KMTs hyperstability would lead to inefficient turnover increasing the chances of generate merotelicity with generation of lagging chromosomes in anaphase. The light green box represents the behaviour of KMT with correct stability.

This mechanism can be understood intuitively. During prophase, improper KMT attachments form quite frequently; however, the high turnover of KMTs, assessed to be around 2-6 min could promote their gradual release from the kinetochore (Zhai et al., 1995). As mitosis progresses, cycles of KMT attachment-detachment could gradually lead to the amphitelic arrangement. However, KMT stabilitymust be controlled to prevent undesirable consequences resulting from excessively stable or unstable attachments (Figure 11). Indeed, if their turnover is too high,

this would favour a poor occupancy at the kinetochore therefore an active SAC and mitotic arrest. On the other hand, a low MT turnover could lead to an accumulation of improperly attached KMTs. If most erroneous attachment are corrected the cell will enter into anaphase but the chance of doing so in the presence of merotelic chromosomes would increase since they are not detected by the SAC, causing aneuploidy (Cimini et al., 2002).

*In **1976**, while neither tubulin isotypes nor post-translational modifications were described yet; Fulton and Simpson had been writing the following:*

"*The surfaces of a tubulin molecule must interact with many other tubulin surfaces […] as well as with associated molecules. […] Many of these structural interactions appear to have been conserved throughout evolution, and this probably imposes severe restraints on variations in the amino acid sequence. […] On the other hand, subtle changes may have occurred that do not alter the basic topology of tubulin but do provide specialized associative properties or binding sites for particular functions"*

Fulton, C. & Simpson, P. A. Cold Spring Harbor, 1976

1.5. The tubulin code

a) Beyond the MAP solo: the tubulin code

MTs exhibit a large number of different functions even within the same cell to support cell motility, cell shape, differentiation, intracellular transport and cell division. This involves different types of MT networks that can organize upon need thanks to the versatile nature of the MTs. Here I will focus on the diversity at the MT level. MT heterogeneity first comes from a variety of α- and β-tubulin isotypes. Despite the little evolutionary freedom (Ludueña, 2013), there are nine genes encoding for α- and for β-tubulin in the human genome. Although some tubulin isotypes have a tissue-specific functional significance (for example, a mutation in TUBB8 disrupts meiotic spindle function leading to female infertility in humans (Feng et al., 2016)), most of the β- and α-tubulin isotypes can participate in mitotic spindle assembly as well as in forming an interphase network (Gu et

al., 1988; Joshi et al., 1987; Lewis et al., 1988). No data so far support the idea of a putative regulation for the expression of specific tubulin isoforms at the G2/M transition, or during axons and new dendritic spines formation for example. However, some isoforms are specifically expressed in some cell types and for example cancer cells. Another mechanism that can provide diversity is through tubulin post-translational modifications (PTMs) that could drive MT functions in a fine way to confer, rapidly, new structures and properties in a time and space-controlled manner acting both in cis and trans on the MT network. Indeed, tubulin PTMs can tune the intrinsic MT properties and provide new docking sites for the binding of MT associated proteins, tuning their function locally (selected review (Janke et al., 2011; Magiera, Singh, et al., 2018; Roll-Mecak, 2020)). MT interacting domains regulate protein-MT interaction. Many MAPs and motors interact directly with the tubulin C-terminal tails on the MT surface; therefore, their binding could be modulated by PTMs on the MTs. This possible dependency makes the tubulin code hypothesis intriguing, indeed. So far, several MT interacting proteins have been shown to change their binding affinities and or activity depending on the tubulin isotypes and PTMs. In this chapter, I will try to review the state-of-the-art of the so-called tubulin code.

b) Tubulin isotypes

Tubulin isotypes arise from the expression of alternative tubulin genes, and their numbers differ largely between species. The core structure of tubulin almost does not diverge, the most variable part is the C-terminal tail, which is the part of tubulin which is exposed on the surface of the MT and generates docking sites that can be altered by tubulin PTMs. α-tubulin in yeast is encoded by two genes, and only one gene for β- tubulin, whereas the human genome contains nine genes for each (Neff et al., 1983; Schatz et al., 1986) (Figure 12). α- tubulin and β- tubulin isotypes are highly conserved in evolution, whereas less common isotypes evolved to achieve novel MT functions. For example, β1-tubulin (encoded by TUBB1) has co-evolved with platelets (D. Wang et al., 1986).

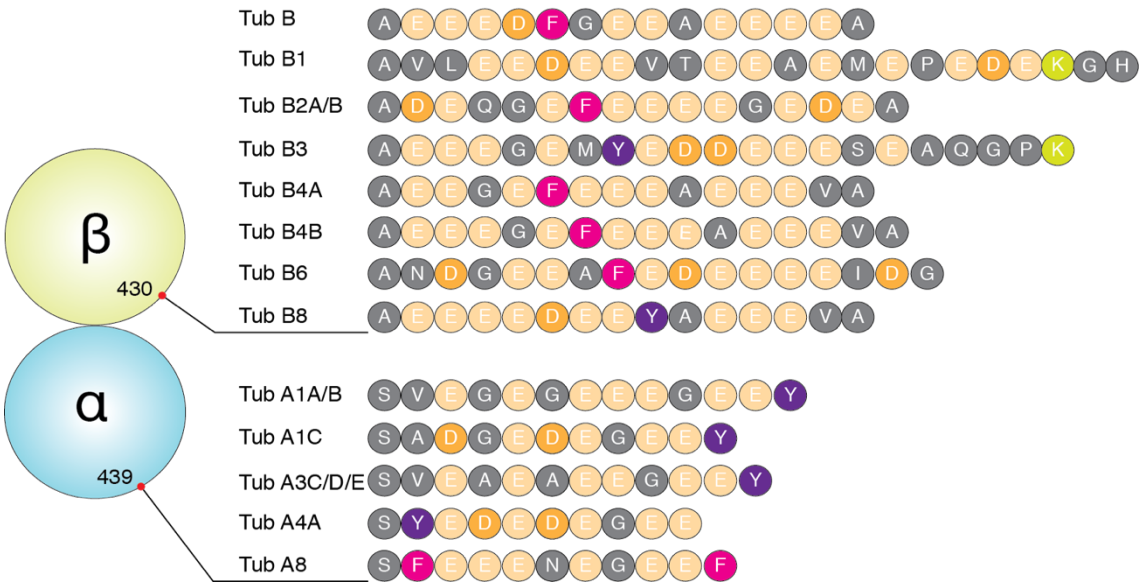

Figure 12 I Tubulin isotypes. Representation of all the human tubulin isotypes. The non-divergent core domains of β-tubulin and α-tubulin are represented by the green and blue sphere, respectively. The numbered red dot depicts the point where the unstructured divergent C-terminal tails start. The color code for the aminoacids in the expanded C-terminal regions represents the aminoacid type.

Albeit no specific functions on controlling MT physical properties have been addressed so far for tubulin isotypes, the absence of TUBB1 leads to severe defects in the architecture of MT arrays in platelets. Neurons express specifically the β3-tubulin isoform. *In-vitro* experiments showed that brain tubulin selectively depleted for β3-tubulin show an increase assembly speed. Moreover, direct experimental evidence with chimeric yeast tubulins demonstrated that a single amino acid difference, such as the presence of a lysine residue in the tail of human β3-tubulin, is sufficient to substantially reduce the run length of kinesin-1 on MT. Interestingly, two α- tubulin isoforms lack the C-terminal tyrosine: α4A-tubulin is naturally detyrosinated (Figure 12) and α8 tubulin has a phenylaniline instead of a tyrosine at the C-terminus. In addition, the β8-tubulin isoform (present only in primates) mutation 292G>A leads to women infertility. It has been proposed that there is a crosstalk between the tubulin isotypes and PTMs (A. Wang et al., 2018). As mentioned above, α4A-tubulin is encoded in its detyrosinated form, but it can be retyrosinated. The presence of this isoform could be explained by the possible need of the cell to directly produce detyrosinated tubulin (Cambray-Deakin et al., 1990). The topology of glutamates within the C-

terminal tail domains could also strongly condition the distribution of PTMs, such as polyglycylation and polyglutamylation. However, the role of tubulin isotypes and how they have evolved is still under investigation.

d) MT Post-Translational Modifications

The first observation that tubulin can undergo post-translational modifications goes back to 1973. α-tubulin tyrosination was first noted in rat brain homogenates (Barra, 1973). Short after, the same group described that tubulin can also be detyrosinated (Hallak et al., 1977). This was the first time that tubulin was described to undergo PTM. In the following paragraphs, I will summarize the milestones of the better-studied tubulin PTMs: acetylation, tyrosination, detyrosination, D2, and D3; phosphorylation, polyglycylation and polyglutamylation. I will dedicate a short chapter to the less known tubulin PTMs polyamination, palmitoylation, arginylation, ubiquitylation, glycosylation, sumoylation and methylation.

i) Tyrosination, detyrosination, Δ2, and Δ3

Tubulin tyrosination was the first MT PTM ever recorded in the scientific literature (Barra, 1973). Tubulin detyrosination came next (Hallak et al., 1977). Most α-tubulin isoforms encode a C-terminal tyrosine, except for TUBA8, in which the last residue is phenylalanine, and TUBA4A that has no C-terminal tyrosine (Ludueña et al., 2008) (Figure 14). Tubulin Tyrosine Ligase (TTL), named according to the PTM it catalyses, was the first enzyme discovered to modify tubulin in 1985 (Schröder et al., 1985); it adds a tyrosine to the C-terminal end of detyrosinated α-tubulin (Figure 13A). On the other hand, its counterpart, the detyrosination enzyme, was long thought to be a member of the carboxypeptidase family CCPs (I will introduce the family later in the following section), which actually catalyse the **Δ**2, and **Δ**3 tubulin (de la Vega et al., 2007; Rogowski et al., 2010) (Figure 13A).

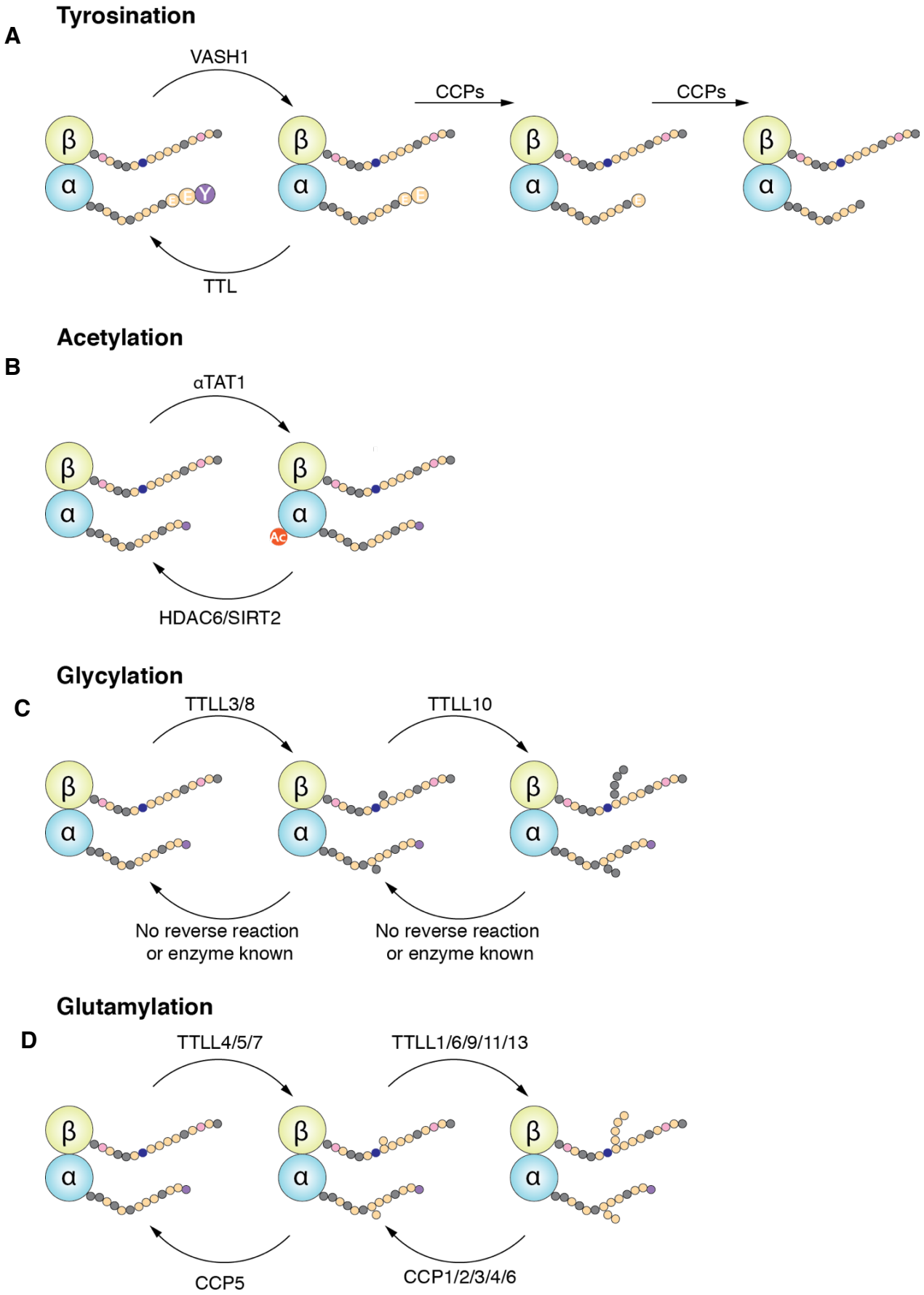
A
Tyrosination
VASH1
CCPs
CCPs
TTL
B
Acetylation
αTAT1
HDAC6/SIRT2
C
Glycylation
TTLL3/8
TTLL10
No reverse reaction
or enzyme known
No reverse reaction
or enzyme known
D
Glutamylation
TTLL4/5/7
TTLL1/6/9/11/13
CCP5
CCP1/2/3/4/6

Figure 13 | Tubulin PTMs, where and who. A) Tyrosination/detyrosination cycle occurring on α-tubulin. On the right of the tyrosination/detyrosination cycle and the formation of **Δ**2, and **Δ**3-tubulin. Bigger circles depict the amino acid that will be removed. B) Acetylation cycle, the acetyl group added by αTAT1 is indicated in orange. C) The Glycylation cycle has two steps, the localization of the branching glycine and the subsequent side chain elongation. It is not clear whether the reverse reaction actually occurs. D) The glutamylation cycle has two subsequent reactions, branching and elongation and the corresponding two reverse reactions. The enzymes involved are known. Glycylation and glutamylation can share the same branching site.

Only, in 2017, a publication in Science by Rogowzki's group shed light on the tubulin carboxypeptidase triggering tubulin detyrosination. As VASH1 (Aillaud et al., 2017; Nieuwenhuis et al., 2017) (Figure 13A). In contrast to tyrosination, which preferentially occurs on free tubulin (Beltramo et al., 1987), detyrosination preferentially occurs on MTs.

Tubulin detyrosination is associated with longer-lived MTs, whereas more dynamic MTs are mainly tyrosinated (Gundersen et al., 1986) . For a long time, it was thought that MT detyrosination confers intrinsic stability to the MT lattice based on many observations. However, recent work using an in-vitro approach with either pure tyrosinated or detyrosinated tubulin showed no intrinsic differences in the dynamic state of the two distinct MT sets (Chen et al., 2021; Gundersen & J.C., 1986).

MT tyrosination/detyrosination is the best-studied MT PTM. Many MT interacting proteins have different binding affinities depending on the MT tyrosination state. For instance, CLIP170 and p150^{glued} (a subunit of the dynein-dynactin complex), two CAP-Gly-domain-containing MAPs, were shown to mislocalise upon TTL silencing in mammalian cells which result in a drop in tyrosinated tubulin (Erck et al., 2005; Peris et al., 2006). Moreover, structural studies of p150^{glued} showed that interaction of their CAP-Gly domain involves the C-terminal tyrosine (Q. Wang et al., 2014). MCAK, a MT destabilising kinesin with no motor activity (Maney et al., 2001; Wordeman & Mitchison, 1995), has a higher activity against tyrosinated tubulin (Peris et al., 2009). In mitosis, its role is essential to maintain k-fibre dynamics for faithful chromosome segregation. Another mitotic motor, CENP-E, guides chromosomes congression by preferentially moving on tyrosinated MTs to navigate correctly towards the

metaphase plate (Barisic et al., 2015). Kinesin-2 processivity increases on detyrosinated MT (Sirajuddin et al., 2014). Despite the central role of this MT PTM, TTL KO mice can surprisingly reach birth although they die shortly after due to brain development defects There is a lack of information about the putative role in the maintenance of tissue homeostasis. Following detyrosination, additional amino acid residues may be removed from the C-terminal tail of α-tubulin to generate Δ2-tubulin (Paturle-Lafanechère et al., 1991) and Δ3-tubulin (Aillaud et al., 2016). This process is catalyzed by enzymes of the CCP family (Berezniuk et al., 2012). Δ2 and Δ3-tubulin are thought to lock MT in a detyrosinated state since TTL cannot add back the C-terminal tyrosine (de la Vega et al., 2007; Rogowski et al., 2010). Indeed, TTL KO increases the abundance of Δ2-tubulin because of the continuous production of detyrosinated MTs that cannot be retyrosinated (Rüdiger et al., 1994) (Figure 7A). The physiological role of these irreversible MT PTMs is still under debate.

ii) Acetylation

In 1983, α-tubulin from flagellar axonemal and cell body of Chlamydomonas was found to have two different isoelectric points (L'Hernault et al., 1983). Two years later, scientists understood that α-tubulin acetylation on Lys40 residue was accountable for the isoelectric shift (L'Hernault et al., 1985). This modification is carried out by α-tubulin acetyltransferase αTAT1 (Akella et al., 2010; Shida et al., 2010) and removed by the deacetylases SIRT2 (North et al., 2003) and HDAC6 (Hubbert et al., 2002). However, other enzymes are likely to act as acetyltransferase on Lys40 (Creppe et al., 2009; Ohkawa et al., 2008; Solinger et al., 2010) (Figure 13B). It is the only MT PTM that occurs at the luminal internal side of MTs (L'Hernault & Rosenbaum, 1985) (Figure 14). Tubulin acetylation of Lys40 was found to mark stable, long-lived MTs with a half-life of more than two hours, including the axonemes of cilia and flagella (which acetylated tubulin is a subcellular marker). α-tubulin Lys40 acetylation protects MTs from depolymerizing drugs activity, such as colchicine and nocodazole, when present

at low doses (LeDizet et al., 1986). Despite these observations, whether acetylated MTs are stable because of acetylation or stable MT structures are better substrates for acetylation is still under debate. Recently, *in-vitro* studies using pure acetylated tubulin suggest intrinsic structural changes of the tubulin polymer that improves the flexibility and resistance to mechanical ageing by reducing interprotofilament sliding (Xu et al., 2017). Recent advances in proteomics have suggested the existence of additional acetylation sites on α- and β-tubulin (Choudhary et al., 2009; N. Liu et al., 2015). One confirmed acetylation event occurs on β-tubulin Lys252 residue, which is expected to regulate MT polymerization (Chu et al., 2011). However, the physiological role of tubulin acetylation is still under investigation. Indeed, the lack of tubulin acetylation upon αTAT1 KO in mice nervous system only results in mild phenotypes such as the loss of touch sensation (Morley et al., 2016). In addition, the lack of tubulin acetylation in the flagellar axoneme leads to male subfertility (Kalebic et al., 2013), maybe because of a reduced MT resistance to mechanical fatigue (Xu et al., 2017).

iii) Polyglycylation

Glycylation is one of the 2 MT PTMs occurring on the tubulin C-terminal tail of both tubulin monomers, the other being polyglutamylation (I will review it in the next chapter). The modification branches the first glycine (Gly) from the γ-carboxyl group of a glutamate (Glu) residue present in the tubulin tails of polymerised MT (Figure 14). It was first described in the axoneme of Paramecium (Redeker et al., 1994). Indeed, MT glycylation is an axoneme related to MT PTM, even though non-tubulin proteins can be targets for this modification. Until 2009, functional experiments assessing the role of MT glycylation were challenging because of the absence of information on the modifying enzymes. Glycylases are members of the TTL family. TTLL3 and TTLL8 catalyse the addition by γ-linking of the first Gly to a Glu residue. TTLL10 catalyses the addition of additional Gly residues by α-linking to another Gly residue (Rogowski et al., 2009) (Figure 13C).

TTLL10 is not active in humans due to the change of two residues in the catalytic domain, and indeed axoneme MT are not polyglycylated in human (Rogowski et al., 2009). The enzymes responsible for the reverse reaction are still unknown. Polyglycylation is a complex MT PTM since the Gly stretches can be of variable length, potentially tuning MAPs activity and/or binding in a graded way instead of the "on/off" behaviour on other mono-modifications. Despite the fact that it is already more than one decade since the discovery of the glycylase family of enzymes, few advances have been made so far to understand the functional and biochemical role of this PTM. Glycylation is primarily found in axonemes and it is crucial for their long-term stability (Grau et al., 2013). It also accumulates in primary cilia in a length-dependent manner, and depletion or overexpression of glycylating enzymes modulates the length of primary cilia in cultured cells (Gadadhar et al., 2017). This strongly suggests that glycylation is essential for the homeostasis of primary cilia. In motile cilia and flagella, ciliary beating is also compromised when polyglycylation is impaired. Recently, the structural basis for this phenotype was characterized as an abnormal conformation of the dynein arms within the sperm axonemes (Gadadhar et al., 2021).

iv) PTMs polyamination, palmitoylation, arginylation, ubiquitylation, glycosylation, sumoylation. and methylation

Other MT PTMs have been described so far, including a plethora of new PTMs such as phosphorylation, polyamination, palmitoylation, arginylation, ubiquitylation, glycosylation, sumoylation and methylation that have been found on tubulin dimers. So far, only a few of them have been characterized in more detail. For instance, phosphorylation on serine 172 of β-tubulin, which is catalyzed by the cyclin-dependent kinase Cdk1, has been shown to affect MT assembly (Fourest-Lieuvin et al., 2006). The recently discovered methylation of α-tubulin K40 (Park et al., 2016) is highly intriguing as it competes with the well-known acetylation of this site. Polyamination is getting increasing attention since it has been recently described to tune MT function in cis, intrinsically stabilising

MT in neurons. The modified residue is usually the Q15 on the β-tubulins. Polyamination is the only modification adding positively charged residues to MTs.

v) Polyglutamylation

At the beginning of the 90s, mass spectrometry of brain tubulin homogenates led to the first observation of MT polyglutamylation (Alexander et al., 1991). As MT polyglycylation, MT polyglutamylation occurs on the C-terminal tail of both α- and β-tubulin on polymerised tubulin (Figure 14). Chemically, the modification branches the first Glu from the γ-carboxyl group of a glutamate residue present in the tubulin tails of polymerised MT to continuing extending the side chain by adding α-linked Glu (Mahalingan et al., 2020). It is thought that the Glu chain starts branching from a preferential Glu residue on the tails without being constrained to any branching site. MT polyglutamylation is particularly abundant in neurons; the first evidence of MT polyglutamylation comes indeed from brain tubulin (Alexander et al., 1991). Later, MT polyglutamylation was also identified in other tissue and cell compartments.

MT polyglutamylation is abundant on axonemal MTs in primary cilia, motile cilia and flagella (Multigner et al., 1996); evolutionarily speaking, it is interesting that polyglutamylation enzymes appear in all the ciliated organisms but are absent from organisms without cilia/flagella such as the yeasts Saccharomyces Cerevisiae or Schizosaccharomyces pombe. Another subcellular MT based structures highly polyglutamylated are the mitotic spindle (Regnard et al., 1999) and the centrioles (Bobinnec et al., 1998).

The first polyglutamylase enzyme to be identified was the murine TTLL1 (Trichet et al., 2000), also named PsG3. The Tubulin Tyrosine Ligase-like (TTLL) family of enzymes is named after their sequence similarity with TTL due to the strong TTL domain homology. This characteristic was essential for the discovery of the TTLL family. Indeed, BLAST and subsequent phylogeny analysis revealed a big family with the presence of 13 different clades conserved in humans, with a high conservation of the TTL and the TTL-extended (flanking regions of the TTL

domain controlling the enzyme activity) domains among orthologues (Janke et al., 2005; van Dijk et al., 2007). As mentioned in the previous chapter, the TTLL family also includes three glycylases: TTLL3, TTLL8 and TTLL10. The active site of TTLL12 has completely degenerated and the role of the putative glutamylase TTLL2 is still under debate. All the other TTLLs are glutamylases that can have specific tissue expression patterns and localisations to subcellular compartments. Glutamylases reaction and substrate specificity have been described by TTLLs overexpression (van Dijk et al., 2007). TTLL4, 5 and 7 carry out the MT branching reaction exclusively while TTLL1, 6, 9, 11 and 13 preferentially elongate the Glu side chain; however, it is still uncertain whether some of these elongation enzymes can also add the branching glutamate under some circumstances. TTLL1 and TTLL9 need co-factors in order to be active (Janke et al., 2005; Kubo et al., 2014). Other regulatory proteins can couple with TTLLs to tune their activity, such as CSAP that binds MT, and docks TTLL5 and 7 to the MT, increasing their polyglutamylation potential (Bompard et al., 2018) (Figure 13D). However, little is known about the regulation of glutamylase activity. Polyglutamylases can also modify a broader range of substrates apart from the MTs including the nucleoproteins NAP1 and NAP2 already described in 2000 (Regnard et al., 2000), other proteins such as RANGAP, SET, ANP23A, ANP23B and nucleolin. However, no glutamylation consensus sequence has ever been pointed out. On the other hand, the cytosol-carboxypeptidases (CCPs) family members catalyse the reverse reaction. The six CCPs of a subfamily of M14 metallocarboxypeptidases catalyse the removal of the polyglutamylated side chain (Kimura et al., 2010; Rogowski et al., 2010). CCPs are exonucleases, with CCP5 being the only family member able to remove the branching Glu (Figure 7D). In contrast, the other members remove the chain of Glu stretch or even a terminal Glu in a peptide or a protein such as myosin light-chain kinase and telokin. CCPs, indeed, can produce **Δ**2, and **Δ**3 α -tubulin (Rogowski et al., 2010). The role of the deglutamylases, apart from CCP5, could be considered redundant and specialised to regulate the brain and cilia/flagella homeostasis. CCP1, CCP4 and CCP6 are tightly linked with neurodegeneration. KO of CCP1 leads to early

cerebellum neurodegeneration in young mice, an effect that CCP6 overexpression can rescue. Under these circumstances, neurodegeneration is caused by hyperglutamylation, which impairs neuron homeostasis by interfering with cellular trafficking and MAPs interactions (Rogowski et al., 2010). The role of CCP2 and CCP3 have been more elusive; however, now it is clear that they participate in the deglutamylation process. CCP2 and CCP3 expression in ciliated tissues and the increase of their expression levels during ciliogenesis suggest that they fulfil specific functions in the regulation of the two PTMs in these organelles. CCP3 seems to catalyse Glu and Asp removal with equal efficiency (Tort et al., 2014). On the other hand, CCP6 could regulate SAC activity since it has been described that it removes the Glu chain from Mad2 (its role in the SAC will be reviewed in the following chapters. In contrast with the TTLL family, which

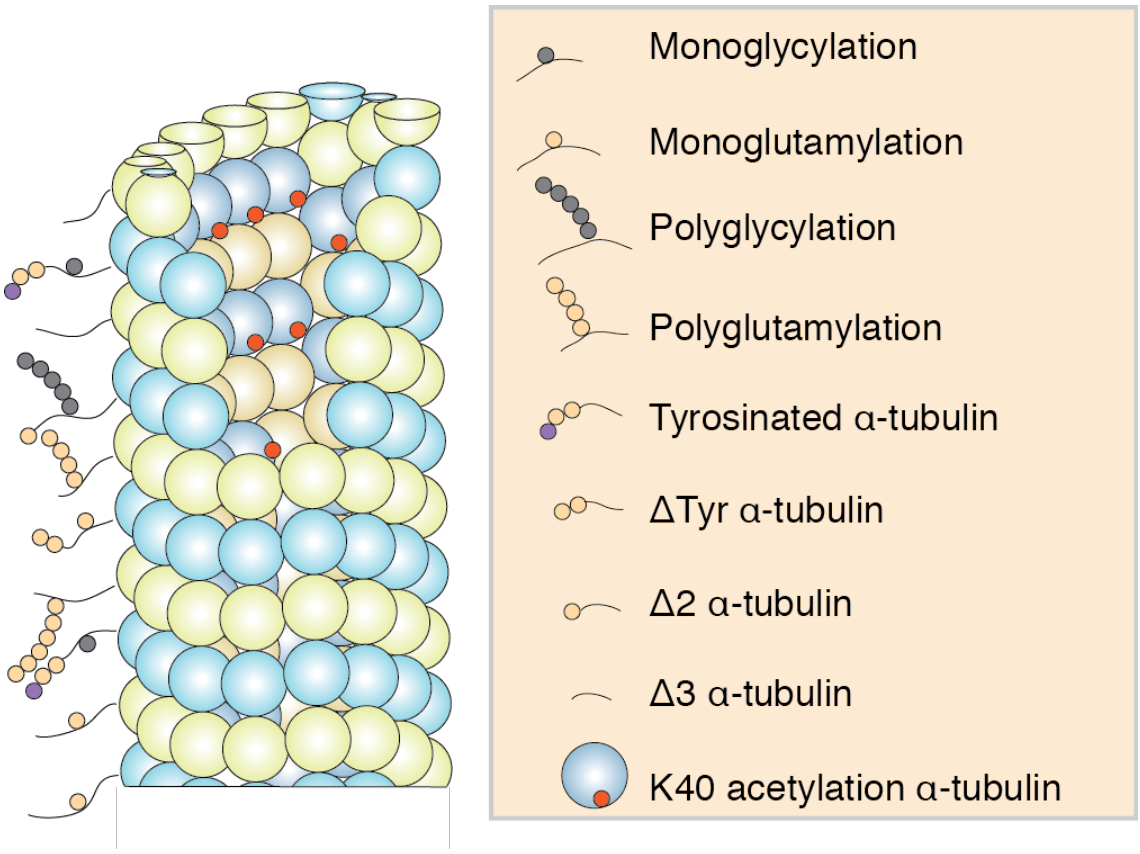

Figure 14 I MT PTMs. 3D reconstruction of a MT with the sites of the main tubulin PTMs. Acetylation is the only luminal PTMs while the MT surface is rich in different PTMs that can create new docking sites for protein interaction. The color code of the tubulin subunits follows the one reported in Figure 3. The luminal side of the tubulin is illustrated in a darker shade.

function preferentially on polymerized tubulin, the deglutamylation reaction occurs mostly on soluble tubulin dimers.

Since the discovery of the enzymes orchestrating the MT polyglutamylation cycle, we have been getting an increasing understanding of the functional consequences of MT polyglutamylation. The first evidence of MT polyglutamylation role in physiology came from the pcd mice model. These animals are affected by early cerebellum neurodegeneration, in particular affecting the Purkinje cells. These mice bear a mutation in the Agtpbd1 gene that gives rise to the CCP1 protein (Fernandez-Gonzalez et al., 2002; Rogowski et al., 2010). MT hyperglutamylation was found to be the cause of nervous tissue degeneration. Interestingly, the co-depletion TTLL1, the main brain glutamylase, was shown to rescue the neurodegenerative phenotype. Brain MTs are generally polyglutamylated. In the brain regions that did not undergo neurodegeneration upon CCP1 loss of function, another carboxypeptidase called CCP6 encoded by the Agbl4 gene was essential to control polyglutamylation in this area (Magiera, Bodakuntla, et al., 2018). However, the co-depletion of CCP1 and CCP6 led to the entire brain neurodegeneration, suggesting that CCP6 loss of function alone can be rescued by CCP1 activity in those areas. MT polyglutamylation is also essential for cilia and flagella. CCP5 loss of function leads to subfertile mice likely due to the hyperglutamylation of the B-Tubule (the axonemal structural part bearing polyglutamylation). TTLL5 leads to retina degeneration; however, it seems that the TTLL5 target substrate in photoreceptor cells is not tubulin. A mutation in TTLL9 human homolog of *Chlamydomonas reinhardii* impairs the MT polyglutamylation pattern leading to a weakening of flagellar motility due to improper modulation of the inner-arm dynein motility in the flagellar axoneme (Kubo et al., 2010). Recently, the Joubert syndrome protein ARL13B trafficking pathway in the cilia was shown to control the import of TTLL5 and TTLL6 in the cilia. Loss of the aforementioned TTLLs result in correct ciliogenesis; nonetheless, it promotes cilia disassembly and disrupts cilia signalling. Remarkably, as in the brain nervous tissue, the phenotype can be rescued by balancing the MT polyglutamylation cycle. Indeed, the depletion of CCP5 restores

the cilia function (He et al., 2018). Up to now, few strong pieces of evidence of how MT polyglutamylation can actually control MAPs, molecular motors or severing enzymes have been provided. The severing enzyme spastin deserves more than a mention. In 2010, it was discovered that MT polyglutamylation levels regulate spastin activity in human cells directing MT network disassembly (Lacroix et al., 2010). In 2016, using human-engineered and differentially modified MT, Roll-Mecak's lab investigated how MT glutamylation actually affect spastin activity finding that MT polyglutamylation works as a nonlinear biphasic tuner. In other words, spastin binding and severing activities are influenced by MT polyglutamylation levels. Short glutamylated side chains avoid the binding of spastin; however, it has the highest activity. As the chain elongates, spastin activity reduces, but binding capability increases until reaching an inflexion point where the slope of the curve changes and decrease until having all the spastin bound but inactive. This aspect is of deep interest since it showed for the first time that MT polyglutamylation acts actually by finely grading proteins functions (Valenstein et al., 2016). Other proteins such as Kinesin-1, tau and dynein show a binding control dependent on MT polyglutamylation levels, as mentioned in the previous chapters.

MT polyglutamylation was also found in the mitotic spindle. Indeed, an increase of MT polyglutamylation is observed in cycling cells, and interphase MTs have low polyglutamylation signal while mitotic MTs present a high level of polyglutamylation (Regnard et al., 1999). It has also been observed that mitotic astral MTs are not polyglutamylated, whereas the central spindle is. It is still not clear whether it is due to a global increase of MT polyglutamylation in the central spindle or, as it is tempting to speculate, k-fibre mainly contributes to the increase of the polyglutamylation observed in this region. I will shed light on this question in the result section of this thesis.

Objectives

2. Objectives

The main goal of this thesis was to shed light on the role of spindle MT polyglutamylation. To answer this question, we aimed at:

1) Identifying the putative polyglutamylase enzyme/s that modify the spindle MTs.
2) Interfere with the expression of the identified enzyme to address the role of spindle MT polyglutamylation during mitosis in HeLa cells
3) Validate the functional analysis on the role of spindle MT polyglutamylation *in-vivo* using zebrafish embryos.
4) Examining the putative role of the identified enzyme in human cancer through a bioinformatic analysis of expression data.

Results

3. Results

3.1 Human meiotic spindle MT polyglutamylation pattern

Thanks to our collaboration with the Eugin fertility clinic, I had access to human oocytes donated to the clinic. I performed immunostainings of oocytes collected at meiosis II to visualize MTs and their polyglutamylation levels. At this stage, the oocyte is called secondary oocyte, and it has already extruded the first polar body (Figure 15A). The oocyte is haploid, and without replicating the genetic material, it enters meiosis II and halts at metaphase II. Interestingly, the MTs of the human meiotic spindle are polyglutamylated (Figure 15A, B), as detected with our polyE home-made antibody (Figure 15A, B). This experiment was performed with eight different human oocytes giving the same positive signal.

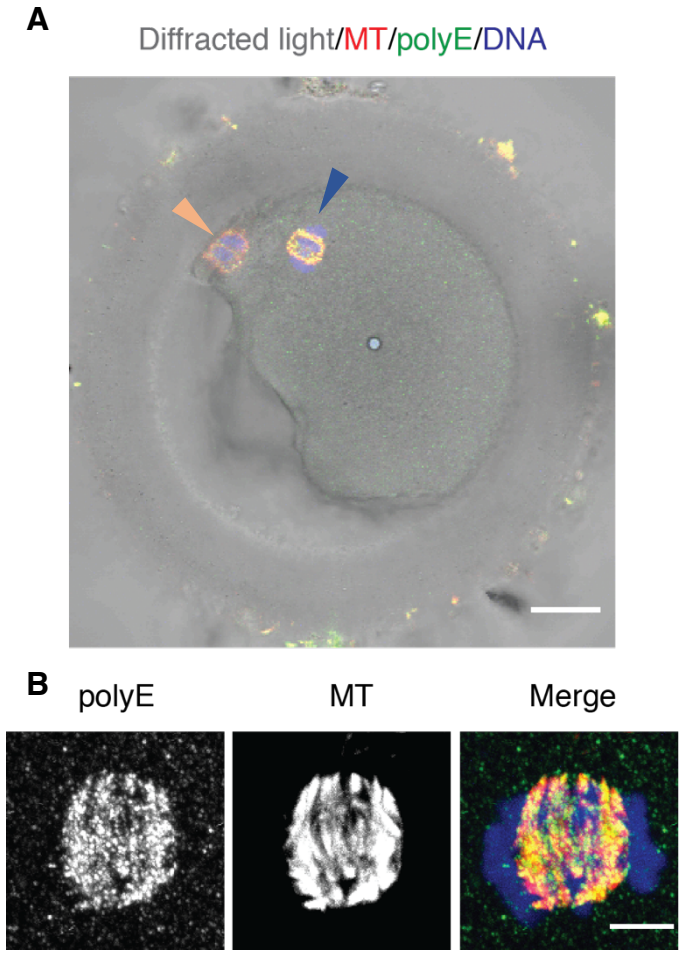

Figure 15 I Human oocyte polyE staining. A) confocal image of the entire oocyte, we can notice the meiotic spindle in metaphase II (blue arrowhead) and the first polar body (orange arrowhead). Scale bar, 20 μm. B) Zoom-in of the metaphase II spindle. MT are in red, polyE in green. The image is then merged with the DNA (blue). Scale bar, 5 μm.

3.2. TTLLs localization and expression profile in HeLa cells

An increase in polyglutamylase activity was previously reported to occur during mitosis (Regnard et al., 1999) as well as the specific polyglutamylation of the spindle MTs (Bobinnec et al., 1998; Lacroix et al., 2010), suggesting that this PTM has a role during cell division.

To address the molecular mechanism and functional implications of the polyglutamylation of spindle MTs, we aimed at identifying the enzyme driving this PTM. I then checked first the interphase and mitotic localization of the 9 TTLL enzymes, classified as glutamylases by exogenously expressing each of them as recombinant proteins with an EGFP tag either at their N- or C-terminus in Hela cells. I also cloned TTLL12 that has a degenerated TTL domain and is thought to

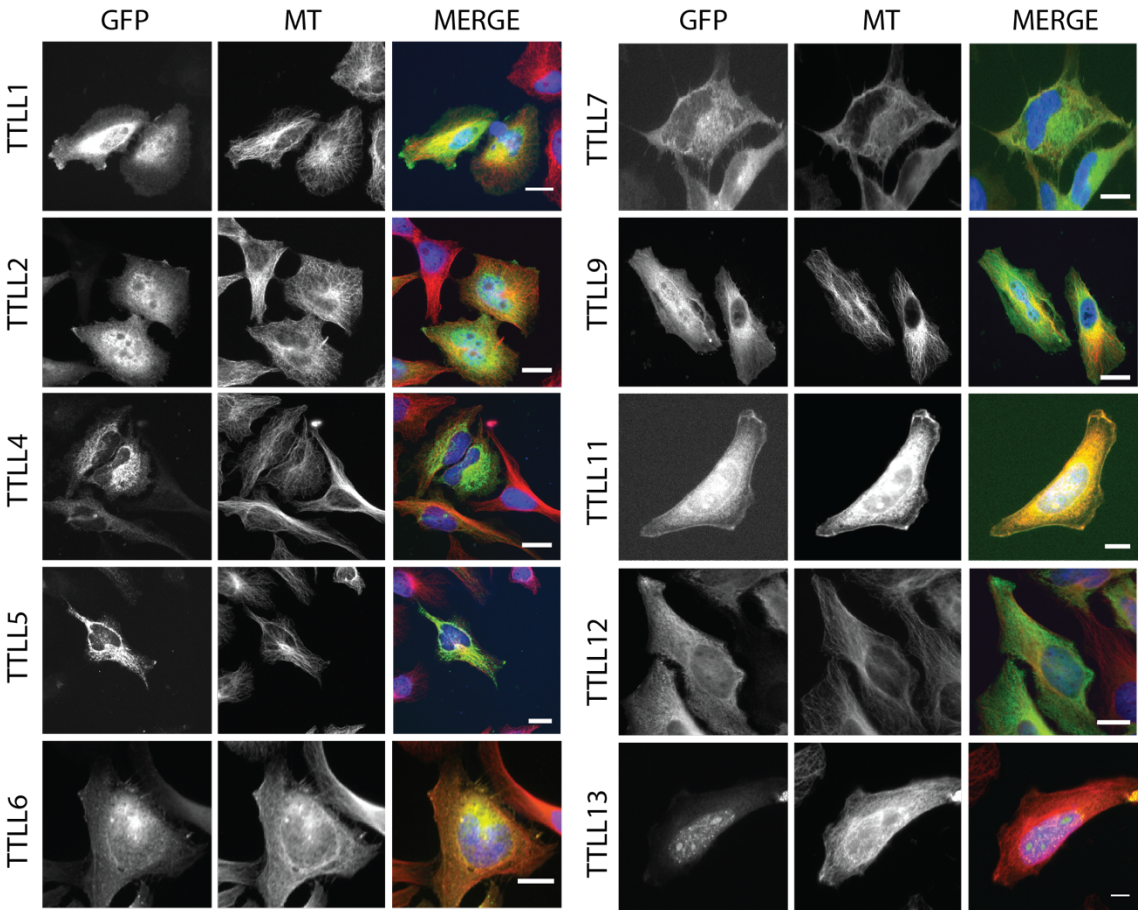

Figure 16 I TTLLs localization in cycling HeLa cells. Fluorescent wide-field images of c-terminal GFP tagged glutamylases in HeLa cells. Tubulin was stained with DM1A antibody (red) and GFP tagging glutamylases with anti-GFP (green), DNA was stained with DAPI (blue). Interphase HeLa cells TTLLs localization. All scale bars are 5 μm.

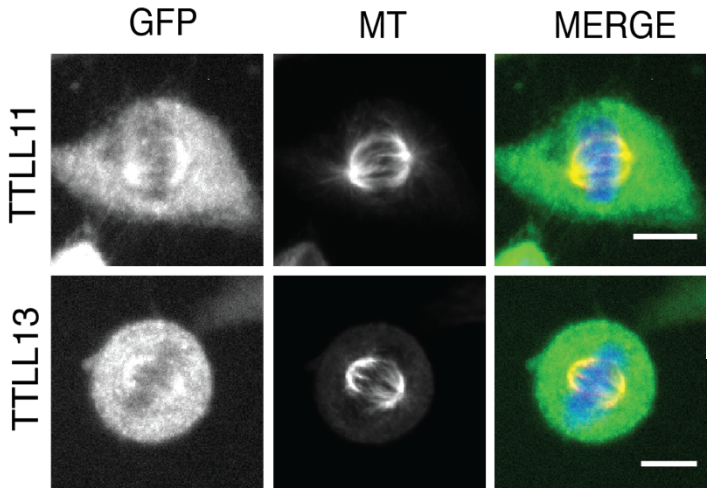

Figure 17 I TTLL11 and TTLL13 mitotic localization. HeLa cell immunofluorescence of GFP tagged TTLL11 and TTLL13. MT are stained with DM1A antibody (red), GFP tagged TTLL are immunostained with a home-made GFP antibody (green). DNA is stained with DAPI (Blue). Scale bars are 10 μm.

be a histone methylase enzyme; however, a putative tubulin modification activity is not ruled out (Wen et al., 2016). I found that in interphase cells, TTLL1, 2, 6, 9, 11, 13 show clear nuclear localization whereas TTLL 4, 5 are cytoplasmic suggesting different regulation mechanisms for the different glutamylases (Figure 16). I then looked at the mitotic localization of the exogenously expressed TTLL glutamylases as recombinant proteins with an EGFP tag either at their N- or C-terminus in Hela cells. I found that only two TTLLs localized to the spindle MTs, TTLL11 and TTLL13 (Figure 17).

3.3. Expression of TTLL glutamylases in HeLa cells and human tissues

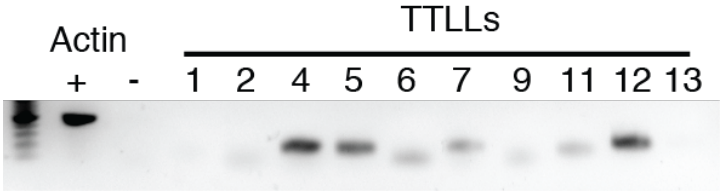

Figure 18 I TTLLs expression profile by RT-PCR. Plus and minus signs indicate the actin primers amplification of retrotranscribed and non-retrotranscribed whole mRNA HeLa cell extract, respectively. Every number indicate the member of TTLL family.

Since we had to check the localization of the TTLL enzymes by exogenous expression of fluorescently tagged proteins, we then aimed at characterizing the expression of the endogenous proteins. I first performed an expression profile of TTLLs in HeLa cells. RT-PCR of the 10 TTLLs under investigation revealed that all except TTLL1, 2 and 13 are expressed in HeLa cells (Figure 18).

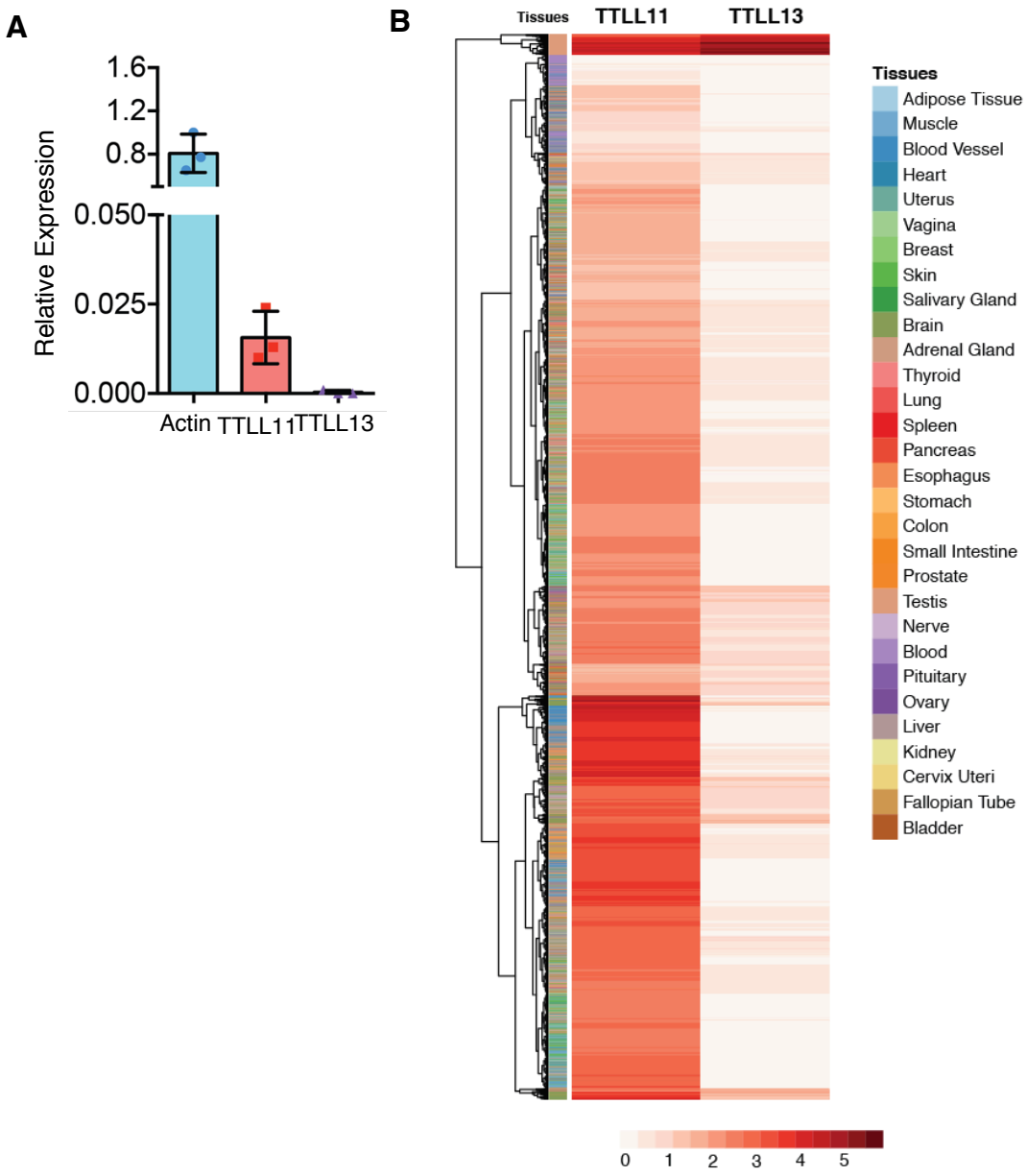

Figure 19 I TTLL11 and TTLL13 localize to the spindle but only TTLL11 is ubiquitous expressed. A) Relative expression of actin, TTLL11 and TTLL13 in HeLa cells detected by RT-qPCR. The plot represent means from N = 3 independent experiments. Error bars represent SD. B) Expression levels of TTLL11 and TTLL13 across human tissues from GTEx illustrated as a red scale in log2(TPM+1).

Since only two TTLL localized to the spindle upon exogenous expression I then focused on these two enzymes and performed a RT-qPCR to check the expression level of TTLL11 and TTLL13 in cycling HeLa cells. The RT-qPCR confirmed the previous results, TTLL13 is not expressed in HeLa cells while

TTLL11 has a low but consistent expression profile (Figure 19A). As a complementary analysis we decided to check for the expression of TTLL11 and TTLL13 in human tissue by querying the GTEx Portal (https://gtexportal.org/home/). We found that TTLL11 is ubiquitously expressed in human tissues whereas TTLL13 is poorly expressed overall (Figure 19B). Altogether our data point at TTLL11 as a solid candidate for driving MT polyglutamylation in the spindle and we focused on this enzyme for further experimental approaches.

3.4. TTLL11 is the primary enzyme catalyzing mitotic spindle MT polyglutamylation

To validate TTLL11 as the enzyme driving mitotic spindle MT polyglutamylation we first tested whether this PTM would be reduced upon silencing the enzyme in HeLa cells. First, I checked the silencing efficiency of TTLL11 using the Darmachon SMARTpool. Since I could not check the levels of the TTLL11 protein due to the lack of available antibodies (commercial or home-made), I first checked whether the siRNAs could silence the expression of the exogenous protein tagged with GFP at the N-terminal upon co-transfection in HeLa cells. This was the case as shown in Figure 20A. In addition, I checked for the levels of endogenous TTLL11 mRNA by qRT-PCR. Also, in this case, I could confirm the silencing efficiency of the TTLL11 Darmachon SMARTpool (Figure 20B). We then went on to investigate the impact of TTLL11 KD on MT polyglutamylation in the spindle. I transfected HeLa cells with either a scrambled control siRNA or the TTLL11 silencing constructs. At 48h after transfection, I fixed the cells in cold methanol and stained them for tubulin and polyglutamylation. The signal for polyE was significantly reduced in spindles assembled in siTTLL11 cells (0.521 ± 0.145 a.u versus 0.821 ± 0.192 a.u. in control; p-value < 0.0001) (Figure 20C).

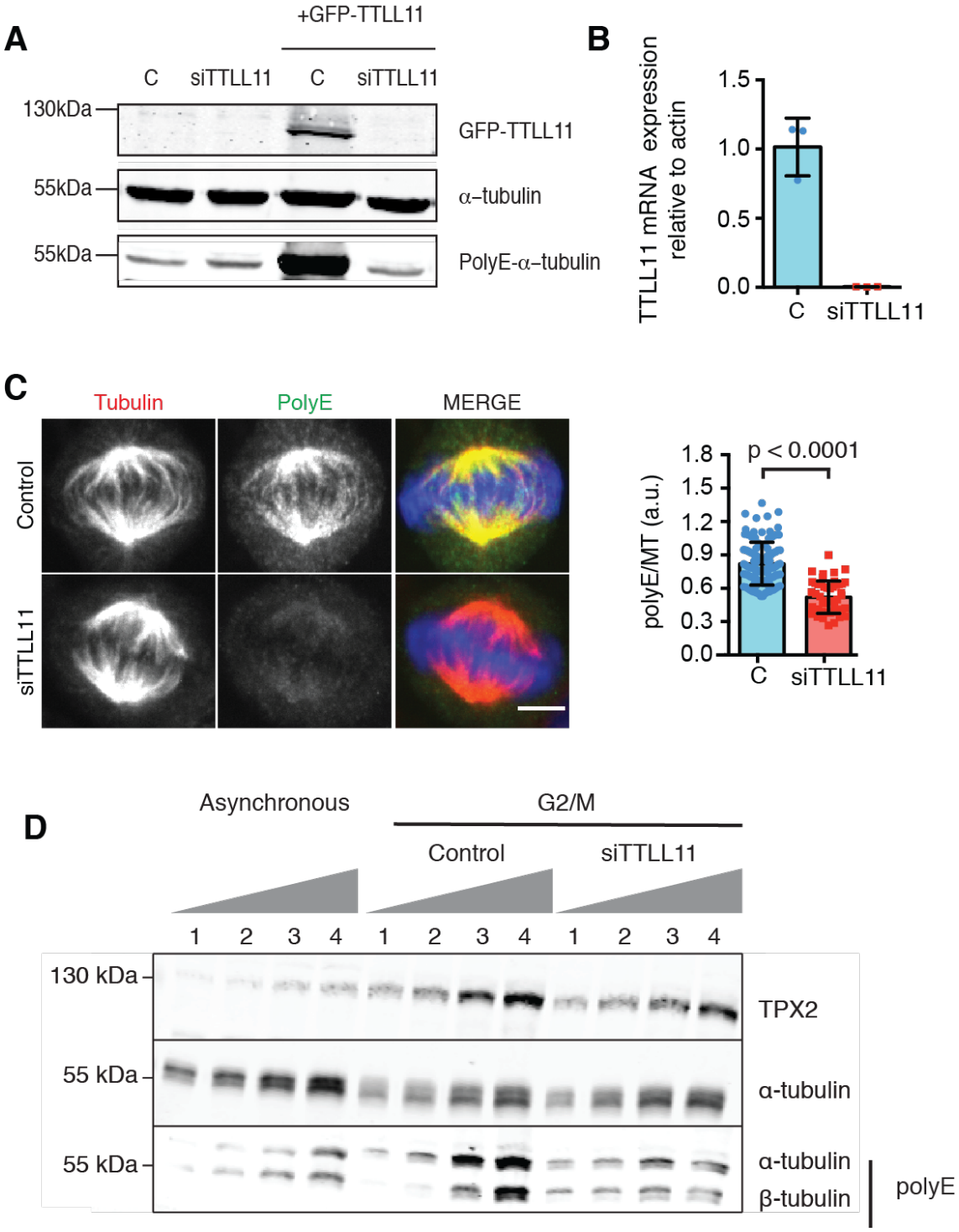
A
+GFP-TTLL11
C
siTTLL11
C
siTTLL11
130kDa
55kDa
55kDa
GFP-TTLL11
α–tubulin
PolyE-α–tubulin
B
TTLL11 mRNA expression relative to actin
1.5
1.0
0.5
0.0
C
siTTLL11
C
Tubulin
PolyE
MERGE
Control
siTTLL11
p < 0.0001
polyE/MT (a.u.)
1.8
1.5
1.2
0.9
0.6
0.3
0.0
C
siTTLL11
D
Asynchronous
G2/M
Control
siTTLL11
1 2 3 4 1 2 3 4 1 2 3 4
130 kDa
55 kDa
55 kDa
TPX2
α-tubulin
α-tubulin
β-tubulin
polyE

Figure 20 I siTTLL11 efficiently silence TTLL11 resulting in a drop in MT polyglutamylation level in the mitotic spindle. A) Western blot analysis of control and siTTLL11 cells expressing GFP-hTTLL11. The blot was probed with an anti-GFP to visualize exogenous GFP-TTLL11, an anti-tubulin as loading control and the anti-polyE antibody. Note that cells overexpressing GFP-TTLL11 have a higher level of polyglutamylated tubulin. Cell lysates were obtained 48h after transfection. (B) TTLL11 expression levels detected by RT-qPCR in control and TTLL11 silenced cells 48 h after transfection. Expression levels represent means from N = 3 independent experiments. Error bars represent SD. Scale bar represent 5 μm. C) Immunofluorescence images of metaphase spindles in control and siTTLL11 cells stained to visualize polyglutamlyted MTs (PolyE, green), tubulin (red) and DNA (blue). The graph shows quantification of the polyE signal normalized on the total tubulin signal in spindles assembled in control and siTTLL11 cells. n (control) = 105 cells and n (siTTLL11) = 59 cells. Representative graph from N=5 independent experiments. Bars represent SD. D) Western blots of Hela cell lysates probed to detect TPX2, Tubulin and Polyglutamylated tubulin (polyE-tubulin). TPX2 peaks in G2/M and was used as a maker for G2/M synchronized cells. For quantification increasing amounts of the cell lysates were loaded for each condition as indicated on top: 1- 15 μg, 2- 25 μg, 3- 35 μg, 4- 45 μg.

Consistently, WB analysis showed that the level of tubulin polyglutamylation in TTLL11-silenced cells was reduced in mitosis compared to controls (Figure 20D). Altogether, these results point at TTLL11 as the polyglutamylase that generates long glutamate chains on the spindle MTs.

3.5. Characterization of MT (poly)glutamylation in interphase and mitotic HeLa cells upon TTLL11 KD

So far, we have investigated how spindle MT polyglutamylation levels are affected by the TTLL11 KD. However, we wanted to understand whether this drop of MT polyglutamylation in mitosis comes from a reduced glutamylation activity directly in this phase or is an indirect effect due to the impairment of MT glutamylation on the interphase MTs. Interphase MTs are monoglutamylated but poorly polyglutamylated. We then explored the landscape of the glutamylation pattern in interphase and mitotic HeLa cells in control and siTTLL11 cells. We found that the GT335 antibody staining changes neither between mitosis and interphase nor between control and siTTLL11 cells both in mitosis and in interphase (Figure 21A). As expected, the polyE levels of MTs changed in mitosis between control and TTLL11 silenced conditions (Figure 21B).

However, in interphase the low levels of MT polyglutamylation are unchanged in control and TTLL11 silenced cells. Therefore, there is an increase in the level of MT polyglutamylation between interphase and mitosis (Figure 21B) in agreement with previous literature (Regnard et al., 1999). These data

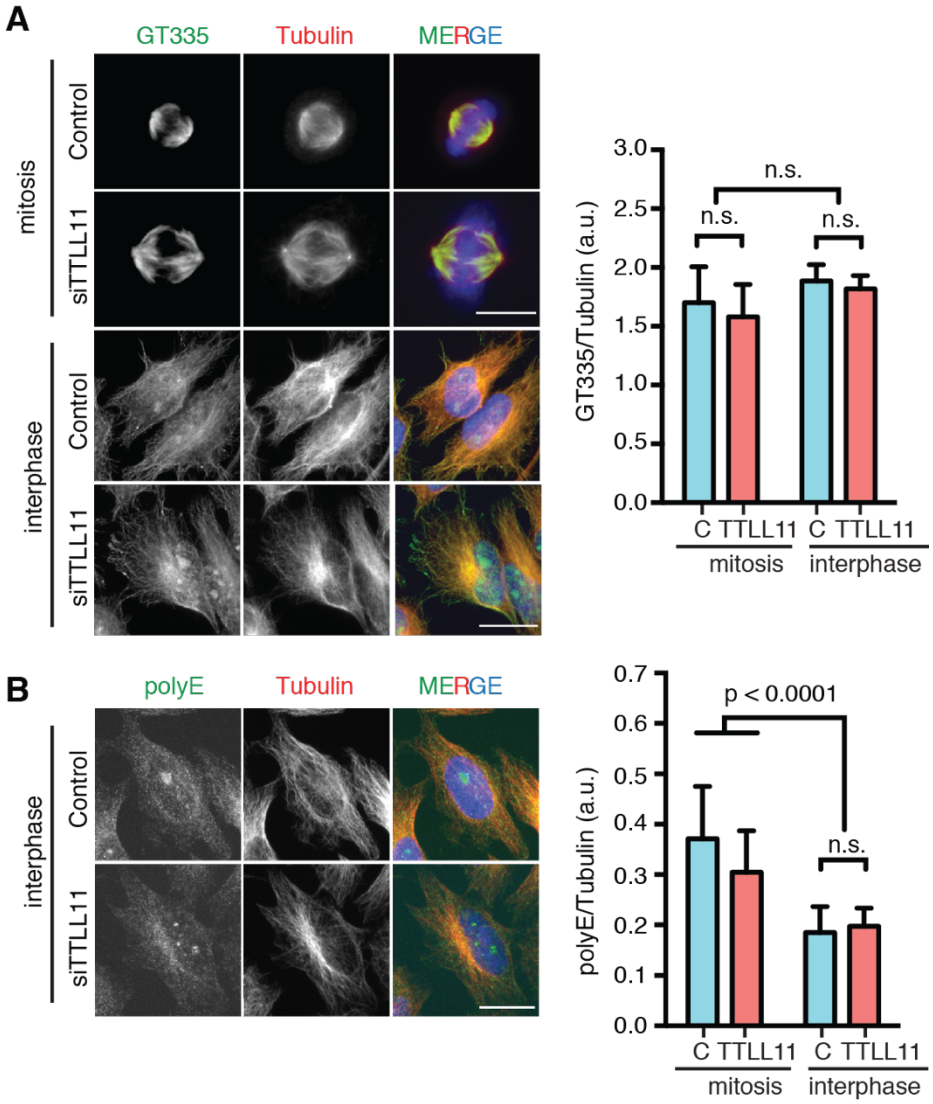

Figure 21 I GTT35 and polyE levels in interphase and mitotic HeLa cells in control and siTTLL11 condition. A) Immunofluorescence images of interphase and mitotic control and siTTLL11 HeLa cells. Tubulin (red), GT335 (green) and DAPI (blue). Scale bars, Interphase, 20 μm; Mitosis, 10 μm. Graph represents means of normalized GT335 signal in the different conditions. Mitosis n (control) = 35 and n (siTTLL11) = 38. Interphase n (control) = 27 and n (siTTLL11) = 33. N = 2. Error bars are SD. p-value are based on two-way ANOVA test with a 95% confidence interval. B) Immunofluorescence images of control and siTTLL11 interphase cells. Tubulin (red) polyE (green) and DAPI (blue). Scale bar, 20 μm. Graph represents means of normalized anti-polyE antibody signal in interphase control and siTTLL11 cells. Mitosis n (control) = 56 and n (siTTLL11) = 54. Interphase n (control) = 14 and n (siTTLL11) = 14. N = 2. Error bars are SD. p-values are based on two-way ANOVA test with a 95% confidence interval.

altogether show a mitotic specificity for the TTLL11 dependent polyglutamylation of MTs.

We then investigated whether some populations of the spindle MTs could be preferentially polyglutamylated. Astral MTs are not polyglutamylated (Regnard et al., 1999). To focus on the spindle MTs we first check whether KMTs are polyglutamylated. We silenced Nuf2, one of the components of the Ncd80 complex at the kinetochore, which is necessary to build K-fibre bundles (DeLuca et al. 2002). I measured the level of polyglutamylation out of the level of total tubulin in the spindle of 4 different conditions in HeLa cells (Figure 9): i) Control cells with the scrambled siRNA transfected; ii) TTLL11 silenced with Darmacon hTTLL11 SmartPool; iii) Nuf2 Darmacon SmartPool and iv) combination of the silencing of TTLL11 and Nuf2. Consistently we found again that spindle MT polyglutamylation levels were higher in control than in the siTTLL11 cells (0,38±

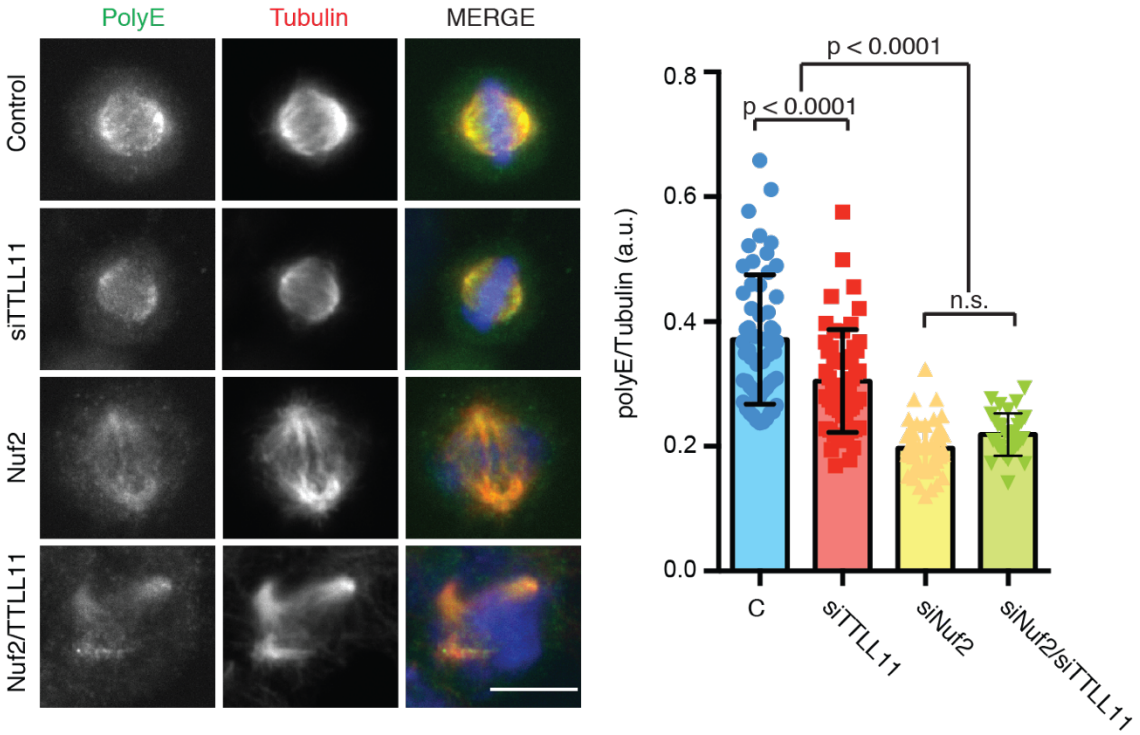

Figure 22 I K-fibre are polyglutamylated in the spindle. Immunofluorescence images in mitotic control, siTTLL11, siNuf2 and co silencing of Nuf2 and siTTLL1 HeLa cells. Tubulin (red), GT335 (green) and DAPI (blue). Scale bar, 10 μm. Graph represents means of normalized polyE signal in the four different conditions. n (control) = 55, n (siTTLL11) = 48, n (siNuf2) = 47, n (siNuf2/siTTLL11) = 33. Representative analysis of N = 2. Error bars are SD. p-values are based on two-way ANOVA test with a 95% confidence interval.

a.u. against 0,29± a.u.; respectively with a ratio comparable to other experiments; p-value < 0.0001). In cells silenced for Nuf2, there was a dramatic drop in MT polyglutamylation levels compared to control cells. The co-silencing of Nuf2 and TTLL11 did not lower the level of polyglutamylation any further (Figure 22). Taken together, these data indicate that the KMTs are the main population of the spindle MTs polyglutamylated by TTLL11.

3.6. TTLL11 is essential for chromosome segregation fidelity

The data so far showed an impaired MT polyglutamylation pattern in the spindle upon TTLL11 silencing. We then use investigated the role of the spindle MT polyglutamylation in mitosis. First, we examined whether spindle assembly and chromosome segregation were impaired. We used time-lapse imaging to monitor TTLL11-silenced HeLa cells undergoing mitosis. I compared control and TTLL11-silenced HeLa cells stably expressing mCherry-H2B/α-tubulin–GFP. Silenced cells assembled bipolar spindles and segregated chromosomes without significant delays compared to control cells (Figure 23A). Consistently, control and TTLL11-silenced cells had a similar mitotic index (Figure 23B). These data indicated that TTLL11 silencing and therefore the reduction of spindle MT polyglutamylation did not induce a SAC-dependent mitotic arrest. We then wondered whether these cells did segregate chromosomes without errors during anaphase. We found that TTLL11-silenced cells showed a significant increase of lagging chromosomes (25.53 ± 5.94 % versus 8.6 ± 2.21 % in control; p= 0.001) (Figure 23D). These data suggested that TTLL11 and spindle MT polyglutamylation are important for the fidelity of chromosome segregation during anaphase.

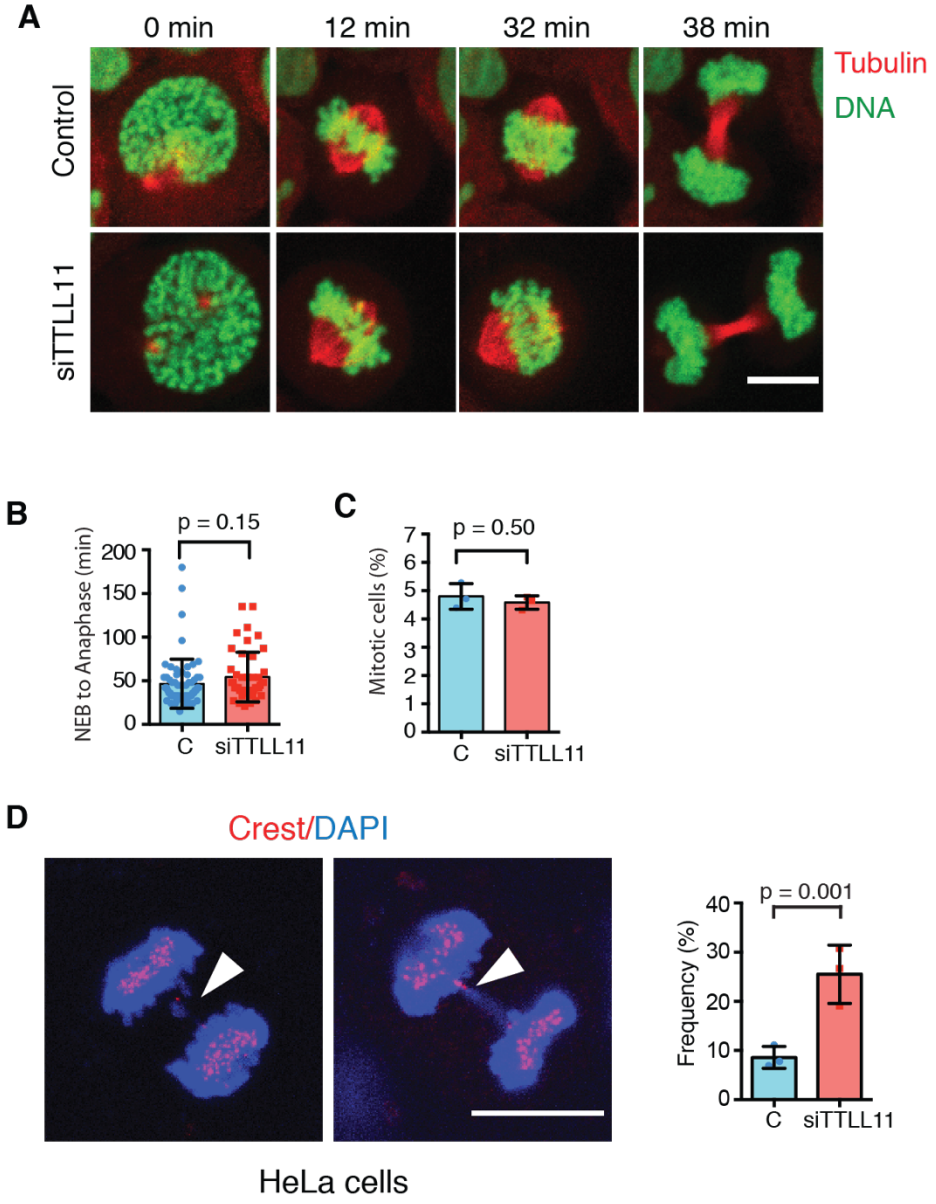

Figure 23 I TTLL11 silencing enhance the presence of anaphase lagging chromosomes without delaying mitosis progression. A) selected frames from time lapse movies of control and siTTLL11 HeLa cells constitutively expressing H2B-mRFP/α-tubulin-GFP. Tubulin, red; DNA, green. Scale bar, 10 μm. B) Representative graph of one of N = 3 experiments showing HeLa cell mitotic timing in control and siTTLL11 condition. n(control) = 66 and n(siTTLL11) = 46. C) Graph showing the mitotic index of control and TTLL11 silenced cells. n = at least 1000 cells for each condition. N= 3. D) Immunofluorescence images of two siTTLL11 anaphase cells having lagging chromosomes (white arrows). The graph shows the mean frequency of anaphase lagging chromosomes in control, at least n(control) = 117 and n(siTTLL11) = 105. p-value is based on $\chi 2$ test with a 95% confidence interval. N = 3. Scale bar is 5 μm. All error bars are SD. p-values are based on unpaired t-test with a 95% confidence interval.

3.7. *ttll11* ensure chromosome segregation fidelity in zebrafish embryos

Based on our results in HeLa cells we decided to explore further the role of TTLL11 and spindle MT polyglutamylation in chromosome segregation fidelity in vivo. We decided to perform experiments in Zebrafish early embryos that develop initially (as all early embryos) through several successive rounds of cell division before gastrulation occurs. Indeed, the first division of the zygote occurs 30 minutes after fertilization, and the embryo reaches the 128-cells stage at 2.3 hours post-fertilization (hpf). At this point, the embryo is known to be in the early blastula stage and starts to transcribe its genomic RNA. From the first division until the 10th cycle of mitosis, all the embryo cells divide synchronously every 15 minutes before slowing down and starting to divide more autonomously (Kane et al., 1993). As all developing embryos, zebrafish relies on a correct and finely tuned cell division to develop.

First, we checked whether mitotic MT polyglutamylation occurs in this organism through development, a data that was not available in the scientific literature. I performed an immunofluorescence protocol to preserve MTs in zebrafish embryos at the blastula stage (4 hpf). I stained the zebrafish embryo for tubulin, polyglutamylation and DNA. We observed a pattern of MT polyglutamylation for the spindle similar to the one observed in HeLa cells. Interphase cells had low MT polyglutamylation signal as well as the astral MTs during mitosis (Figure 14A). The pattern of MT polyglutamylation in zebrafish embryo therefore resembles the one in HeLa cells, suggesting that the zebrafish orthologous *ttll11* might regulate spindle MT polyglutamylation. We then looked at the expression profile of *ttll11* mRNA in zebrafish embryos from the 4-cell stage until 24hpf. In this time interval, we took nine timepoints to extract the mRNA of the cell mass and amplified it with *ttll11* primers. We found that *ttll11* mRNA is present at all the developmental stages investigated (Figure 24B). Based on zebrafish embryo biology, we can conclude that there is a maternal pool of *ttll11* mRNA since the genomic DNA is not transcribed until the 128- cell stage.

Moreover, the mRNA is most probably actively transcribed upon the midblastula transition.

To evaluate whether t*tll11* is involved in the polyglutamylation of the zebrafish embryonic spindle, I cloned t*tll11* in a pCS2 vector for expression in zebrafish as a recombinant protein with EGFP on its N-terminus. Then, we used

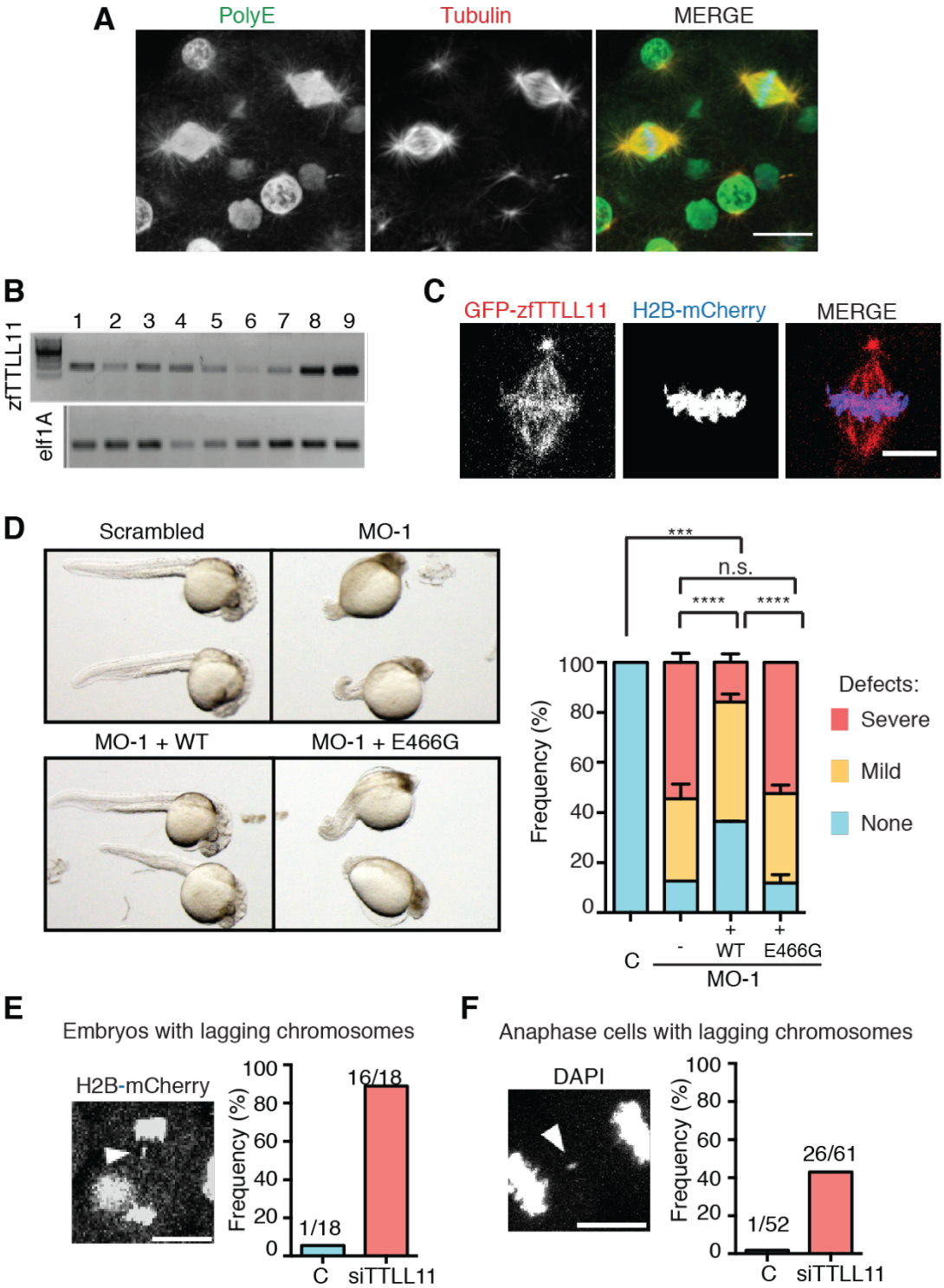

Figure 24 l Spindle MTs polyglutamylation by *ttll11* is required for chromosome segregation fidelity in zebrafish embryos. A) Immunofluorescence images of zebrafish embryos (4 hpf) showing high levels of spindle MT polyglutamylation. PolyE, green; Tubulin, red and DNA, blue. Scale bar, 20 μm. B) Semi-quantitative PCR for *ttll11* at different stages of embryo development: 1- 4cell; 2- 8cell; 3- 64cell; 4- 256cell; 5- Sphere; 6- Shield; 7- 70% epiboly; 8- 90% epiboly; 9) 24hpf. eef1A was amplified as control. C) Fluorescent image of GFP-*ttll11* localization to the zebrafish embryo spindle. GFP, red; H2B-mCherry, blue. Scale bar, 20 μm. D) Zebrafish embryos (36 hpf) injected with scrambled MO, MO-1 targeting *ttll11*, MO-1 co-injected with *ttll11* mRNA or MO-1 co-injected with catalytically inactive *Ttll11*-E466G mRNA. n(control) = 31, n(MO-1) = 20, n(MO-1+WT) = 30 and n(MO-1+E466G) = 20 The graph is a cumulative bar plot of embryo phenotypes at 36hpf representative from four experiments (minimum n = 21). (***) < p <0.001, (****) = p < 0.0001, p-values based on χ2 test with a 95% confidence interval. E) Still image from a time lapse recording of an anaphase cells in a MO-1 injected embryo showing a lagging chromosome (white arrow). The graph represents the frequency of embryos showing at least one anaphase with a chromosome mis-segregation event during the time lapse imaging period for control and MO-1 injected embryos. Graph for N = 3 independent experiments (minimum n = 4). Scale bar, 10 μm. F) Immunofluorescence image of an anaphase cell with a lagging chromosome (arrow) in a zebrafish embryo (sphere stage). The graph represents the frequency of anaphase mis-segregation events on total anaphases in control and MO-1 injected embryos. Graph for N = 3 independent experiments (minimum n = 6). Scale bar, 10 μm.

the mMESSAGE mMACHINE SP6 to produce the suitable EGFP-*ttll11* mRNA to inject into the zebrafish zygotes expressing H2B-mTomato. I analysed the images under an SP8 microscope, and found that EGFP-Ttll11 localizes to the spindle of the zebrafish blastula cells, further confirming the observation done in HeLa cells (Figure 24C).

We then address the role of Ttll11 in zebrafish early embryo development and, in particular, determine whether its glutamylase activity is required. We decided to KD *ttll11* using morpholinos (from now on MO-1) that targets the 5'-UTR of the *ttll11* mRNA. To test the specificity of the MO-1 mediated KD, we co-inject the MO-1 with WT *ttll11* mRNA. We designed the experiment with four conditions.: control condition injected with a scrambled morpholino, injection of MO-1, co-injection of MO-1 and WT *ttll11* mRNA and co-injection of MO-1 and *ttll11*·E466G. *ttll11*·E466G is an enzymatic dead version of *ttll11* that we generated by exchanging the glutamate residue 466 with a glycine (from now on: *ttll11*·E466G) (van Dijk et al., 2007) to test whether the Ttll11glutamylation activity is important for the development of zebrafish embryos. Scrambled-morpholino injected embryos developed normally while MO-1 injected embryos developed abnormally, showing either a tilted tail or an overall impairment in 60% of the

cases. Co-injection of MO-1 and WT *ttll11* rescued almost entirely the embryo early development. The co-injection of MO-1 and enzymatic dead *ttll11*·E466G did not rescue the phenotype, supporting the hypothesis that *Ttll11* glutamylase activity is essential for zebrafish development (Fig 24D).

Our data indicated that *Ttll11* plays a pivotal role in this developing organism. We then decided to investigate further whether the downregulation of *ttll11* impaired chromosome segregation fidelity like in HeLa cells. I monitored anaphase in 2 different ways, by live embryo imaging and in fixed embryos. First, in the live imaging, I counted the embryos that showed at least one lagging chromosome event over a time period of 2 hours. Upon MO-1 injection, the frequency of embryos showing such phenotype was 16 out of 18 embryos (Figure 24E). In contrast, scrambled morpholino injected embryos had only one embryo out of 18 showing anaphase lagging chromosomes (Figure 24E). Comparable results were obtained counting the lagging chromosome frequency in fixed embryos (Figure 24F). Measuring the aberrant anaphase present in control and

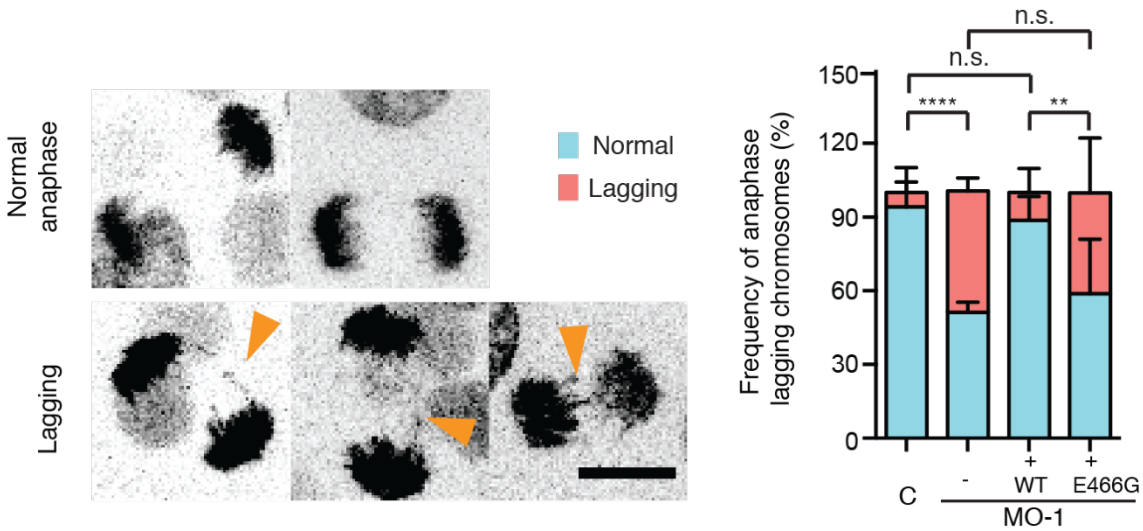

Figure 25 I co-injection of MO-1 and WT *ttll11* rescue the lagging chromosome phenotype in zebrafish embryos. Immunofluorescence images of zebrafish embryos (4 hpf) showing representative correct anaphases and anaphases with lagging chromosomes. The bar graph represents the mean frequency of N = 3 experiment of anaphases showing lagging chromosomes. The total number of embryos represented in the graph are n (Control) = 12, n (MO-1) = 11, n (MO-1 + WT) = 14 and n (MO-1 + E446G) = 8. The total number of anaphases counted are n (Control) = 41, n (MO-1) = 46, n (MO-1 + WT) = 39 and n (MO-1 + E446G) = 31. Error bar represent the SD. Scale bar is 10 μm. (**) = $p < 0.01$, (****) = $p < 0.0001$, p-values based on $\chi 2$ test with a 95% confidence interval.

ttll11-injected fixed embryos, we observed a clear increase of anaphase lagging chromosomes in morpholino injected embryos. Altogether, these data point to an essential role of Ttll11 in chromosome segregation fidelity during early embryonic development. In addition to the zebrafish phenotype rescue experiment at 36 hpf showed in Figure 24D, we also tried to rescue the lagging chromosome phenotype on zebrafish embryos. Also in this case, the embryos successfully revert the lagging chromosomes phenotype upon co-injection of MO-1 and the WT *ttll11*. Moreover, the co-injection of the *ttll11·E466G* an MO-1, was not rescuing the phenotype (Figure 25), confirming that the *ttll11* MT polyglutamylation activity is fundamental for error-free anaphases.

To determine the fate of the lagging chromosomes generated in *ttll11* KD, we imaged zebrafish embryos expressing H2A-mCherry at the sphere stage.

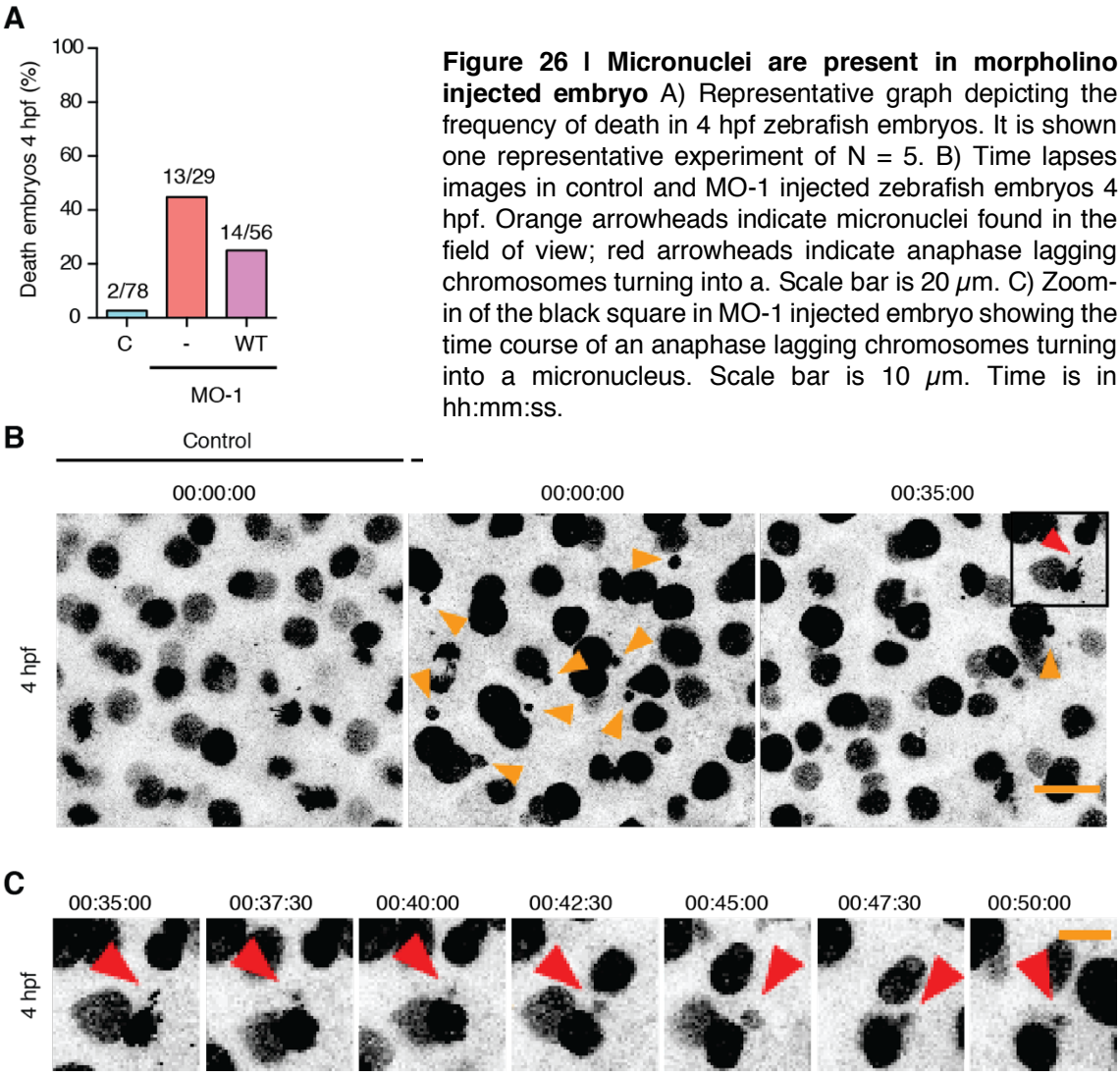

Figure 26 I Micronuclei are present in morpholino injected embryo A) Representative graph depicting the frequency of death in 4 hpf zebrafish embryos. It is shown one representative experiment of N = 5. B) Time lapses images in control and MO-1 injected zebrafish embryos 4 hpf. Orange arrowheads indicate micronuclei found in the field of view; red arrowheads indicate anaphase lagging chromosomes turning into a. Scale bar is 20 μm. C) Zoom-in of the black square in MO-1 injected embryo showing the time course of an anaphase lagging chromosomes turning into a micronucleus. Scale bar is 10 μm. Time is in hh:mm:ss.

First, we detected an increase in mortality during development (Figure 26A). Indeed, almost half of the embryos injected with MO-1 died by 4h hpf. This phenotype was partially rescued by the co-injection of *ttll11* mRNA. We then decided to follow the development of the embryos by time-lapse imaging microscopy over two hours to address the nature of their increased mortality. The imaging had enough time resolution to follow single chromosomes over anaphase, telophase, and interphase. As seen in Figure 24E, *ttll11* KD often generated laggards in anaphase blastula cells. We followed the laggards over anaphase up to interphase and observed that frequently the anaphase laggards formed micronuclei (Figure 26B, C). Moreover, the micronuclei were accumulating over time. Altogether these results corroborate the ones obtained in HeLa cells. Here, we show that zebrafish spindle MT are highly polyglutamylated and TTLL11 zebrafish ortholog localizes to the mitotic spindle during development. Moreover, *ttll11* is expressed already in the zygote. *ttll11* KD experiments revealed that the protein polyglutamylation activity is necessary for proper embryo development. Further analysis show that chromosome segregation fidelity is compromised in the absnece of TTLL11, increasing the formation of anaphase laggards, often ending in micronuclei formation resulting in an increase of embryonic lethality.

3.8. TTLL11 expression is downregulated in tumours and correlates negatively with aneuploidy scores

Aneuploidy is one of the most salient hallmarks of cancer. Approximately 86% of solid tumours are aneuploid (Zasadil et al., 2013). Aneuploidy is the irreversible consequence of chromosome missegregation, generating CIN. In cells showing CIN, we can observe a persistent defect in chromosome segregation fidelity. Since TTLL11 downregulation promotes lagging chromosomes and micronuclei, we wondered whether its activity could be compromised in cancer cells. To address the issue, we collaborated with Serrano's laboratory, in particular with Miquel Anglada-Girotto, a PhD student in the lab.

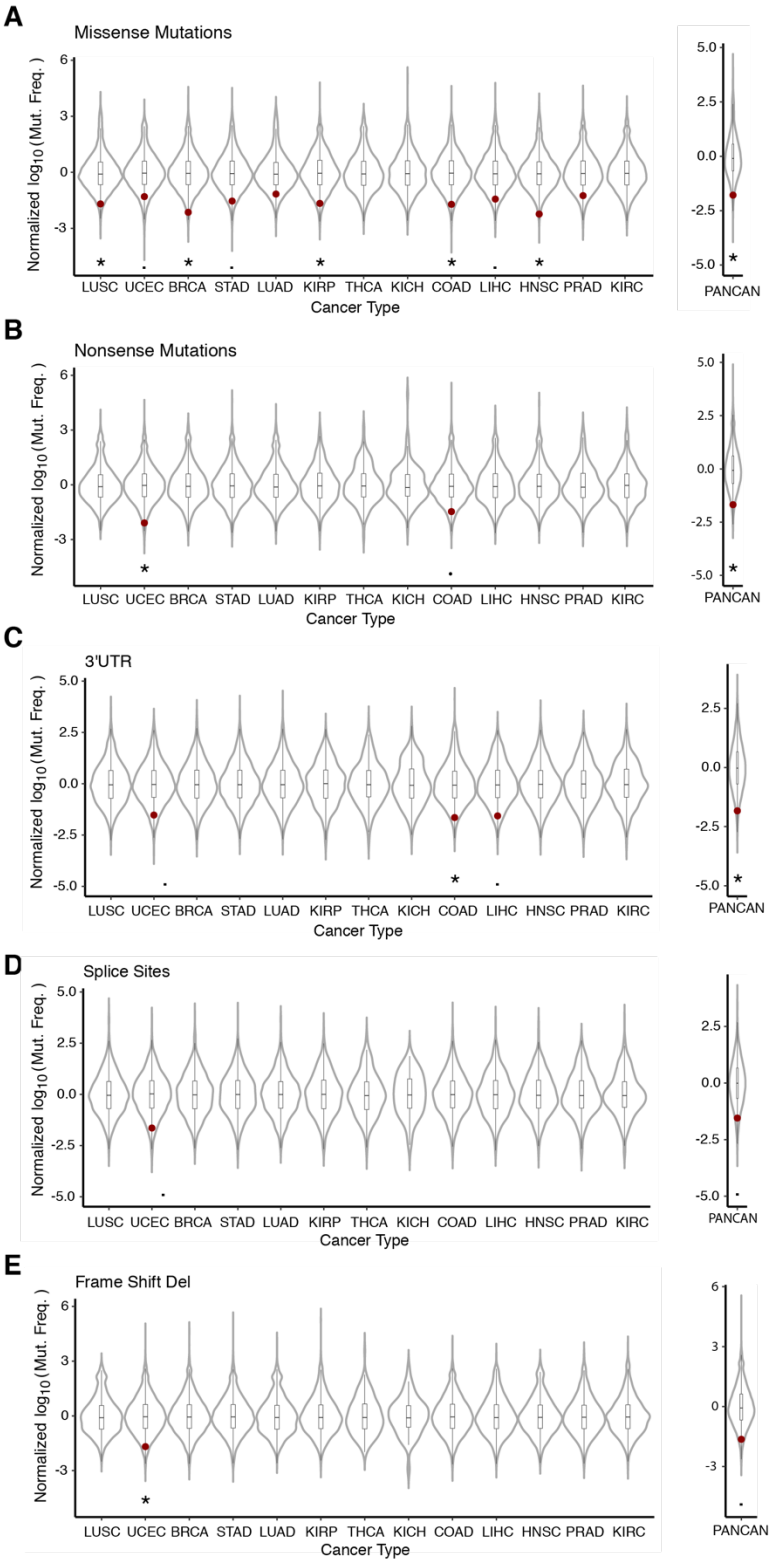

Figure 27 | TTLL11 is rarely mutagenized in tumors. Mutation. Frequencies per kilobase for every detected gene across 13 different cancer types. PANCAN represents the median mutation frequency per kilobase for every gene across cancers. TTLL11 is highlighted in red. Mutation frequencies are reported by their predicted type of effect: A) missense mutation, B) nonsense mutation, C) 3'UTR, D) splice site, E frameshift deletion. p-values:(*) 0.05 (.) 0.01, based on one-sided one-sample Z tests.

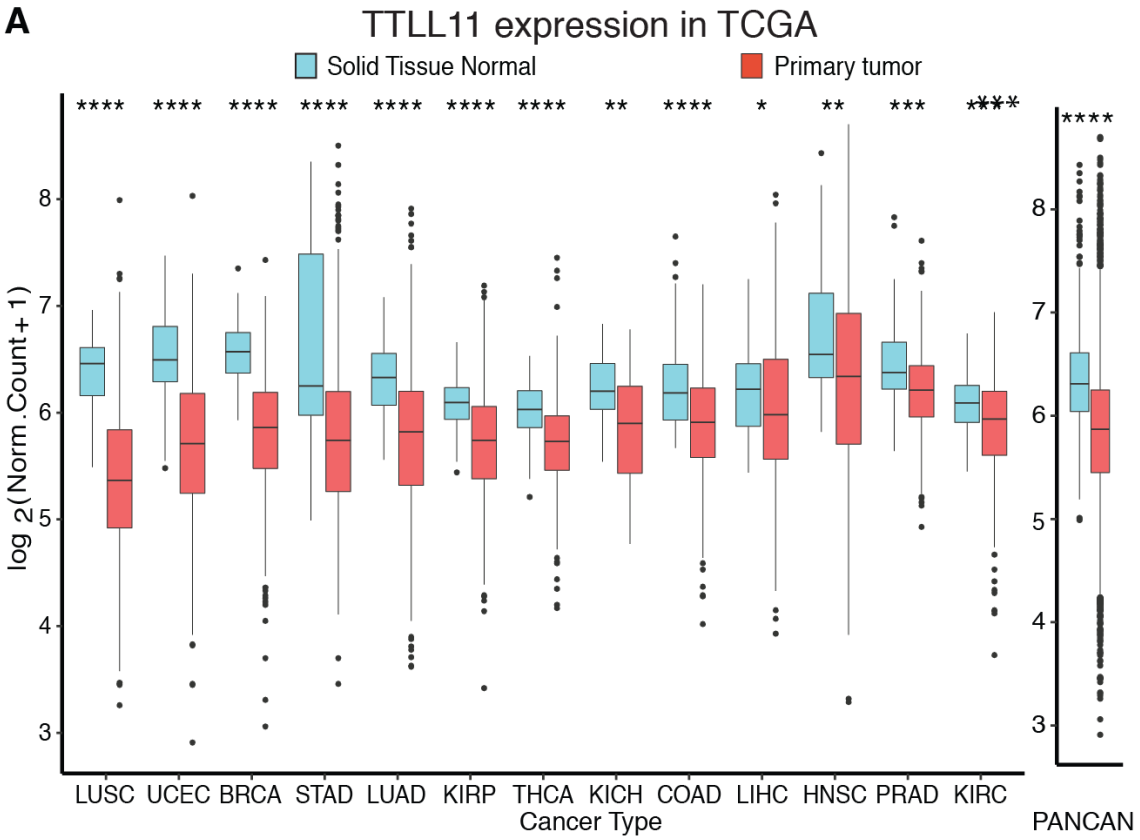
A
TTLL11 expression in TCGA
Solid Tissue Normal
Primary tumor
log 2(Norm.Count+1)
LUSC UCEC BRCA STAD LUAD KIRP THCA KICH COAD LIHC HNSC PRAD KIRC
Cancer Type
PANCAN

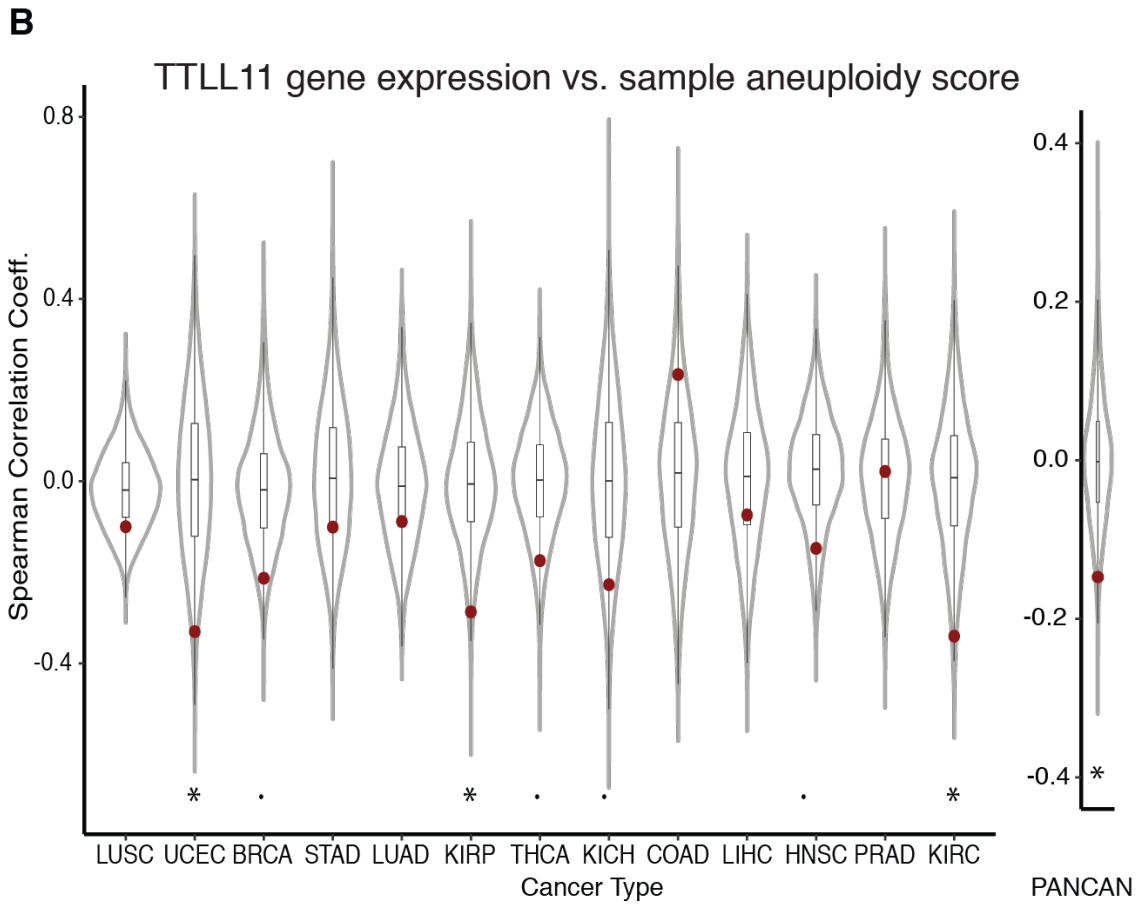
B
TTLL11 gene expression vs. sample aneuploidy score
Spearman Correlation Coeff.
LUSC UCEC BRCA STAD LUAD KIRP THCA KICH COAD LIHC HNSC PRAD KIRC
Cancer Type
PANCAN

Figure 28 | TTLL11 expression level is downregulated in tumors and correlates negatively with aneuploidy scores. (A) Normalized expression of *TTLL11* in solid tissue normal and primary tumor samples across 13 different cancer types, separately and combined (PANCAN). p-values: (****) ≤ 0.0001 (***) ≤ 0.001 (**) ≤ 0.01 (*) ≤ 0.05, based on unmatched Wilcoxon Rank Sum tests. (B) Spearman correlation coefficients of normalized gene expression and sample aneuploidy scores for every gene across 13 different cancer types. PANCAN represents the median correlation coefficient for every gene across cancers. *TTLL11* is highlighted in red. p-values: (*) ≤ 0.05 (.) ≤ 0.01, based on one-sided one-sample Z tests.

Our collaborator analyzed the TTLL11 expression data in thirteen human tumors and healthy control tissue counterparts (For the extended tumor name, see Annex). We collected the data by querying “The Cancer Genome Atlas” (TCGA) database, which has a downloadable publicly available dataset on gene expression and function parameters like normalized copy number variation (CNV) and classification of the somatic mutations, among 13 selected human tumors and their counterparts. At first, we decided to analyze whether TTLL11 in this cancer cohort could be positively or negatively correlated with missense, nonsense, frameshift, 3’ UTR or intronic spaces mutation frequencies. Miquel Anglada-Girotto performed the bioinformatic analysis. We found that the rate of missense mutations in the TTLL11 gene in cancer cells is significantly lower than expected (Figure 27), suggesting that this enzyme’s loss of function could jeopardize cell survival. This may indicate that there could be other mechanisms to lower TTLL11 activity and ne could involve changes in gene expression. Therefore, we wanted to understand whether there was a change in expression levels. Strikingly, we found that TTLL11 expression is significantly downregulated in all the tumors reported, and the significant decrease could also be detected in the pan-cancer data (Figure 28A). When analyzing a potential correlation between TTLL11 expression levels and aneuploidy in cancer, we found a clear negative correlation between TTLL11 expression levels and the aneuploidy scores of the different tumors (Figure 28B) (A.M. Taylor et al., 2018).

Interestingly, TTLL11 is the only glutamylase systematically downregulated in the selected tumors. The other TTLLs show neither upregulation nor downregulation (Figure 29). Altogether these data show a coherent vision of the downregulation of TTLL11 and thereby spindle MT

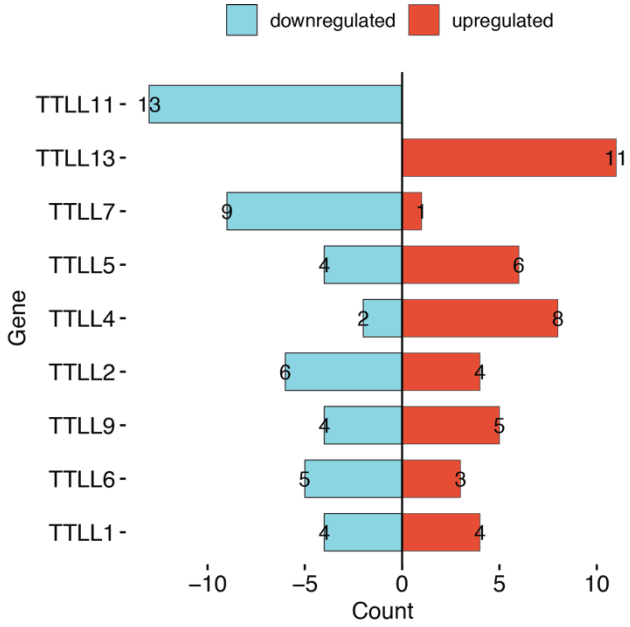

Figure 29 I Differential expression analysis of TTLLs. We performed a Wilcoxon Rank Sum test for every type of cancer to assess statistically the differences in log-normalized read counts of *TTLL1, TTLL2, TTLL4, TTLL5, TTLL6, TTLL7, TTLL9, TTLL11* and *TTLL13* between primary tumors and unmatched solid tissue normal samples. This consistent downregulation in tumours is not found for any of the other TTLL glutamylase enzymes; p-value = 6.272*10^-7 (Binomial Test).

polyglutamylation in aneuploidy and cancer. This bioinformatic profiling of TTLL11 expression in human cancer samples fit well with what we previously described in HeLa cells and zebrafish embryos, underlying an essential role of TTLL11 and its subsequent spindle MT polyglutamylation in chromosome segregation fidelity.

3.9. Polyglutamylation defines spindle MT dynamic properties

We showed that TTLL11 is fundamental to ensure chromosome segregation fidelity in HeLa cells and zebrafish embryos. Bioinformatics analysis of cancer tissue expression data provides further support for this essential function. We therefore wanted to address the mechanism at play. Different mechanisms may promote chromosome segregation errors, including a weakened spindle assembly checkpoint, defects in error correction of kinetochore-MT attachments, multipolar spindle formation and MT partial stabilization (Levine et al., 2018; Musacchio et al., 2007b; Zasadil et al., 2013). We first checked whether the SAC and the kinetochore-MT attachment error correction mechanism were functional in TTLL11-silenced cells.

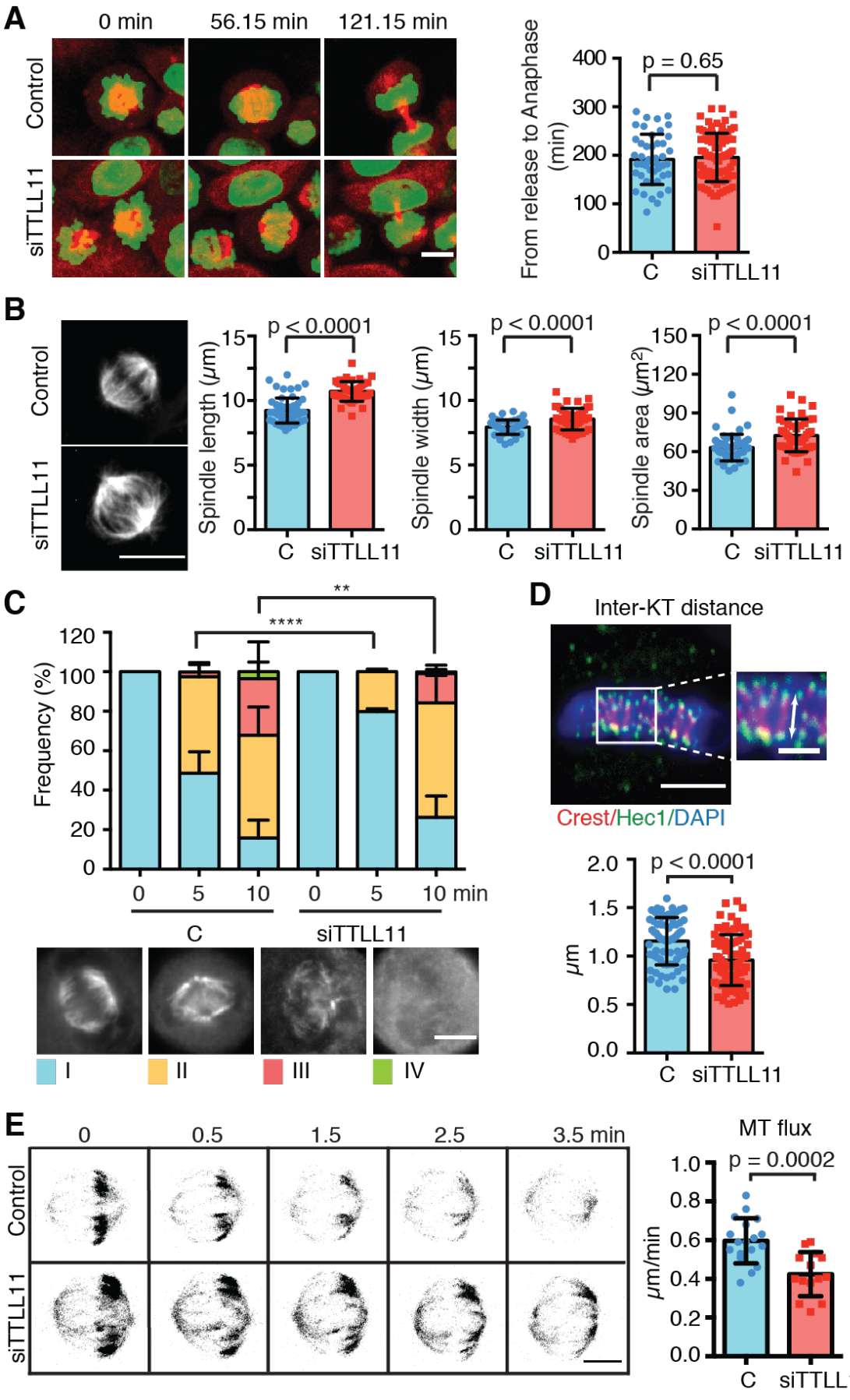
A
0 min
56.15 min
121.15 min
Control
siTTLL11
From release to Anaphase (min)
p = 0.65
C
siTTLL11
B
Control
siTTLL11
Spindle length (μm)
p < 0.0001
Spindle width (μm)
p < 0.0001
Spindle area (μm²)
p < 0.0001
C
siTTLL11
C
Frequency (%)
**
****
0
5
10
0
5
10 min
C
siTTLL11
I
II
III
IV
D
Inter-KT distance
Crest/Hec1/DAPI
μm
p < 0.0001
C
siTTLL11
E
0
0.5
1.5
2.5
3.5 min
Control
siTTLL11
MT flux
μm/min
p = 0.0002
C
siTTLL11

Figure 30 I Spindle MTs are more stable upon spindle silencing. A) Time lapse images of control and siTTLL11 HeLa H2B-mRFP/α-tubulin-GFP cells released from a STLC treatment. Time is in min. Tubulin, red and DNA, green. Scale bar, 10 μm. Cumulative frequency of cells entering anaphase over time. n (control) = 46 and n (siTTLL11) = 87. N = 3. B) Representative image of a HeLa cell under control and siTTLL11 conditions showing the differences in size. Graphs showing the spindle length, width and area quantified for at least 47 cells for each measurement. Graphs are representative of N=3 independent experiments. Scale bars, 10 μm. Error bars represent SD. C) Quantification of cold induced K-fibre stability over time in control and siTTLL11 cells classified according to the four categories shown. n (control) = at least 43 cells and n (siTTLL11) = at least 57 cells per experiment N = 3. Scale bar, 10 μm. (**) < p <0.01, (****) = p < 0.0001, p-values based on χ2 test with a 95% confidence interval. Error bars represent SD. D) Immunofluorescence image of a metaphase cell showing the aligned chromosomes (blue) and markers for the kinetochores, CREST (red) and Hec1 (green). The inlaid shows the interkinetochore distance measured with a white arrow. The graph corresponds to n (control) = 72 kinetochore pairs from 16 cells; n (siTTLL11) = 82 kinetochore pairs from 18 cells. Representative graph of N = 4 independent experiments. Error bars are SD. Scale bar, 5 μm. Scale bar zoom in 1 μm. C) Confocal images showing the poleward movement of photoactivated tubulin (dark grey) at the spindle equator (T0) over time (in min.) in control and siTTLL11 cells. The graph shows the velocity of the poleward flux in control (n = 18) and siTTLL11 (n = 14) cells from three independent experiments. Scale bar, 5 μm. A, B, D, E) p-values are based on t-test with a 95% confidence interval.

Hela cells were incubated with an Eg5 inhibitor (STLC) to generate monopolar spindles that accumulate erroneous KMT attachments, promoting a SAC-dependent mitotic arrest (Dudka et al., 2018a). TTLL11-silenced cells efficiently arrested in mitosis indicating that they have a fully functional SAC. We then quantified the time required for the cells to correct the erroneous attachments and enter anaphase after STLC washout as a readout of the activity of the error correction mechanism (Dudka et al., 2018a; M. A. Lampson et al., 2004). TTLL11-silenced cells entered anaphase with similar kinetics to the control cells (Figure 30A), suggesting that erroneous kinetochore-MT attachments are corrected as efficiently in the absence of TTLL11 as in control cells. We did not observe multipolar spindles in TTLL11 silenced cells or in morphants zebrafish embryos, nor any delay in mitotic progression, ruling out that the observed chromosome segregation defects could occur as a consequence of problems in bipolar spindle assembly.

However, we found that spindles assembled in siTTLL11 cells were overall larger. Immunofluorescence experiments in HeLa cells fixed with cold methanol showed that mitotic spindles are 16% longer upon TTLL11 silencing. The pole-to-pole measure showed that spindles in control cells are 9.24±0.98 μm long on

average whereas, they are 10,72±0.77 μm long (Figure 30B; p-value<0,0001;) in siTTLL11 cells. Other morphological parameters such as the area and width were analyzed. The spindle area in TTLL11-silenced cells was 13% bigger than in control cells, precisely it was 63,16±10,37 μm^2 and 72,56±12,63 μm^2 (Figure 30B; p-value< 0,0001) for control and silenced mitotic spindle, respectively. Spindle width at the equatorial region was also larger in siTTLL11 cells by 8%: 7,93±0.55 μm in control cells and 8,55±0.85 μm in TTLL11 silenced cells (Figure 30B; p-value <0,0001). These data suggest that MTs could be partially stabilized when their polyglutamylation is reduced. Consistent with this idea, in TTLL11-silenced cells the k-fibres were more resistant to cold-induced MT depolymerization (Figure 30C). HeLa cells were placed at 4ºC and fixed at different time points (5 min, 10 min, 20 min and 30 min), to monitor MT depolymerization. The quantification of the MT remaining in the mitotic cells at the different time points showed that k-fibres had an increased stability in TTLL11-silenced cells (Figure 30C). We also checked the interkinetochore distance to test whether the lack of TTLL11 and the subsequent spindle MT polyglutamylation drop would affect the pulling forces exerted from the k-fibres on the bio-oriented chromosomes. CREST antibody and an anti-Hec1 antibody were used to stain the kinetochore by IF. CREST detects kinetochore centromere proteins, whereas Hec1, also known as Ndc80, is part of the Ndc80 complex and is responsible for interactions with the KMTs. We found that the TTLL11 silenced cells had a shorter interkinetochore distance. In control cells have the average distance was1.25±0.04 μm while it was 1.02±0.04 um in the siTTLL11 cells (Figure 30D; p-value<0,0001). This indicated that there was lower tension acting upon sister kinetochores in the silenced cells. Altogether these data consistently pointed to a partial stabilization of the spindle MTs in TTLL11-silenced cells. To obtain further support for this idea, I used HeLa cells stably expressing H2B–RFP/PA-α-tubulin–GFP. This cell line expresses photoactivable tubulin, which allows us to follow the spindle flux within the mitotic spindle by live imaging of the poleward directed movement of a tubulin stripe photoactivated close to the metaphase plate. We found that the velocity of the spindle flux was significantly

reduced in the TTLL11-silenced cells (Figure 30E; 0.42±0.11 μm/min versus 0.59±0.12 μm/min in control; p=0.0002), again pointing at a reduced dynamics of the spindle MTs.

Altogether our data consistently show that reducing TTLL11-dependent MT polyglutamylation results in the partial stabilization of the spindle MTs. Previous work showed that an increased MT stability and assembly rate compromise chromosome segregation fidelity (Bakhoum, Genovese, et al., 2009; Bakhoum, Thompson, et al., 2009; Dudka et al., 2018a; Ertych et al., 2014) because of unresolved merotelic attachments during anaphase (Cimini et al., 2001a; S. L. Thompson et al., 2008). We conclude that TTLL11 dependent polyglutamylation fine-tunes the dynamics of the spindle MTs to ensure chromosome segregation fidelity by preventing cells from entering anaphase with unresolved erroneous kinetochore attachments.

Discussion

4. Discussion

4.1. The TTLL enzyme family, a divergent evolution from TTL

Mitotic spindle MTs are polyglutamylated in HeLa cells (Regnard et al., 1999), RPE1, human oocyte and zebrafish embryos (this work). Despite the relatively widespread polyglutamylation of MTs across systems, no information on the enzyme(s) and the function of this PTM in the mitotic spindle was available at the beginning of this work. TTLL enzymes catalyze the polyglutamylation and polyglycilation of various substrates. They belong to a large family of conserved eukaryotic proteins with a TTL homology domain. Moreover, some of them have an additional conserved extended domain that seems indispensable for glutamylation activity (van Dijk et al., 2007). Unlike the TTL enzyme that catalyzes the tyrosination of soluble tubulin, MTs are the substrate for TTLLs. Indeed, all the TTLLs autonomous glutamylase enzymes (4, 5, 6, 7, 11, 13) have a cationic-MTBD, recognizing MTs through multivalent interactions (Garnham et al., 2016). Among the TTLLs, the aminoacid sequences outside the catalytic domains and the position of the homology domains are poorly conserved (van Dijk et al., 2007), likely providing the specificity for different substrate and type of catalytic activity within the family (van Dijk et al., 2008). In addition, these divergent regions may contain regulatory domains that could account for the specific functions of the different TTLLs in time and in space, articulating the tubulin code.

Since we identified TTLL11 as the polyglutamylase driving spindle MT polyglutamylation in human cells and zebrafish embryos, we explored the relationship among paralogs and orthologs in the TTLL family to gain better insights into the glutamylase enzymes. Even if the role of MT polyglutamylation has started to raise interest and has been investigated extensively, at least in flagella, cilia and axons, the actual role of every single glutamylase enzyme is far from being elucidated and understood.

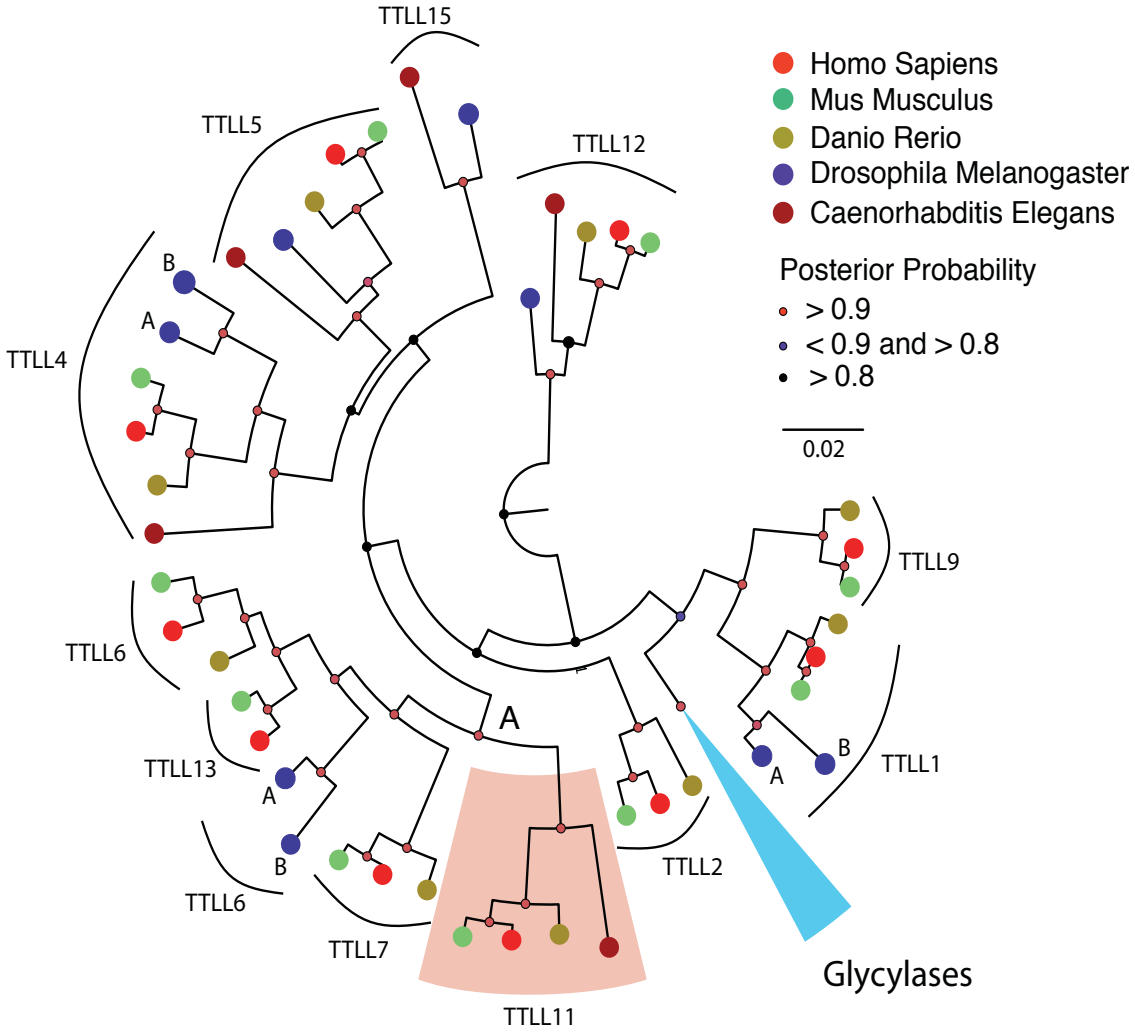

Figure 31 I Phylogenetic tree of TTLLs enzymes. The tree includes all the TTLL enzymes from *Homo sapiens*, *Mus musculus, Danio rerio, Drosophila Melanogaster* and *Caenorhabditis elegans*. It was developed with posterior probability algorithm. The TTLL11 branch is highlighted with a red shadow. The position of the glycylases is indicated with a light blue cone.

According to our phylogenetic study and previous studies (Figure 31) (Janke et al., 2005; van Dijk et al., 2007), in eukaryotes, TTLLs can be categorized into multiple conserved subtypes. I assembled a phylogenetic tree selecting enzymes from *Homo sapiens*, *Mus musculus, Danio rerio, Drosophila Melanogaster* and *Caenorhabditis elegans* (Figure 31). It shows that TTLL6, 7, 11 and 13 belong to the same clade starting from node A (Figure 31). This clade includes all the enzymes known to have an autonomous glutamylase function and trigger a side-chain elongation reaction. However, it is not possible to rule out that they could also have an initiation activity as suggested by functional and

crystallography studies (Garnham et al., 2016; van Dijk et al., 2007). Our analysis shows that not all the TTLLs are present in all the five organisms selected in this study. This may be due to incomplete information in the databases. However, in some cases, we can speculate that the function of a missing paralog could be compensated by the expression of another TTLL that could function in multiple processes. This could be the case for the TTLL11 paralog in *Caenorhabditis elegans*. Indeed, *ttll11* is the only glutamylase catalyzing side-chain elongation present in this organism, and there it has been described to be required for cilia function (O'Hagan et al., 2017). Since no other enzyme can elongate glutamate side-chains in this organism, it is possible that *ttll11* participates in multiple processes. There are no reports in the literature for the putative role of TTLL11 in cilia in other organisms. Preliminary data that I obtained upon silencing TTLL11 in RPE1 suggest that in these cells, TTLL11 is not required for cilia assembly (data not shown).

4.2. TTLL11-mediated spindle MT polyglutamylation

In agreement with previous data, we showed here that MTs are polyglutamylated in the spindles of HeLa cells and zebrafish embryos. Through a localization screen, I found that TTLL11 localizes the spindle MT in both systems. TTLL11 was previously shown to be a glutamylase that preferentially catalyzes glutamate side-chain elongation on the alpha-tubulin C-terminal tail domain (van Dijk et al., 2007). Consistently our results show the spindle MT polyglutamylation level is significantly reduced when TTLL11 is silenced. Additional experiments confirmed the specific activity of TTLL11 on mitotic MTs. Indeed, we did not find any difference in interphase MT polyglutamylation levels in control and siTTLL11 cells (Figure 21). Therefore, we conclude that TTLL11-dependent MT polyglutamylation is mitosis specific. Interestingly, upon silencing Nuf2 and, therefore, in the absence of k-fibres (J.G. DeLuca et al., 2002), the level of MT polyglutamylation in the spindle dropped dramatically. Moreover, the

co-silencing of Nuf2 and TTLL11 did not reduce the level of spindle MT polyglutamylation any further. These data indicate that TTLL11 may act with some preference for the KMTs. However, it is also possible that the high levels of polyglutamylation of the KMTs are a consequence of their lower dynamics, increasing the chances of getting post-translationally modified. Alternatively, cells could use the TTLL11 natural kinetics and affinity toward particular structures such as the k-fibre to tune their stability. In contrast, short-living interpolar-MTs, even if polyglutamylated, probably would not show significantly altered dynamics. Although we found here that MT polyglutamylation increases moderately MT dynamics in mitosis, it is not a general rule. Indeed, this PTM is particularly enriched in the brain where MTs are relatively stable. Moreover, MT polyglutamylation was shown to act as a rheostat for spastin (Valenstein & Roll-Mecak, 2016), tuning MT severing activity as a function of the glutamate side-chain length. The MT polyglutamylation rheostat-like function could then generate a mitotic environment rich of new docking sites that may allow the spatial-temporal regulation of mitotic MT dynamics properties.

4.3. The control of spindle length

Mitotic spindle assembly and kinetochore-MT attachment require the fine regulation of several motors, MAPs and severing enzymes. Altogether they orchestrate the self-assembly and the homeostasis of the mitotic spindle. Many factors and processes can be involved in maintaining a given steady-state size or, better, steady-state spindle length since it has been reported that spindle size proportionally changes upon length (Barisic et al., 2021; Hara et al., 2013). We initially noticed that the size of the HeLa cell spindles increased upon TTLL11 silencing. Indeed, spindles were significantly longer by 13% (Figure 30B). In the last two decades, different experimental approaches have led to the identification of hundreds of proteins required for spindle assembly and chromosome segregation. Some of them were proposed to participate in defining spindle length. These proteins have different activities such as MT nucleation in mitosis, γ-tubulin /γ-TuRC and TPX2; MT depolymerization, KIF18A and MCAK; MT

severing, katanin; spindle pole focusing, dynein and HSET; motors involved in spindle bipolarity, Eg5 and Hklp2. We checked whether the localization of some of these proteins could be altered in spindles assembled in TTLL11-silenced cells to test if any of them could respond to changes in MT polyglutamylation levels. We investigated the localization of TPX2 in the mitotic spindle in control and TTLL11-silenced cells. TPX2 is important for the recruitment of the γ-TuRC in the RanGTP and Augmin pathways. We found a significant increase in TPX2 localization along the spindle (Figure 32A). The data is interesting since it would indirectly indicate an increase in MT nucleation activity. Therefore, we tested

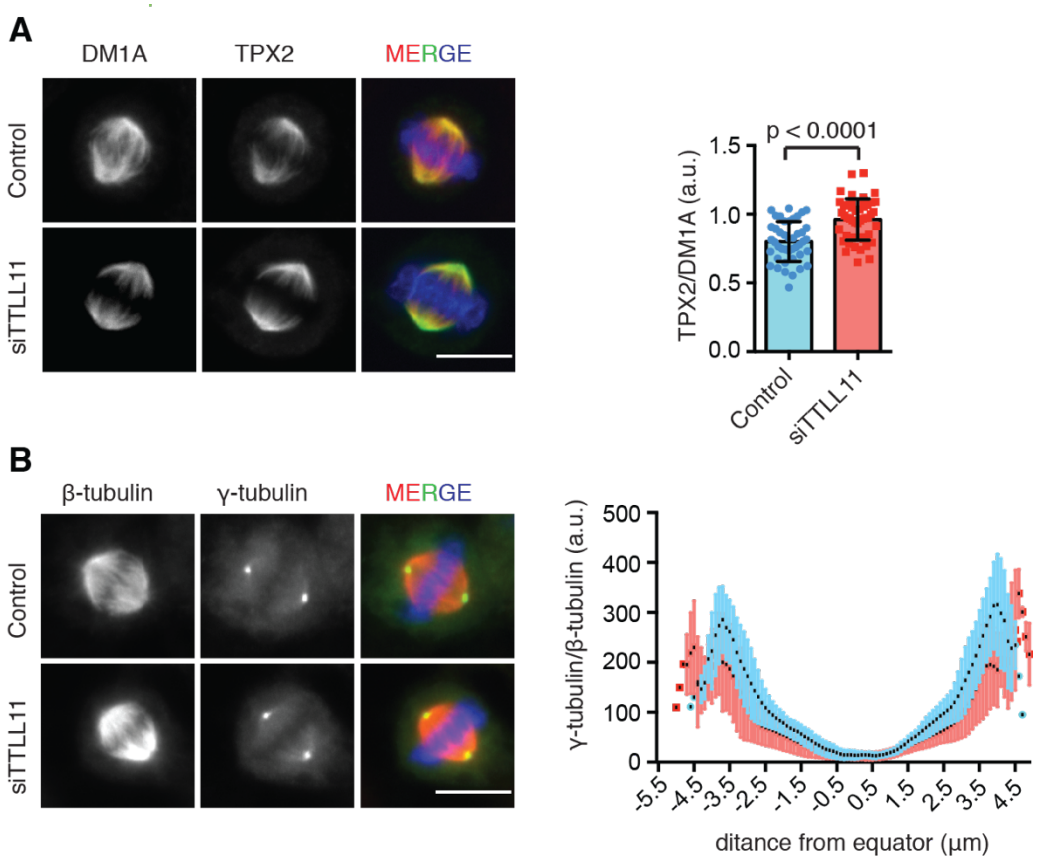

Figure 32 I Localization of TPX2 and γ-tubulin to the mitotic spindle. A) Immunofluorescence images of metaphase spindles in control and siTTLL11 cells stained for TPX2. The graph shows the quantification of the TPX2 signal normalized on the total tubulin signal. n (control) = 43 cells and n (siTTLL11) = 48 cells B) Immunofluorescence images of metaphase spindles in control and siTTLL11 cells stained for γ-tubulin. The graph represents the pole-to-pole normalized intensity profile of the γ-tubulin signal n(control) = 21 and n(siTTLL11) = 22. One representative experiment of N = 2. Scale bars, 10 μm. Error bars represent SD. Tubulin (red), protein of interest (green) and DAPI (blue). p-values are based on t-test with a 95% confidence interval.

whether γ-tubulin/γ-TuRC localization could confirm an increase in MT nucleation in the TTLL11-silenced cells. We used a different quantification approach because of the uneven distribution of γ-tubulin along the spindle and profiled the level of γ-tubulin from pole-to-pole. This revealed a mild decrease in the levels of γ-tubulin/γ-TuRC along the spindle (Figure 32B); however, the difference was not significant. These data are preliminary, and further experiments are required to address whether MT nucleation could be altered depending on the levels of MT polyglutamylation. We then analyzed the localization of the severing enzyme katanin, involved in the spindle poleward flux and the regulation of MT minus-ends dynamics. In this case, we did not appreciate any difference in the level of

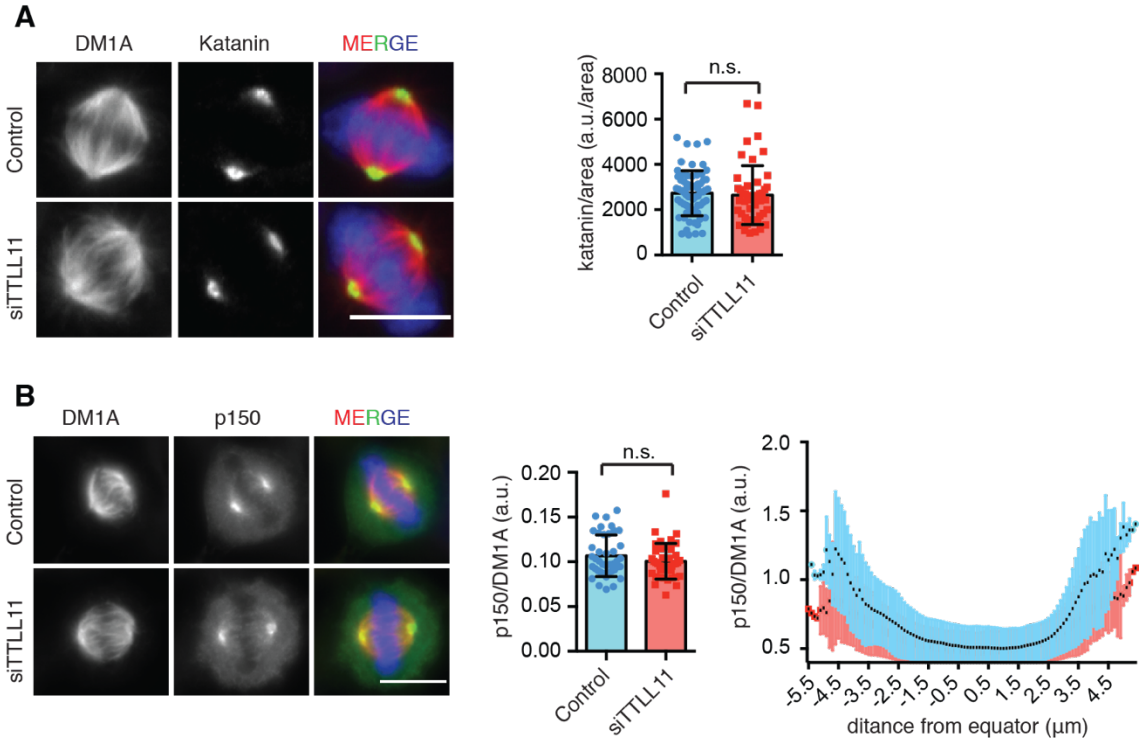

Figure 33 I Localization of Katanin and p150 to the mitotic spindle. A) Immunofluorescence images of metaphase spindles in control and siTTLL11 cells stained to visualize Katanin. The graph shows the quantification of the Katanin signal normalized on the total tubulin signal. n (control) = 66 cells and n (siTTLL11) = 49 cells. B) Immunofluorescence images of metaphase spindles in control and siTTLL11 cells stained for p150. The bar plot shows quantification of the p150signal normalized on the total tubulin signal. n (control) = 41 cells and n (siTTLL11) = 42 cells. The second graph represents the pole-to-pole normalized intensity profile for the p150 signal, n(control) = 24 and n(siTTLL11) = 24. One representative experiment of N = 2. Scale bars, 10 µm. Error bars represent SD. Tubulin (red), protein of interest (green) and DAPI (blue). p-values are based on t-test with a 95% confidence interval.

localization of katanin to the mitotic spindle (Figure 33A). We also quantified the level of p150, a subunit of the cytoplasmic dynein, like we did for the γ-tubulin/γ-TuRC. Also, in this case, we appreciated a mild decrease in the localization of p150 along the spindle (Figure 33B). However, we never observed problems in pole focusing and chromosomes congression, indicating that the minus-end directed motor dynein activity does not seem to be impaired upon TTLL11 silencing. Finally, we analyzed whether the plus-end directed motors Eg5 and Hklp2, directly responsible for tuning spindle length, localized correctly to the mitotic spindle. Also, in this case, we did not notice any impairment in the localization of any of the two motor proteins (Figure 34A, B). Despite the fact that we did not observe significant changes in the localization of a few spindle proteins in many cases, we cannot rule out that these and/or other spindle proteins could

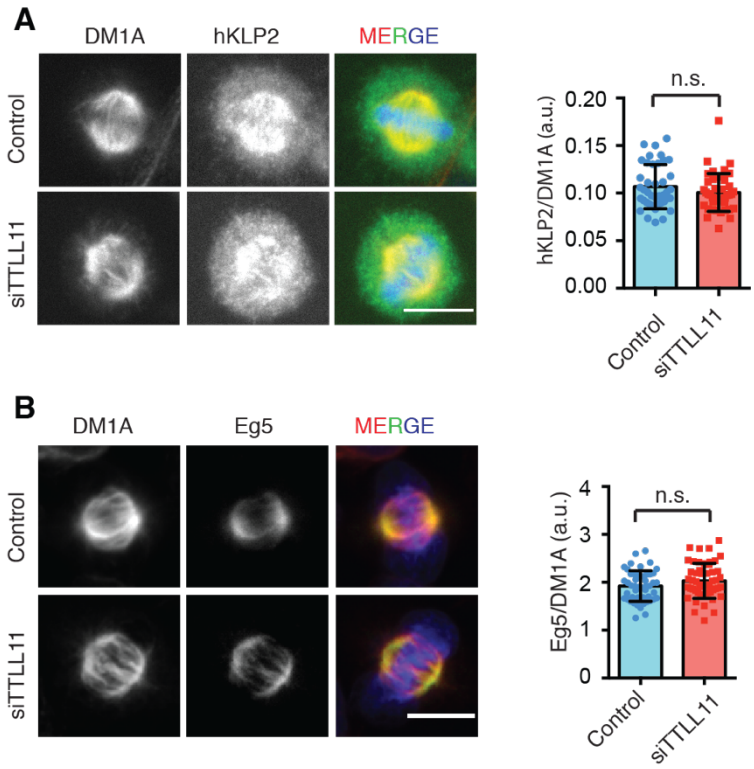

Figure 34 I Localization of Hklp2 and Eg5 to the mitotic spindle. A) Immunofluorescence images of metaphase spindles in control and siTTLL11 cells stained to visualize HKLP2. The graph shows the quantification of the HKLP2 signal normalized on the total tubulin signal. n (control) = 45 cells and n (siTTLL11) = 51 cells. B) Immunofluorescence images of metaphase spindles in control and siTTLL11 cells stained to visualize Eg5. The graph shows the quantification of the Eg5 signal normalized on the total tubulin signal. n (control) = 41 cells and n (siTTLL11) = 43 cells. One representative experiment of N = 2. Scale bars, 10 μm. Error bars represent SD. Tubulin (red), protein of interest (green) and DAPI (blue). p-values are based on t-test with a 95% confidence interval.

show altered kinetics to non-polyglutamylated spindle MTs and altogether contribute to the change in spindle size.

4.4. Regulation of MT dynamics

The spindle flux involves the addition/removal of tubulin subunits at the MT ends. Intuitively, keeping all the other spindle parameters constant, we could think that a slower poleward MT flux could result in an increased spindle length, and vice versa, a faster poleward flux could generate shorter spindles. Although this seems to apply to *Drosophila* embryos (Rogers et al., 2004) and *Xenopus* egg extracts (Gaetz et al., 2004), human cells do not show this reciprocity (Barisic et al., 2021). Indeed, it has been reported that the spindle size positively correlates with spindle poleward flux in U2OS cells (Steblyanko et al., 2020). In addition, stable end-on k-MT attachments display reduced flux, which still positively correlates with spindle size (Steblyanko et al., 2020). Our results show that the spindle flux has a reduced speed in the larger spindles assembled in TTLL11-silenced cells (Figure 30E). Although these data seem to contradict previous reports, they suggest that the spindle MT dynamics may be (slightly) reduced in TTLL11 silenced cells. It is also possible that the overall change of the spindle MT polyglutamylation pattern may trigger a spindle wide response that could modulate spindle size and spindle poleward flux oppositely as a result of a wide range of altered molecular interactions.

As another way to evaluate changes in the spindle MT dynamics, we analyzed interkinetochore distance that is a direct readout of the forces pulling the sister chromatids apart. We found that the distance between the two sister kinetochores is reduced in TTLL11-silenced cells (Figure), meaning less tension pulling the two kinetochores apart. Although reduced intra-kinetochore tension is thought to indirectly sustain the SAC due to KMT attachment instability triggered by AuroraB kinetochore gradient (Dudka et al., 2018b) and, therefore, poor kinetochore occupancy, it is possible that the tension is not low enough to be sensed by the SAC. In fact, mitosis progression is not altered in TTLL11-silenced

cells. Moreover, the SAC efficiently arrests these cells in mitosis when challenged by incubation with an Eg5 inhibitor that promotes spindle monopolarity, generating many syntelic chromosome attachments (Figure 30A). The slightly reduced interkinetochore tension could be due to the reduced KMT flux. Indeed, since the k-fibre flux generates part of the pulling forces required for chromosome segregation in anaphase, it is also likely to participate in generating interkinetochore tension in metaphase. However, there are controversial results (Buster et al., 2007; J.G. DeLuca et al., 2006; Dudka et al., 2018b; Maiato et al., 2005; Wandke et al., 2012) suggesting that other factors can generate interkinetochore tension.

KMT flux and the KMT turnover are two uncoupled mechanisms. However, there is a strong interconnection between the two phenomena. MCAK that is directly involved in the KMT error correction mechanism controlling KMT turnover, also regulates the flux. Some data support the idea for a direct role of the spindle flux in generating error-free anaphases that may be due to an interplay between MT flux and turnover. Cells co-silenced for MCAK and KIF2A do not show spindle flux and have more segregation errors than fluxing cells depleted only for MCAK (Ganem et al., 2005). Moreover, another evidence showing the interconnection between MT poleward flux and KMT turnover comes from the possibility of calculating the KMT turnover rate from spindle MT flux experiments. Indeed, MT photoactivation experiments in metaphase spindles allow measuring the half-life of the spindle MT population by fitting the normalized intensity of the fluxing speckles over time with a double-exponential curve (Girão & Maiato, 2020). In addition, k-fibres in TTLL11-silenced cells are more resistant to cold-induced depolymerization (Figure 30C). Altogether our data point toward the partial stabilization of the spindle MTs, in particular, the k-fibre when MT polyglutamylation is abolished through TTLL11 silencing. This stabilization may lead to more robust kinetochore-MT attachments that may favour the entry into anaphase in the presence of erroneous attachments that result in lagging chromosomes in anaphase and chromosome segregation defects. The increase of MT stability could be the primary cause of lagging chromosomes in anaphase

in Hela cells and zebrafish embryos (Figure 23D; 24E, F; 25). Interestingly, we found that TTLL11 seems to be systematically downregulated in a wide range of human cancers, suggesting a clear role of this enzyme in keeping the correct ploidy of the cell.

4.5. How does TTLL11 downregulation promote lagging chromosomes in anaphase and aneuploidy?

The SAC prevents chromosome segregation errors by delaying anaphase onset until all the kinetochores are captured by spindle MTs. When a cell bypasses the SAC, for example, because of the lack of some SAC component like MAD2 (Foijer et al., 2017), the duration of mitosis represents the time required by the cell to destroy cyclin B. Under these conditions, there is a complete loss of control on the kinetochore-MT attachment status that leads to chromosome segregation errors and aneuploidy. The SAC is not an all-or-nothing response; indeed, unattached kinetochores tune the strength of the signal. Hence, mutations in SAC components may “weaken” the checkpoint and result in a premature anaphase entry, increasing the chances of chromosome missegregation. Indeed it has been shown that SAC weakening promotes aneuploidy and CIN *in-vivo* (Suijkerbuijk et al., 2010). For example, mutation of BUBR1 causes mosaic variegated aneuploidy that leads to an increased level of tumorigenesis. Nonetheless, cells showing aneuploidy and CIN usually have a functional SAC and do not enter anaphase anticipatedly. This indicates that SAC misfunction is not the main source of mitotic errors observed in human cancer cells (Holland et al., 2012). In fact, work from many groups has provided evidence that explains aneuploidy in cancer cells as a consequence of erroneous merotelic attachments that the SAC does not sense and result in chromosome segregation errors (Cimini et al., 2001b; Thompson et al., 2011).

Three main processes driving merotelic attachment in a non-physiological frequency have been identified so far: the timing of centrosome separation, centrosome amplification, and KMT altered stability. In the first two scenarios, the

spindle usually shows transient multipolarity and altered mitotic phases dynamics and possible delayed anaphase entry due to SAC persistent activation. The main mechanism triggering both events involves an impaired geometry of the mitotic spindle configuration (Nam et al., 2016). On the other hand, a slight increase in MT stability does not drive SAC activation and does not alter centrosome dynamics and number (Bakhoum, Genovese, et al., 2009; Bakhoum, Thompson, et al., 2009).

Our data show that reducing spindle MT polyglutamylation through TTLL11 silencing generates lagging anaphase chromosomes in HeLa cells and zebrafish embryos. Moreover, bioinformatics analysis shows that TTLL11 downregulation is correlated with cancer cell aneuploidy. Although one possibility could be that spindle MT polyglutamylation could be required for SAC function, neither the mitotic index nor the mitotic timing in HeLa cells seems to be affected in TTLL11 silenced cells (Figure 23A, B, C). As explained in the introduction (Section 1.4.), syntelic and monotelic MT kinetochore attachments trigger SAC response delaying anaphase until they are corrected and the SAC is satisfied, or if they are not corrected, they trigger exit from mitosis without chromosome segregation, the cell entering into G1 in a tetraploid configuration. Our data suggest that preventing spindle MT polyglutamylation does not generate persistent syntelic or monotelic kinetochore MT attachments. When we challenged silenced cells by inducing a prolonged spindle monopolarity, thereby increasing the frequency of erroneous kinetochore attachments, cells arrested properly in mitosis (Figure 30A). If their SAC had been weakened, they would not have arrested as control cells. These data indicate that TTLL11 silencing and the reduction of spindle MT polyglutamylation does not alter SAC signalling. We conclude that anaphase laggards in the absence of TTLL11 and spindle MT polyglutamylation are due to unresolved merotelic chromosomes.

It was shown that merotelic chromosomes are the most common cause of segregation errors leading to cell aneuploidy and CIN. Despite this, there is currently no mechanism described to prevent or correct these types of erroneous attachments. The main physiological mechanism involved in avoiding merotelic

KMT attachment involves stringent geometric constraints and KMT dynamics (M.A. Lampson & Grishchuk, 2017). Merotelic and other types of erroneous kinetochore-MT attachments frequently form at the beginning of mitosis because MTs emanate radially from the centrosomes and around the chromosomes that are scattered in the nucleoplasmic environment. As mitosis progresses, MTs organize into a bipolar spindle leading to a geometric constrain, meaning that MTs have increased chances to catch the kinetochore oriented toward the corresponding spindle pole and much fewer chances to catch the other opposite oriented kinetochore, thereby favouring correct amphitelic configurations (R.B. Nicklas, 1997). However erroneous attachments can occur anyway, including merotelic attachments that are not sensed by the SAC and therefore are particularly dangerous for genome stability. So, how can a correct configuration of the kinetochore-MT interface be secured to ensure error-free anaphase? Several data support that KMT attachment stability is related to a narrow range of MT dynamics. Indeed, KMT stability defines the KMT turnover rate. The mechanism can be understood intuitively.

KMT interface is highly dynamic during prophase and becomes more stable in metaphase, however keeping a certain degree of turnover. Therefore, KMTs may be released due to their turnover rate as metaphase approaches. In the early phases of mitosis, there are random captures of KMTs that may be released while new MTs become captured by the kinetochore. As mitosis advances, the stringent geometric constraint will favour the attachment of correctly oriented MTs and, therefore, the establishment of amphitelic KMTs. If some merotelic KMTs persist over prophase and reach metaphase (lasting 10-20 minutes (M.A. Lampson & Grishchuk, 2017)), they will be released thanks to the MT turnover rate (2-6 min (Zhai et al., 1995)) to be replaced by correct amphitelic KMTs (Figure 35).

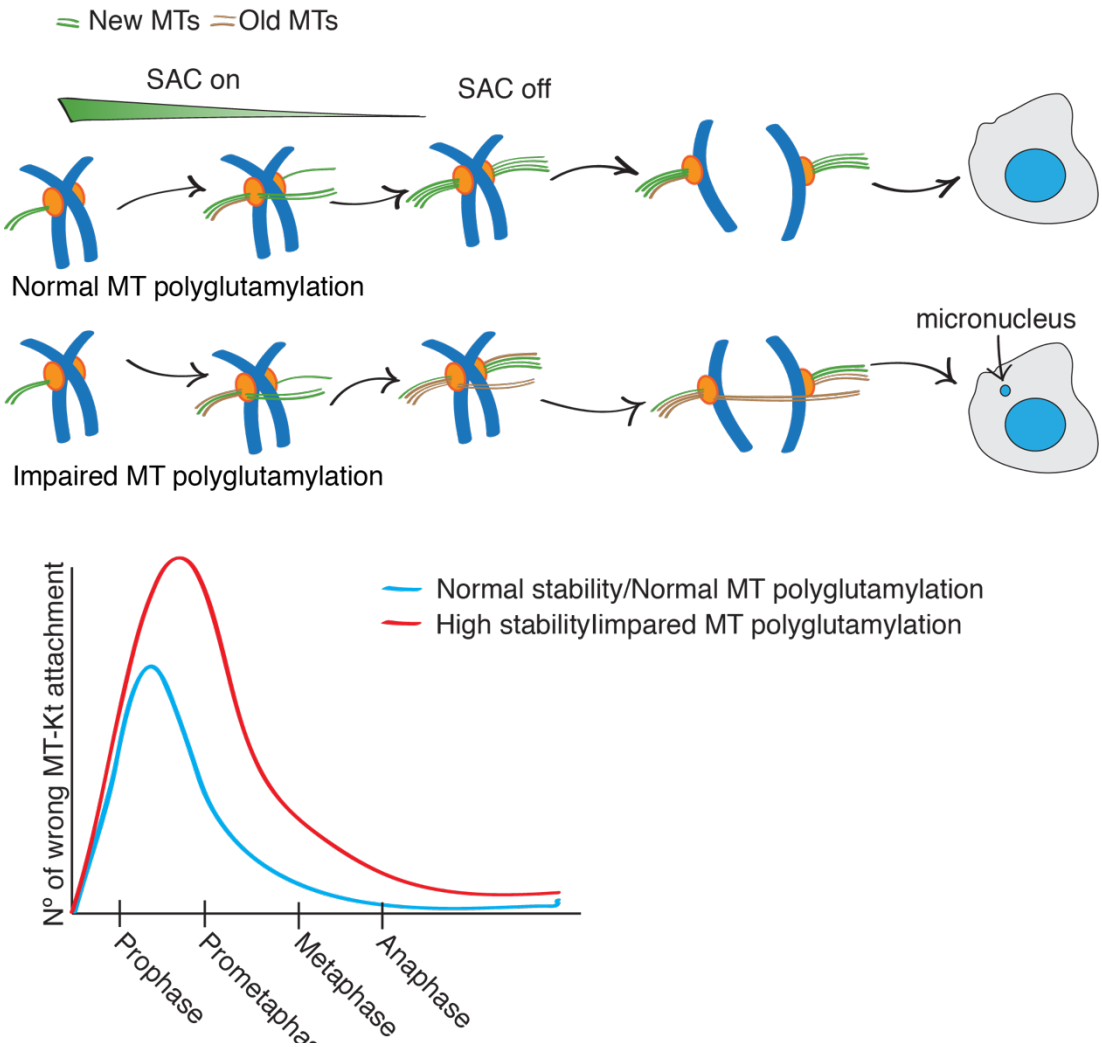

Figure 35 I Possible model of aneuploidy driven by impaired MT polyglutamylation. A) The MTs are captured by the kinetochores from many angles, generating erroneous KMT attachments. However, in the presence of correct MT polyglutamylation level the turnover of the KMTs is defined in the narrow range required for error correction of all these erroneous attachments leading to faithful anaphase. When MT polyglutamylation is impaired the k-MTs are slightly more stable leading to persistent merotelic attachments that are not sensed by the SAC. Anaphases show lagging chromosomes that can finally end forming a micronucleus in G1 and aneuploid cells. B) Schematic representation of KMTs dynamics throughout mitosis. At the beginning of mitosis and during prophase, the level of erroneous KMT attachments are comparable in control and TTLL11 silenced cells. However, control cells do not accumulate erroneous KMT attachments due to the kinetochore geometric constraint achieved by the alignment of chromosomes on the metaphase plate. Instead TTLL11 silenced cells have an increased stability of KMT attachments that are not as easily corrected leading to a higher probability to enter anapahse in the presence of merotelic chromosomes not sensed by the SAC. The graph shows that the time of mitosis is comparable in both scenario since the SAC is not activated.

In this view, the stability of KMTs is undoubtedly essential. Indeed, since mitotic timing is limited, the turnover rate must match this mitotic clock. For example, if the KMT stability increases while the mitotic timing remains the same,

the chances of reaching the metaphase-anaphase transition with merotelic kinetochore increases due to a longer half-life of the KMTs (Figure 35).

In conclusion, our data suggest that spindle MT polyglutamylation is required to establish the narrow range of MT dynamics required for chromosome segregation fidelity. In the absence of polyglutamylation, cells enter anaphase in the presence of unresolved merotelic chromosomes due to excessively stable kinetochore-MT attachments and generate laggards and aneuploidy. Polyglutamylation of MTs may define the correct balance of binding affinities and activity of the associated proteins. This balance may be lost in cancer cells that we found here downregulate TTLL11. Indeed, an imbalance of binding of several proteins may generate the hyper-stability of the kinetochore-MT attachments observed in cancer cells with CIN compared to stable diploid cells (Bakhoum, Thompson, et al., 2009; Dudka et al., 2018a; M. A. Lampson et al., 2004; Zasadil et al., 2013).

Conclusions

5. Conclusions

1) We identified TTLL11 as the polyglutamylase that modifies MTs specifically in mitosis.
2) Exogenously expressed TTLL11 localizes to the spindle in Hela cells and zebrafish embryo cells.
3) TTLL11 downregulation impairs zebrafish development
4) TTLL11 is required for chromosomes segregation fidelity in HeLa cells and zebrafish embryos
5) Ttll11 catalytic activity is necessary for chromosome segregation fidelity and embryonic development in zebrafish
6) TTLL11 and spindle MT polyglutamylation defines the dynamics of the spindle MTs in the narrow range required for faithful chromosome segregation.
7) TTLL11 is systematically downregulated in human cancer
8) TTLL11 expression levels correlate negatively with aneuploidy in human cancer.
9) We propose that the MT polyglutamylation in the spindle by TTLL11 provides a novel mechanism to ensure genome stability

Materials and Methods

6. Materials and Methods

Cell lines and plasmids

HeLa cells were grown at 37ºC in a 5% CO2 humid atmosphere in Dulbecco's Modified Eagle Medium (DMEM) supplemented with 4,5g/L Glucose and 4,5g/L Glutamine, 10% fetal bovine serum, 100 units/ml penicillin and 100 µg/ml streptomycin. Stable HeLa cell lines expressing H2B–mRFP/α-tubulin-GFP and H2B–mRFP/PA-α-tubulin–GFP (kind gift from P. Meraldi, University of Geneva) were grown in the presence of 400 µg /ml G418 and 20 µg/ml puromycin.

Plasmid and RNAi transfection

To express fluorescently labelled proteins, cells were transfected for 48h using Lipofectamine 2000 (Invitrogen) with 1 µg of human TTLL11 tagged with GFP at either ends. hTTLL11, coming from hTTLL11 cloned in a peYFP-C1 vector (kind gift from C. Janke, Institut Curie, 91405 Orsay, France), was subcloned in peGFP-N1 and peGFP-C1 vectors (van Dijk et al., 2007). To perform RNA interference (RNAi), HeLa cells were transfected at a 50—60% confluence using 500 pM RNAiMAX (Invitrogen) with 100nM siRNAs during 48h. siRNA SMARTpool (Dharmacon, SO-2796953G) was used with the following sequences: TTLL11#1 5'- UGACGGAGAUGGUGCGUAA-3'; TTLL11#2 5'-GAGUUUCAUUUCACGACAA -3'; TLL11#3 5'- UCAAAUGGUGAAAGACGAU -3'; TTLL11#4 5'- GGAUUCUGCCUGACGAGUU-3'; Nuf2 5'-AAGCATGCCGTGAAACGTATA -3'. The silencing construct against Nuf2 was used with the following sequence: 5'- AAGCATGCCGTGAAACGTATA -3' (J.G. DeLuca et al., 2002)

SDS-PAGE and Western blot analysis

For western blot analysis the following primary antibodies were used: rabbit anti-polyE antibody (polyE, home-made, 1,1 µg/ul) diluted 1:1000, mouse anti- α-tubulin (DM1A, Sigma T9026) diluted 1:1000; rabbit anti-GFP (GFP, home-made,

0,6 µg/ul) diluted 1:500. Western blots were developed with Odyssey CLx imaging system (LI-COR Bioscience).

Immunofluorescence microscopy

HeLa cells were grown on glass coverslip and fixed in ice-cold methanol for 3min at -20Cº. The following primary antibody were used: rabbit anti-polyE antibody (polyE, home-made, 1,1 µg/ul) diluted 1:1000, mouse anti-α-tubulin (DM1A, Sigma T9026) diluted 1:1000; rabbit anti-GFP (GFP, home-made, 0,6 µg/µl) diluted 1:1000; rabbit anti-β-tubulin (Abcam ab6046) diluted 1:500; mouse anti-γ-tubulin (Sigma, T6557) diluted 1:1000; mouse anti-glutamylated tubulin (GT335; Enzo 804-885) diluted 1:1000; human anti-centromere proteins (CREST, Antibodies Incorporated 15-235) diluted 1:100; anti-Hec1 (Hec1, Genentek GTX70268) diluted 1:100; rabbit anti-p150 (BD Bioscience, 610474), diluted 1:750; rabbit anti-Eg5 (BD Bioscience, 61186) diluted 1:1000; rabbit anti-TPX2 (home-made, 2 µg/µl) diluted 1:2000; rabbit anti-katanin (KATNB1, Proteintech, 14969-1AP) diluted 1:500; rabbit anti-Hklp2 (home-made, 0,8 µg/µl). DNA was counterstained with DAPI (1µg/ml; Sigma-Aldrich) diluted 1:1000. Antibodies were diluted in the following buffer: PBS 1x, 0,1% Triton-X-100 (v/v), 0,5% BSA (w/v) Images were acquired with Leica DEI 6000B microscope mounted with a DF2 90000GT camera.

Quantification of immunofluorescence samples

The length of HeLa cells metaphase spindles was obtained by tracing a line manually from pole-to-pole using ImageJ. ImageJ scale was checked for correct pixel/µm conversion. To quantify the level of tubulin (poly), glutamylation in interphase and mitotic cells, the signal intensity for the selected antibody was normalized with the DM1A tubulin signal. To limit signal fluctuation, the following formula was used:

$$NormalizedIntensity_x = \frac{RawIntensity_x - (Area * \overline{Noise_x})}{RawIntensity_{tub} - (Area * \overline{Noise_{tub}})}$$

where x is the protein or PTM of interest, Area is the circular ROI drawn around the metaphase spindle and must be identical for both signals, $\overline{Noise}$ is the mean of the average intensity signal of 3 random areas within the cell around the spindle. For p150 and γ-tubulin we also profiled the protein levels along the spindle. In this case, we measured the intensity from pole-to-pole on a two µm wide rectangle. The length of pole-to-pole distance was then binned in 0.1 µm, and the corresponding intensity values of the protein of interest and the MTs were retrieved for every bin. The signal of the protein of interest was normalized by the MT intensity value for every bin. The measurements from different cells were then aligned at the metaphase equator chosen as the lowest normalized intensity value. Average and SD were calculated for every bin, and control and TTLL11-silenced cell values were plotted together.

The inter-kinetochore distance was obtained by tracing manually a straight line between sister chromatids centromeres detected with Hec1 (Hec1, Genetex GTX70268) antibody connected with CREST (CREST, Antibodies Incorporated 15-235) staining in metaphase spindles. Measurements were only validated for a given spindle when obtaining at least five different values was possible. The lagging chromosome frequency was assessed in fixed HeLa cells stained with DAPI (1µg/ml; Sigma-Aldrich) diluted 1:1000 to detect DNA and centromeres with an anti-CREST (CREST, Antibodies Incorporated 15-235) diluted 1:100. It was calculated by monitoring lagging chromosomes (showing both DNA and centromere positive signals) in the two main masses of separating chromosomes in at least 121 anaphase cells. Data were then analyzed with Prism6 (Graphpad).

K-fibre cold stable assay

Hela cells were cultured on 18mm round coverslips in DMEM. Cells were washed three times for 5 min in PBS 1x. The medium was replaced by cold L15 medium at 4ºC, and cells were placed on ice. Coverslips were retrieved at given time points and cells fixed in ice-cold methanol at -20ºC for 3 min. Slides were stained for anti-α-tubulin (DM1A, Sigma T9026) diluted 1:1000 and DNA (DAPI 1µg/ml;

Sigma-Aldrich) diluted 1:1000. The quantification of K-fiber stability upon cell incubation on ice over time was obtained by scoring the status of the k-fibre microtubules among four arbitrarily defined classes.

Live cell imaging

HeLa cells stably expressing H2B–mRFP/α-tubulin-GFP were cultured in a 35/10 mm glass bottom, four-compartment dish (Grainer Bio-one) and imaged using a 60x oil-immersion 1.4 NA objective on Andor Dragon Fly Spinning Disk confocal microscope. For imaging purposes, culture cell media was replaced with one without phenol red. Several random fields were selected for imaging to increase the possibility of visualizing mitotic events. Every field was imaged every 2-3 minutes over 6 hours taking a 15 µm Z-volume divided into 5-7 intervals depending on the experiment. Movies were then processed using ImageJ (ref. NIH Image to ImageJ: 25 years of image analysis). The STLC release experiment was performed by adding 10 µM STLC to growing HeLa cells for 2 h. The STLC was then washed out by 4 washes in warm PBS 1x and one with DMEM. Cells were placed under the microscope Andor Dragon Fly Spinning Disk microscope and imaged using a 60x oil-immersion 1.4 NA objective. Every field was imaged every 2-3 minutes for 6h taking a 15 µm Z-volume divided into 5-7 intervals depending on the experiment. The time required for cells to enter into anaphase was calculated from the time of the first wash. All displayed images represent the maximum intensity projection of z-stacks. Andor Dragon Fly system was equipped with an iXON-EMCCD Du-897 camera, and Andor QI imaging software was used for images acquisition.

RT-qPCR HeLa cells TTLLs expression

For the RT-qPCR in HeLa cell, a normal asynchronous Hela cell population was harvested, and the mRNA was isolated with TRIzol Reagent (Invitrogen). Total mRNA was quantified with a NanoDrop spectrophotometer and retro-transcribed in cDNA with the Superscript III (Invitrogen, 12574-026). cDNA was used for

quantitative PCR with reverse transcription (RT-qPCR) analysis with SYBR green (Thermo Fischer). Oligonucleotide sequences are indicated in Table 1, Annex.

Tubulin poleward flux measurement

HeLa cells stably expressing H2B–RFP/PA-α-tubulin–GFP were cultured in a 35/10 mm glass bottom, 4 compartments dish (Grainer Bio-one). For imaging, cells were kept at 37ºC using an Okolab stage top chamber (UNO-T-H-CO2) and imaged using a 63x oil-immersion 1.4 NA objective lens on a Leica TCS SP5 confocal microscope. Images were acquired using the LAS X software. Bipolar spindles were identified by looking at the H2B–mRFP signal. PA-GFP–α-tubulin was activated in thin stripes (1-2 µm wide, as long as the metaphase plate) on one side of the metaphase plate with a 405 nm laser (100%). GFP fluorescence was captured every 8-10 s for 270 s. The poleward microtubule flux rate was calculated, generating a kymograph of the fluorescent speckle (Girao et al., 2020) using ImageJ.

Zebrafish Husbandry, Strains

Zebrafish (Danio rerio) were maintained as previously described (W. Westerfield, The Zebrafish Book: A Guide for the Laboratory Use of Zebrafish (Brachydanio rerio) (Univ. of Oregon Press, 1995)). Wild-type embryos were obtained from the AB strain natural crosses and were kept in an incubator at 28ºC until the sphere stage (Kimmel et al., 1995). All protocols used for the experiments have previously been approved by the Institutional Animal Care and Use Ethics Committee (PRBB–IACUEC). The transgenic fish line Tg(actb2:h2a-mCherry) (Zfin: e103Tg) was used for in vivo imaging experiments.

zfTTLL11 cloning, RT-PCR and mutagenesis

Total RNA was isolated from 24 hpf zebrafish embryos using tripleXtractor direct RNA (mirage biomedicals, GK23.0100) and reverse transcribed using an Xpert cDNA Synthesis kit (mirage biomedical GK80.0100). *ttll11* (ZDB-GENE-061013-747) cDNA was amplified using Phusion HF (Thermofisher F530S) and cloned

into pCS2 vector (BamHI-EcoRI linearised) through Gibson cloning, using the following primers:

TTLL11-pCS2-Fw:

5’—CTACTTGTTCTTTTTGCAGGATCCATGAGCGATCACTACGAGAGAGT—3’

TTLL11-pCS2-Rv:

5’—GCTCGAGAGGCCTTGAATTCTCAGTTGTCTGTGTTGGCTTTAGCAG—3’

To visualize the protein, a Gibson system was used to subclone ttll11 into a pCS2 vector containing a GFP at the N-terminal end (XhoI linearised) to obtain the GFP-zfTTLL11 fusion protein. The following primers were used:

TTLL11-GFP-GibpCS2-Fw:

CAAGGAATTCAAGGCCTCTCGAATGAGCGATCACTACGAGAGAGT

TTLL11-GFP-GibpCS2-Rv:

ACTCACTATAGTTCTAGAGGCTCAGTTGTCTGTGTTGGCT

For the semi-quantitative RT-PCR, zebrafish embryos at different stages of development were collected to extract mRNA with tripleXtractor direct RNA (mirage biomedicals, GK23.0100) and reverse transcribed using an Xpert cDNA Synthesis kit (mirage biomedical GK80.0100). 35 ng of cDNA were used for each stage of the RT-PCR reaction (Tm=57ºC; 33 cycles), and cDNA was amplified using GoTaq DNA polymerase (Promega, M7805). Oligonucleotide sequences are indicated in Table 1, Annex.

The pCS2-ttll11 construct was used to generate the mutated zfTTLL11·E466G version with QuickChange Site-Direct Mutagenesis kit (Agilent) with the following primers:

Fw: 5'-CTTGAAGCCTGTTTTTATTAGGAGTCAATGCCAATCCCAGC-3'

Rv: 5'-GCTGGGATTGGCATTGACTCCTAATAAAACAGGCTTCAAG-3'

Morpholinos, mRNA synthesis and microinjection

Morpholino antisense oligonucleotides were designed and purchased from Gene Tools, LLC. To inhibit *ttll11*, we used a blocking translation MO (CGGCTGATTTGTTATCTCATCTAGG) and a standard control MO

(CCTCTTACCTCAGTTACAATTTATA) as a negative control. We injected 2,8 ng of morpholino into one-cell stage embryos.

All capped mRNAs were synthesised using mMessage mMachine SP6 (Ambion, AM1340M). For the rescue experiments, 200 pg of ttll11 mRNA was injected together with the indicated MO. 200 pg of E466G mRNA (ttll11 mutated version) was injected together with the indicated MO as a negative control of the rescue experiments. GFP-Ttll11 mRNA was injected into one-cell stage embryos to visualise protein localisation. A PV820 microinjector (WPI) combined with an M3301R micro-manipulator was used to perform the microinjections.

Zebrafish immunofluorescence

Zebrafish embryos at the sphere stage (2.5-4 hpf) were dechorionated and incubated overnight at room temperature (RT), shacking in the microtubule fixative solution (Tran et al., 2012). The MT-fixative was discarded and the embryos were put in methanol at -20ºC overnight. After fixation was completed, zebrafish embryos were transferred in a clean tube and washed 3 times during 5 min with Tergitol solution (PBS 1x, tergitol 0.1% v/v) at room temperature for rehydration. Embryos were then moved to a 96-well plate, and an overnight wash with the anti-autofluorescence buffer (PBS 1x, 100mM NaBH4) was performed at RT gently shaking. Embryos were then washed 5x with TBS 1x followed by a blocking step with TBS 1x with 2% BSA during 30 minutes RT gently shaking. Anti-polyE (1,1 µg/ml, homemade) and -β-tubulin (clone E7; Hybridoma Bank at University of Iowa) primary antibodies were added both at 1:200 dilution and left ON at 4ºC gently shaking. After primary antibody incubation, 5 TBS 1x quick washes were performed, and secondary antibodies Alexa Flour (Invitrogen) at 8 µg/ml were added for 3 hours at RT gently shaking. Embryos were then rinsed twice in TBS 1x and then left 20 minutes in DAPI (1 µg/ml; Sigma Aldrich) diluted 1:500, rinsed twice with TBS 1x and a last washed ON at 4ºC in TBS1x before mounting. Embryos were then transferred in a tube containing low melting agarose at 42ºC diluted in TBS 1x and immediately placed in a Mattek dish with a 7mm diameter glass bottom and oriented with epithelial layer cells toward the

glass slide before the agarose solidified. Once the agarose was stiff, it was covered with TBS 1x to avoid evaporation.

Zebrafish fixed and live embryo imaging

Fixed embryos were imaged in glass-bottom Mattek dishes using a 63x oil-immersion 1.4 NA objective on a TCS SP8 inverted Leica confocal microscope. Laser intensity used changed through experiments according to the tubulin levels detected. For zfTTLL11 localization experiments, zebrafish eggs were fertilized, collected and microinjected with *ttll11* mRNA with a micromanipulator (M3301R, WPI World precision instruments). The quantity injected is relative to the one specified in the "Morpholinos, mRNA synthesis and microinjection" section, according to the experiment. Embryos at the sphere stage were manually dechorionated and moved in a tube containing low melting agarose at 42ºC diluted in TBS 1x and immediately in a Mattek dish with 7mm diameter glass bottom and oriented with epithelial layer cells toward the glass slide before the agarose solidified. Embryos were imaged under an Andor Revolution HD Spinning Disk microscope with a 60x, 1.4 NA oil objective with 2 min time-lapse intervals taking images every 2 µm in a 20 µm volume. iXON- EMCCD Du-897 camera and Andor IQ Imaging software was used for image acquisition. For anaphase lagging chromosome experiments in live embryos, zebrafish eggs coming from the Tg(bactin:H2AmCherry) were fertilized, collected and microinjected with either scramble or MO-1 (as in "Morpholinos, mRNA synthesis and microinjection"). Embryos were collected as abovementioned but laid on a 35/10 mm glass bottom, 4 compartment dish (Grainer Bio-one). Embryos were imaged using a Leica TCS SP8 confocal microscope equipped with an Argon laser. The objective used is an HC PLAN APO 63x 1.4 NA. Images were acquired simultaneously using the LAS X software every 45s-75s according to the experiments imaging a Z-volume 20 µm every 2 µm. All the live imaging experiments were performed at RT.

Morphological zebrafish analysis

Zebrafish embryos at 36 hpf were anaesthetized with tricaine methanesulfonate (MS-222, Sigma Aldrich). The morphological phenotype was evaluated on-site with an Olympus SZX16 scope equipped with an Olympus DP73 camera. Representative images were analyzed with ImageJ.

TCGA Data

The XenaBrowser(Goldman et al., 2020) was used to obtain publicly available data on pan-cancer normalised gene expression, copy number variation, and somatic mutations in patients from The Cancer Genome Atlas (TCGA). The aneuploidy scores were obtained directly from Taylor et al.(Taylor et al., 2018). Gene lengths were obtained from the latest human genome reference (GRCh38) made available through the object "ens.gene.ann.hg38" in the R package GeneBreak. From all cancer types available in TCGA, only those with at least 20 samples of solid tissue normal and primary tumour in the gene expression matrix (n=13) were considered. The complete analysis pipeline is available at https://github.com/MiqG/Zadra_2021.

Differential expression analysis of TTLL11

A Wilcoxon Rank Sum test was performed for every type of cancer to assess the differences in log-normalised read counts of TTLL11 between primary tumours and unmatched solid tissue normal samples statistically. We performed a Wilcoxon Rank Sum test for every cancer type to statistically assess the differences in log-normalised read counts of TTLL1, TTLL2, TTLL4, TTLL5, TTLL6, TTLL7, TTLL9, TTLL11 and TTLL13 between primary tumours and unmatched solid tissue normal samples.

Association between TTLL11 expression and sample aneuploidy

The Spearman correlation between log-normalised read counts of every gene and corresponding sample aneuploidy score was computed for every type of cancer. Then, we assessed how likely it is to obtain the correlation coefficient of TTLL11 with respect to the rest of the genes. We standardised the correlation

coefficients and computed the one-sided p-value of the correlation of TTLL11 with respect to the full distribution. Finally, to have an overview of the association between TTLL11 expression and aneuploidy across cancers concerning the rest of the genes, we computed the median correlation coefficient across all cancer types and re-computed the p-value as explained.

Mutation frequency of TTLL11

For every type of cancer and annotated mutation effect, we computed the mutation frequency per gene. We divided it by the corresponding gene length to obtain the frequency of mutation per kilobase. Then, we followed the same procedure explained above to get the one-sided p-value of the standardised mutation frequency of TTLL11 per kilobase across cancer types and the mutation effect with respect to the rest of the genes.

Sequence sampling

Amino acid sequences were retrieved from ensembl (www.ensembl.org). Annotated canonical sequences of human (GRCh38.p13) TTLLs and their orthologous were used for the following species: Mus Musculus (GRCm39), Danio Rerio (GRCz11), Drosophila Melanogaster (BDGP6.32) and Caenorhabditis Elegans (WBcel235). Transcripts used in the phylogenetic analysis are reported in Table S5. (Assembled genome IDs of the different species between brackets).

Alignment estimation and phylogeny using Bali-phy

Popular alignment tools fail to provide a reliable alignment due to the highly divergent protein sequence employed in this analysis (Suchard et al., 2006). Hence, Bali-phy v.3 (B. D. Redelings, 2021) was implemented to analyse the TTLL aminoacidic dataset; this program uses a model-based approach, so the alignment is calculated alongside the phylogenetic analysis using Bayesian inference. This method estimates the alignment with a likelihood averaged across several alignments (B. Redelings, 2014). This multiple alignment approach is

superior for assessing alignment in highly divergent sequences than the most common alignment tool as MAFT and MUSCLE (Katoh et al., 2019). Moreover, it overcomes the alignment-guided tree that relies already on a tree topology for estimating the alignment (Suchard & Redelings, 2006). The analysis was run three times to check for convergence among different runs. Parameters used were -alphabet Amino-Acids -smodel gtr. Rates.gamma -imodel rs07(Katoh et al., 2019).

Human oocyte immunofluorescence

Oocytes at the germinal vesicle stage were cultured in vitro for 27 hours. Time zero is considered the moment of aspiration from the donor. Oocytes were rinsed in pre-warmed PBS, fixed in pre-warmed 4% PFA in PBS for 10 min at RT, washed in PBT (PBS 0.1% Tween-20) and stored in PBT at 4C until processing. For immunostaining, oocytes were permeabilised in 0.2% Triton X-100 in PBS for 15 min, then blocked in a solution of 5% normal goat serum, 2% BSA and 0.1%. Tween-20 in PBS, and incubated overnight in a mouse monoclonal anti-α-tubulin antibody (T6199; Sigma Aldrich; Merck KGaA, Darmstadt, Germany) diluted 1:100 in blocking solution. Once washed in PBT, samples were incubated for 1h at RT in secondary Alexa Fluor 488 goat anti-mouse IgG (1:500; Molecular Probes, USA). After washing, samples were counterstained for actin in 1:100 Alexa Fluor. 568-Phalloidin (Molecular Probes, USA) and chromatin in 50 µg/ml Hoechst 33342 (Molecular Probes, USA). Oocytes were mounted in Vectashield (Vector Laboratories, USA) using wax cushions to avoid compression and preserve the three-dimensional structure.

Human oocyte imaging

Stained oocytes were imaged using a Zeiss Lsm780 laser scanning confocal equipped with a 405nm diode laser, a multiline 458/488//514 nm argon laser, and a 561nm diode-pumped solid-state lasers (DPSS). Fixed samples were imaged through a 63× glycerol objective every 0.5µm. Only spindles arranged perpendicular to the purpose were considered for analysis. The samples were

imaged the same day they were stained. Imaging data were analysed using the open-source image processing software ImageJ.

Bibliography

7. Bibliography

Aillaud, C., Bosc, C., Peris, L., Bosson, A., Heemeryck, P., Van Dijk, J., . . . Moutin, M. (2017). Vasohibins/SVBP are tubulin carboxypeptidases (TCPs) that regulate neuron differentiation *Science, 358*(6369), 1448-1453. doi:10.1126/science.aao4165

Aillaud, C., Bosc, C., Saoudi, Y., Denarier, E., Peris, L., Sago, L., . . . Moutin, M. (2016). Evidence for new C-terminally truncated variants of α- and β-tubulins *Mol Biol Cell, 27*(4), 640-653. doi:0.1091/mbc.E15-03-0137

Akella, J. S., Wloga, D., Kim, J., Starostina, N. G., Lyons-Abbott, S., Morrissette, N. S., . . . Gaertig, J. (2010). MEC-17 is an alpha-tubulin acetyltransferase *Nature, 467*(7312), 218-222. doi:10.1038/nature09324

Alexander, J. E., Hunt, D. F., Lee, M. K., Shabanowitz, J., Michel, H., Berlin, S. C., . . . Frankfurter, A. (1991). Characterization of posttranslational modifications in neuron-specific class III beta-tubulin by mass spectrometry. *Proc Natl Acad Sci U S A, 88*(11), 4685-4689. doi:10.1073/pnas.88.11.4685

Amaro, A., Samora, C. P., Holtackers, R., Wang, E., Kingston, I. J., Alonso, M., . . . Meraldi, P. (2010). Molecular control of kinetochore-microtubule dynamics and chromosome oscillations. *12, 4*(319-329). doi:10.1038/ncb2033

Andrews, P. A., Ovechkina, Y., Morrice, N., Wagenbach, M., Duncan, K., Wordeman, L., & Swedlow, J. R. (2004). Aurora B regulates MCAK at the mitotic centromere *Dev Cell, 6*(2), 253-268. doi:10.1016/s1534-5807(04)00025-5

Baas, P. W., Rao, A. N., Matamoros, A. J., & Leo, L. (2016). Stability properties of neuronal microtubules. *Cytoskeleton (Hoboken), 73*(9), 442-460. doi:10.1002/cm.21286

Bakhoum, S. F., Genovese, G., & Compton, D. A. (2009). Deviant kinetochore microtubule dynamics underlie chromosomal instability. *Curr Biol, 19*(22), 1937-1942. doi:10.1016/j.cub.2009.09.055

Bakhoum, S. F., Genovese, G., & Compton, D. A. (2009). Deviant kinetochore microtubule dynamics underlie chromosomal instability. *Curr Biol, 19*(22), 1927-1942. doi:10.1016/j.cub.2009.09.055

Bakhoum, S. F., Silkworth, W. T., Nardi, I. K., Nicholson, J. M., Compton, D. A., & Cimini, D. (2014). The mitotic origin of chromosomal instability. *Curr Biol, 24*(4), R148-149. doi:10.1016/j.cub.2014.01.019

Bakhoum, S. F., Thompson, S. L., Manning, A. L., & Compton, D. A. (2009). Genome stability is ensured by temporal control of kinetochore-microtubule dynamics. *Nat Cell Biol, 11*(1), 27-35. doi:10.1038/ncb1809

Bakhoum, S. F., Thompson, S. L., Manning, A. L., & Compton, D. A. (2009). Genome stability is ensured by temporal control of kinetochore-microtubule dynamics. *Nat Cell Biol., 11*(1), 27-35. doi:10.1038/ncb1809

Barisic, M., Rajendraprasad, G., & Steblyankoa, Y. (2021). The metaphase spindle at steady state – Mechanism and functions of microtubule poleward flux. *Seminars in Cell & Developmental Biology, 117*, 99-117.

Barisic, M., Silva e Sousa, R., Tripathy, S. K., Magiera, M. M., Zaytsev, A. V., Pereira, A. L., . . . Maiato, H. (2015). Mitosis. Microtubule detyrosination guides

chromosomes during mitosis *Science, 348*(6236), 799-803. doi:10.1126/science.aaa5175

Barra, H. S. R., J. A. Arce, C. A. Caputto, R. (1973). a Soluble Preparation From Rat Brain That Incorporates Into Its Own Proteins [14C]Arginine By a Ribonuclease-Sensitive System and [14C]Tyrosine By a Ribonuclease-Insensitive System. *J Neurochem, 20*(1), 97-108. doi:10.1111/j.1471-4159.1973.tb12108.x

Beltramo, D. M., Arce, C. A., & Barra, H. S. (1987). Tubulin, but not microtubules, is the substrate for tubulin:tyrosine ligase in mature avian erythrocytes *J Biol Chem, 262*(32), 15673-15677.

Berezniuk, I., Vu, H. T., Lyons, P. J., Sironi, J. J., Xiao, H., Burd, B., . . . Fricker, L. D. (2012). Cytosolic carboxypeptidase 1 is involved in processing α- and β-tubulin *J Biol Chem, 287*(9), 6503-6517. doi:10.1074/jbc.M111.309138

Berry, R. W., & Shelanski, M. L. (1972). Interactions of Tubulin with Vinblastine and Guanosine Triphosphate. *J. Mol. Biol., 71*, 71-80. doi:10.1016/0022-2836(72)90401-9

Bettencourt-Dias, M., & D.M., G. (2007). Centrosome biogenesis and function: centrosomics brings new understanding. *Nat Rev Mol Cell Biol, 8*(6), 451-463. doi:10.1038/nrm2180

Bobinnec, Y., Moudjou, M., Fouquet, J. P., Desbruyères, E., Eddé, B., & Bornens, M. (1998). Glutamylation of centriole and cytoplasmic tubulin in proliferating non-neuronal cells *Cell Motil Cytoskeleton, 39*(3), 223-232. doi:10.1002/(SICI)1097-0169(1998)39:3<223::AID-CM5>3.0.CO;2-5

Bompard, G., van Dijk, J., Cau, J., Lannay, Y., Marcellin, G., Lawera, A., . . . Rogowski, K. (2018). CSAP Acts as a Regulator of TTLL-Mediated Microtubule Glutamylation *Cell Rep, 25*(10), 2866-2877.e2865. doi:10.1016/j.celrep.2018.10.095

Borisy, G. G., & Taylor, E. W. (1967). The mechanism of action of colchicine. Colchine binding to sea urchin eggs and the mitotic apparatus. *J Cell Biol, 34*(2), 535–548. doi:10.1083/jcb.34.2.535

Brinkley, B. R., & Cartwright, J. (1975). Cold-labile and cold-stable microtubules in the mitotic spindle of mammalian cells. *Ann N Y Acad Sci, 253*, 428-439. doi:10.1111/j.1749-6632.1975.tb19218.x

Buster, D. W., Zhang, D., & Sharp, D. J. (2007). Poleward tubulin flux in spindles: regulation and function in mitotic cells. *Mol Biol Cell, 18*(8), 3094-3104. doi:10.1091/mbc.e06-11-0994

Cambray-Deakin, M. A., & Burgoyne, R. D. (1990). The non-tyrosinated M alpha 4 alpha-tubulin gene product is post-translationally tyrosinated in adult rat cerebellum. *Brain Res Mol Brain Res, 8*(1), 77-81. doi:10.1016/0169-328x(90)90012-3

Caplow, M., & Shanks, J. (1996). Evidence that a single monolayer tubulin-GTP cap is both necessary and sufficient to stabilize microtubules. *Mol Biol Cell., 7*(4), 663-675. doi:10.1091/mbc.7.4.663

Carazo-Salas, R. E., Guarguaglini, G., Gruss, O. J., Segref, A., Karsenti, E., & Mattaj, I. W. (1999). Generation of GTP-bound Ran by RCC1 is required for chromatin-induced mitotic spindle formation *Nature, 400*(6740), 178-181. doi:10.1038/22133

Carmena, M., Wheelock, M., Funabiki, H., & Earnshaw, W. C. (2012). The chromosomal passenger complex (CPC): from easy rider to the godfather of mitosis. *Nat Rev Mol Cell Biol, 13*(12), 789-803. doi:10.1038/nrm3474

Cavazza, T., & Vernos, I. (2016). The RanGTP Pathway: From Nucleo-Cytoplasmic Transport to Spindle Assembly and Beyond *Front Cell Dev Biol, 11*(3), 82. doi:10.3389/fcell.2015.00082

Cheeseman, I. M., Chappie, J. S., Wilson-Kubalek, E. M., & Desai, A. (2006). The conserved KMN network constitutes the core microtubule-binding site of the kinetochore. *Cell, 127*(5), 983-997. doi:10.1016/j.cell.2006.09.039

Cheeseman, I. M., & Desai, A. (2008). Molecular architecture of the kinetochore-microtubule interface *Nat Rev Mol Cell Biol, 9*(1), 33-46. doi:10.1038/nrm2310

Chen, J., Kholina, E., Szyk, A., Fedorov, V. A., Kovalenko, I., Gudimchuk, N., & Roll-Mecak, A. (2021). α-tubulin tail modifications regulate microtubule stability through selective effector recruitment, not changes in intrinsic polymer dynamics. *Dev Cell, 56*(14), 2016-2028. doi:10.1016/j.devcel.2021.05.005

Choudhary, C., Kumar, C., Gnad, F., Nielsen, M. L., Rehman, M., Walther, T. C., . . . Mann, M. (2009). Lysine acetylation targets protein complexes and co-regulates major cellular functions *Science, 325*(5942), 834-840. doi:10.1126/science.1175371

Chu, C., Hou, F., Zhang, J., Phu, L., Loktev, A. V., Kirkpatrick, D. S., . . . Zou, H. (2011). A novel acetylation of β-tubulin by San modulates microtubule polymerization via down-regulating tubulin incorporation *Mol Biol Cell, 22*(4), 448-456. doi:10.1091/mbc.E10-03-0203

Cimini, D. (2008). Merotelic kinetochore orientation, aneuploidy, and cancer. *Biochim Biophys Acta, 1786*(1), 32-40. doi:10.1016/j.bbcan.2008.05.003

Cimini, D., Fioravanti, D., Salmon, E. D., & Degrassi, F. (2002). Merotelic kinetochore orientation versus chromosomemono-orientation in the origin of lagging chromosomes in human primary cells. *J Cell Biol, 115*(3), 507-515.

Cimini, D., Howell, B., Maddox, P., Khodjakov, A., Degrassi, F., & Salmon, E. D. (2001a). Merotelic kinetochore orientation is a major mechanism of aneuploidy in mitotic mammalian tissue cells. *J Cell Biol, 153*(3), 517-527. doi:10.1083/jcb.153.3.517

Cimini, D., Howell, B., Maddox, P., Khodjakov, A., Degrassi, F., & Salmon, E. D. (2001b). Merotelic kinetochoreorientation is a major mechanism of aneuploidy in mitotic mammalian tissue cells. *J Cell Biol, 153*(3), 517-527. doi:10.1083/jcb.153.3.517

Cimini, D., Moree, B., Canman, J. C., & E.D., S. (2003). Merotelic kinetochore orientation occurs frequently during early mitosis in mammalian tissue cells and error correction is achieved by two different mechanisms *J Cell Biol, 116*(20), 4213-4225. doi:10.1242/jcs.00716

Creppe, C., Malinouskaya, L., Volvert, M., Gillard, M., Close, P., Malaise, O., . . . Nguyen, L. (2009). Elongator controls the migration and differentiation of cortical neurons through acetylation of alpha-tubulin *Cell, 136*(3), 551-564. doi:10.1016/j.cell.2008.11.043

de la Vega, M. R., Sevilla, R. G., Hermoso, A., Lorenzo, J., Tanco, S., Diez, A., . . . Avilés, F. X. (2007). Nna1-like proteins are active metallocarboxypeptidases of a new and diverse M14 subfamily. *FASEB J., 21*(3), 851-865. doi:10.1096/fj.06-7330com

DeLuca, J. G., Gall, W. E., Ciferri, C., Cimini, D., Musacchio, A., & Salmon, E. D. (2006). Kinetochore Microtubule Dynamics and Attachment Stability Are Regulated by Hec1. *Cell, 127*(5), 968-982. doi:10.1016/j.cell.2006.09.047

DeLuca, J. G., Moree, B., Hickey, J. M., Kilmartin, J. V., & Salmon, E. D. (2002). hNuf2 inhibition blocks stable kinetochore-microtubule attachment and induces mitotic cell death in HeLa cells. *J Cell Biol, 159*(4), 549-555. doi:10.1083/jcb.200208159

Desai, A., & Mitchison , T. J. (1997). Microtubule polymerization dynamics. *Annu. Rev. Cell Dev., 13*, 83-117.

Dhonukshe, P., Vischer, N., & Gadella, W. J. (2006). Contribution of microtubule growth polarity and flux to spindle assembly and functioning in plant cells. *J Cell Biol, 119*(15), 3193-3205. doi:10.1242/jcs.03048

Ding, R., McDonald, K. L., & McIntosh, J. R. (1993). Three-dimensional reconstruction and analysis of mitotic spindles from the yeast, Schizosaccharomyces pombe *J Cell Biol, 120*(1), 141-151. doi:10.1083/jcb.120.1.141

Drechsel, D. N., & Kirschner, M. W. (1994). The minimum GTP cap required to stabilize microtubules *Curr. Biol., 4*(12), 1053-1061. doi: 10.1016/s0960-9822(00)00243-8

Dudka, D., Noatynska, A., Smith, C. A., Liaudet, N., McAinsh, A. D., & Meraldi, P. (2018a). Complete microtubule-kinetochore occupancy favours the segregation of merotelic attachments. *Nat Commun, 9*(1), 2042. doi:10.1038/s41467-018-04427-x

Dudka, D., Noatynska, A., Smith, C. A., Liaudet, N., McAinsh, A. D., & Meraldi, P. (2018b). Complete microtubule–kinetochore occupancy favours the segregation of merotelic attachments. *Nat Commun, 9*, 2042. doi:10.1038/s41467-018-04427-x

Dujardin, D., Wacker, U. I., Moreau, A., Schroer, T. A., Rickard, J. E., & De Mey, J. R. (1998). Evidence for a role of CLIP-170 in the establishment of metaphase chromosome alignment. *J Cell Biol, 141*(4), 849-862. doi:10.1083/jcb.141.4.849

Erck, C., Peris, L., Andrieux, A., Meissirel, C., Gruber, A. C., Vernet, M., . . . Wehland, J. (2005). A vital role of tubulin-tyrosine-ligase for neuronal organization *Proc Natl Acad Sci U S A, 102*(22), 7853-7858. doi:10.1073/pnas.0409626102

Ertych, N., Stolz, A., Stenzinger, A., Weichert, W., Kaulfuss, S., Burfeind, P., . . . Bastians, H. (2014). Increased microtubule assembly rates influence chromosomal instability in colorectal cancer cells. *Nat Cell Biol, 16*(8), 779-791. doi:10.1038/ncb2994

Feng, R., Sang, Q., Kuang, Y., Sun, X., Yan, Z., Zhang, S., . . . Wang, L. (2016). Mutations in TUBB8 and Human Oocyte Meiotic Arrest. *N Engl J Med, 374*, 223-232. doi:10.1056/NEJMoa1510791

Fernandez-Gonzalez, A., La Spada, A. R., Treadaway, J., Higdon, J. C., Harris, B. S., Sidman, R. L., . . . Zuo, J. (2002). Purkinje cell degeneration (pcd) phenotypes caused by mutations in the axotomy-induced gene, Nna1 *Science, 295*(5561), 1904-1906. doi:10.1126/science.1068912

Flemming, W. (1882). Zellsubstanz, kern und zelltheilung.

Foijer, F., Albacker, L. A., Bakker, B., Spierings, D. C., Yue, Y., Xie, S. Z., . . . Sorger, P. K. (2017). Deletion of the MAD2L1 spindle assembly checkpoint gene is tolerated in mouse models of acute T-cell lymphoma and hepatocellular carcinoma *eLIFE, 6*, e20873. doi:10.7554/eLife.20873

Funabiki, H. (2019). Correcting aberrant kinetochore microtubule attachments: a hidden regulation of Aurora B on microtubules *Curr Opin Cell Biol, 58*, 24-41. doi:10.1016/j.ceb.2018.12.007

Gadadhar, S., Alvarez-Viar, G., Hansen, J. N., Gong, A., Kostarev, A., Ialy-Radio, C., . . . C., J. (2021). Tubulin glycylation controls axonemal dynein activity, flagellar beat, and male fertility *Science, 371*(6525), eabd4914. doi:10.1126/science.abd4914

Gadadhar, S., Dadi, H., Bodakuntla, S., Schnitzler, A., Bièche, I., Rusconi, F., & Janke, C. (2017). Tubulin glycylation controls primary cilia length. *J Cell Biol, 216*(9), 2701-2713. doi:10.1083/jcb.201612050

Gaetz, J., & Kapoor, T. M. (2004). Dynein/dynactin regulate metaphase spindle length by targeting depolymerizing activities to spindle poles. *J Cell Biol, 166*(4), 465-471. doi:10.1083/jcb.200404015

Ganem, N. J., & Compton, D. A. (2006). Functional role of puleward microtubule flux during mitosis. *Cell Cycle, 5*(5), 481-485. doi:10.4161/cc.5.5.2519

Ganem, N. J., Upton, K., & Compton, D. A. (2005). Efficient mitosis in human cells lacking poleward microtubule flux. *Curr Biol, 15*(20), 1827-1832. doi:10.1016/j.cub.2005.08.065

Gard, D. L., & Kirsclmer, M. W. (1987). Microtubule assembly in cytoplasmic extracts of Xenopus oocytes and eggs. *J Cell Biol., 105*(5), 2191–2201. doi:10.1083/jcb.105.5.2191

Garnham, C. P., Vemu, A., Wilson-Kubalek, E. M., Yu, I., Szyk, A., Lander, G. C., . . . Roll-Mecak, A. (2016). Multivalent Microtubule Recognition by Tubulin Tyrosine Ligase-Like Family Glutamylases. *Cell, 161*(5), 1112-1123. doi:10.1016/j.cell.2015.04.003

Gergely, F., Draviam, V. M., & Raff, J. W. (2003). The ch-TOG/XMAP215 protein is essential for spindle pole organization in human somatic cells *Genes Dev, 17*(3), 336-341. doi:10.1101/gad.245603

Girao, H., & Maiato, H. (2020). Measurement of Microtubule Half-Life and Poleward Flux in the Mitotic Spindle by Photoactivation of Fluorescent Tubulin. *Methods Mol Biol, 2101*, 235-246. doi:10.1007/978-1-0716-0219-5_15

Girão, H., & Maiato, H. (2020). Measurement of Microtubule Half-Life and Poleward Fluxin the Mitotic Spindle by Photoactivation of FluorescentTubulin. *Cytoskeleton Dynamics. Methods in Molecular Biology, 2101*, 235-246. doi:10.1007/978-1-0716-0219-5_15

Goldman, M. J., Craft, B., Hastie, M., Repecka, K., McDade, F., Kamath, A., . . . Haussler, D. (2020). Visualizing and interpreting cancer genomics data via the Xena platform. *Nat Biotechnol, 38*(6), 675-678. doi:10.1038/s41587-020-0546-8

Goshima, G., Mayer, M., Zhang, N., Stuurman, N., & Vale, R. D. (2008). Augmin: a protein complex required for centrosome-independent microtubule generation within the spindle. *JCB, 181*(3), 421-429. doi: 10.1083/jcb.200711053

Grau, B. G., Curto, G. G., Rocha, C., Magiera, M. M., Sousa, P. M., Giordano, T., . . . Janke, C. (2013). Tubulin glycylases and glutamylases have distinct functions in stabilization and motility of ependymal cilia *J Cell Biol, 202*(2), 441-451. doi:10.1083/jcb.201305041

Griffis, E. R., Stuurman, N., & Vale, R. D. (2007). Spindly, a novel protein essential for silencing the spindle assembly checkpoint, recruits dynein to the kinetochore *J Cell Biol, 177*(6), 1005-1015. doi:10.1083/jcb.200702062

Gu, W., Lewis, S. A., & Cowan, N. J. (1988). Generation of antisera that discriminate among mammalian alpha-tubulins: introduction of specialized isotypes into cultured cells results in their coassembly without disruption of normal microtubule function. *J Cell Biol, 106*(6), 2011-2022. doi:10.1083/jcb.106.6.2011

Gudimchuk, N., Vitre, B., Kim, Y., Kiyatkin, A., Cleveland, D. V., Ataullakhanov, F. I., & Grishchuk, E. L. (2013). Kinetochore kinesin CENP-E is a processive bi-directional tracker of dynamic microtubule tips *Nat Cell Biol, 15*(9), 1079-1088. doi:0.1038/ncb2831

Guimaraes, G. J., Dong, Y., McEwen, B. F., & Deluca, J. G. (2008). Kinetochore-microtubule attachment relies on the disordered N-terminal tail domain of Hec1. *Curr Biol, 18*(22), 1778-1784. doi:10.1016/j.cub.2008.08.012

Gundersen, G. G., & J.C., B. (1986). Microtubule arrays in differentiated cells contain elevated levels of a post-translationally modified form of tubulin *Eur J Cell Biol, 42*(2), 288-294.

Hallak, M. E., Rodriguez, J. E., Barra, H. S., & Caputto, R. (1977). Release of tyrosine from tyrosineted tubulin.Some common factors that affect this process and the assembly of tubulin. *FEBS Journal, 73*(2), 147-150. doi:10.1016/0014-5793(77)80968-x

Hara, Y., & Kimura, A. (2013). An allometric relationship between mitotic spindle width, spindle length, and ploidy in Caenorhabditis elegans embryos. *Mol Biol Cell, 24*(9), 1411-1419. doi:10.1091/mbc.E12-07-0528

Harris, P. (1961). Electron microscope study of mitosis in sea urchin blastomers. *J Biophys Biochem Cytol, 11*(2), 419-431. doi:10.1083/jcb.11.2.419

Hayden, J. H., Bowser, S. S., & Rieder, C. L. (1990). Kinetochores capture astral microtubules during chromosome attachment to the mitotic spindle: direct visualization in live newt lung cells *J Cell Biol, 111*(3), 1039-1045. doi: 10.1083/jcb.111.3.1039

He, K., Ma, X., Xu, T., Li, Y., Hodge, H., Zhang, Q., . . . Hu, J. (2018). Axoneme polyglutamylation regulated by Joubert syndrome protein ARL13B controls ciliary targeting of signaling molecules *Nat Commun, 9*(1), 3310. doi:10.1038/s41467-018-05867-1

Heald, R., Tournebize, R., Habermann, A., Karsenti, E., & Hyman, A. (1997). Spindle assembly in Xenopus egg extracts: respective roles of centrosomes and microtubule self-organization *J Cell Biol, 138*(3), 615-628. doi:10.1083/jcb.138.3.615

Holland, A. J., & Cleveland, D. W. (2012). Losing balance: the origin and impact of aneuploidy in cancer. *EMBO Rep., 13*(6), 501-514. doi:10.1038/embor.2012.55

Howell, B. J., McEwen, B. F., Canman, J. C., Hoffman, D. B., Farrar, E. M., Rieder, C. L., & Salmon, E. D. (2001). Cytoplasmic dynein/dynactin drives kinetochore protein transport to the spindle poles and has a role in mitotic spindle checkpoint inactivation *J Cell Biol, 155*(7), 1159-1172. doi:10.1083/jcb.200105093

Hubbert, C., Guardiola, A., Shao, R., Kawaguchi, Y., Ito, A., Nixon, A., . . . Yao, T. (2002). HDAC6 is a microtubule-associated deacetylase *Nature, 417*(6887), 455-458. doi:10.1038/417455a

Hughes, A. F., & Swann, M. M. (1948). Anaphase movements in the living cell. *J Exp Biol, 25*(1), 45-72. doi:10.1242/jeb.25.1.45

Inouéa, S., & Dan, K. (1951). Birefringenoe of the dividing cell. *Journal of Morphology, 89*(3), 423-455. doi:10.1002/jmor.1050890304
Janke, C., & Bulinski, J. C. (2011). Post-translational regulation of the microtubule cytoskeleton: mechanisms and functions. *Nat Rev Mol Cell Biol, 12*(12), 773-786. doi:10.1038/nrm3227
Janke, C., Rogowski, K., Wloga, D., Regnard, C., Kajava, A. V., Strub, J., . . . Eddé, B. (2005). Tubulin polyglutamylase enzymes are members of the TTL domain protein family *Science, 308*(5729), 1758-1762. doi:10.1126/science.1113010
Joglekar, A. P., Bouck, D. C., Molk, J. N., Bloom, K. S., & Salmon, E. D. (2006). Molecular architecture of a kinetochore–microtubule attachment site. . *Nat Cell Biol, 8*(6), 581-585. doi:10.1038/ncb1414
Joshi, H. C., Yen, T. J., & D.W., C. (1987). In vivo coassembly of a divergent beta-tubulin subunit (c beta 6) into microtubules of different function. *J Cell Biol, 105*(5), 2179-2190. doi:10.1083/jcb.105.5.2179
Kalab, P., Weis, K., & Heald, R. (2002). Visualization of a Ran-GTP Gradient in Interphase and Mitotic Xenopus Egg Extracts. *Science, 295*(5564), 2452-2456. doi:10.1126/science.1068798
Kalantzaki, M., Kitamura, E., Zhang, T., Mino, A., Novák, B., & Tanaka, T. U. (2015). Kinetochore–microtubule error correction is driven by differentially regulated interaction modes. *Nat Cell Biol, 17*(4), 421-433. doi:10.1038/ncb3128
Kalebic, N., Sorrentino, S., Perlas, E., Bolasco, G., Martinez, C., & Heppenstall, P. A. (2013). αTAT1 is the major α-tubulin acetyltransferase in mice. *Nat Commun, 4*, 1962. doi:10.1038/ncomms2962
Kane, D. A., & Kimmel, C. B. (1993). The zebrafish midblastula transition *Development, 119*(2), 447-456.
Kapoor, T. M., Lampson, M. A., Hergert, P., Cameron, L., Cimini, D., Salmon, E. D., . . . Khodjakov, A. (2006). Chromosomes can congress to the metaphase plate before biorientation. *Science, 311*(5759), 388-391. doi:10.1126/science.1122142
Karess, R. (2005). Rod–Zw10–Zwilch: a key player in the spindle checkpoint. *Trends Cell Biol, 15*(7), 386-392. doi:10.1016/j.tcb.2005.05.003
Karsenti, E., & Vernos, I. (2001a). The Mitotic Spindle: A Self-Made Machine. *Science, 294*(5542), 543-547. doi:10.1126/science.1063488
Karsenti, E., & Vernos, I. (2001b). The mitotic spindle: a self-made machine *Science, 294*(5542), 543-547. doi:10.1126/science.1063488
Kato, H., Jiang, J., Zhou, B., Rozendaal, M., Feng, H., Ghirlando, R., . . . Bai, Y. (2013). A conserved mechanism for centromeric nucleosome recognition by centromere protein cenp-c. *Science, 340*(6136), 1110-1113. doi:10.1126/science.1235532
Katoh, K., Rozewicki, J., & Yamada, K. D. (2019). MAFFT online service: multiple sequence alignment, interactive sequence choice and visualization. *Brief Bioinform, 20*(4), 1160-1166. doi:10.1093/bib/bbx108
Kimmel, B., Ballard, W. W., Kimmel, S. R., Ullmann, B., & Schilling, T. F. (1995). Stages of embryonic development of the zebrafish. *Dev Dyn, 203*(3), 253-310. doi:doi: 10.1002/aja.1002030302
Kimura, Y., Kurabe, N., Ikegami, K., Tsutsumi, K., Konishi, Y., Kaplan, O. I., . . . Setou, M. (2010). Identification of tubulin deglutamylase among Caenorhabditis elegans and mammalian cytosolic carboxypeptidases (CCPs) *J Biol Chem, 285*(30), 22936-22941. doi:10.1074/jbc.C110.128280

Kirschner, K., & Mitchison, T. (1986). Beyond self-assembly: from microtubules to morphogenesis *Cell, 45*(3), 329-342. doi:10.1016/0092-8674(86)90318-1
Kitagawa, K., & Hieter, P. (2001). Evolutionary conservation between budding yeast and human kinetochores. *Nat Rev Mol Cell Biol, 9*(2), 678-687. doi:10.1038/35089568
Knowlton, A. L., Lan, W., & Stukenberg, P. T. (2006). Aurora B is enriched at merotelic attachment sites, where it regulates MCAK *Curr Biol, 16*(17), 1705-1710. doi:10.1016/j.cub.2006.07.057
Kubo, T., Yanagisaw, H., Liu, Z., Shibuya, R., Hirono, M., & Kamiya, R. (2014). A conserved flagella-associated protein in Chlamydomonas, FAP234, is essential for axonemal localization of tubulin polyglutamylase TTLL9. *Mol Biol Cell., 25*(1), 107-117. doi:10.1091/mbc.E13-07-0424
Kubo, T., Yanagisawa, H., Yagi, T, Hirono, M., & Kamiya, R. (2010). Tubulin polyglutamylation regulates axonemal motility by modulating activities of inner-arm dyneins. *Curr Biol, 20*(5), 441-445. doi:10.1016/j.cub.2009.12.058
Kuersten, S., Ohno, M., & Mattaj, I. W. (2001). Nucleocytoplasmic transport: Ran, beta and beyond. *Trends Cell Biol, 11*(12), 497-503. doi:10.1016/S0962-8924(01)02144-4
L'Hernault, S. W., & J.L., R. (1983). Chlamydomonas alpha-tubulin is posttranslationally modified in the flagella during flagellar assembly. *J Cell Biol, 97*(1), 258-263. doi:10.1083/jcb.97.1.258
L'Hernault, S. W., & Rosenbaum, J. L. (1985). Chlamydomonas alpha-tubulin is posttranslationally modified by acetylation on the epsilon-amino group of a lysine *1985, 24*(2), 473-478. doi:10.1021/bi00323a034
Lacroix, B., van Dijk, J., Gold, N. D., Guizetti, J., Aldrian-Herrada, G., Rogowski, K., . . . Janke, C. (2010). Tubulin polyglutamylation stimulates spastin-mediated microtubule severing. *J Cell Biol, 189*(6), 945-954. doi:10.1083/jcb.201001024
Lampson, M. A., & Grishchuk, E. L. (2017). Mechanisms to Avoid and Correct Erroneous Kinetochore-Microtubule Attachments. *Biology (Basel), 6*(1), 1. doi:10.3390/biology6010001
Lampson, M. A., Renduchitala, K., Khodjakov, A., & Kapoor, T. M. (2004). Correcting improper chromosome-spindle attachments during cell division. *Nat Cell Biol, 6*(3), 232-237. doi:10.1038/ncb1102
Lecland, N., & Luders, J. (2014). The dynamics of microtubule minus ends in the human mitotic spindle. *Nature cell biology, 16*(8), 770-778. doi:10.1038/ncb2996
LeDizet, M., & Piperno, G. (1986). Cytoplasmic microtubules containing acetylated alpha-tubulin in Chlamydomonas reinhardtii: spatial arrangement and properties. *J Cell Biol, 103*(1), 13-22. doi:10.1083/jcb.103.1.13
Levine, M. S., & Holland, A. J. (2018). The impact of mitotic errors on cell proliferation and tumorigenesis. *Genes Dev, 32*(9-10), 620-638. doi:10.1101/gad.314351.118
Lewis, S. A., & Cowan, N. J. (1988). Complex regulation and functional versatility of mammalian alpha- and beta-tubulin isotypes during the differentiation of testis and muscle cells *J Cell Biol, 106*(6), 2023-2033. doi:10.1083/jcb.106.6.2023
Liu, D., Vader, G., Vromans, M. J. M., Lampson, M. A., & S.M.A., L. (2009). Sensing chromosome bi-orientation by spatial separation of aurora B kinase from kinetochore substrates. *Science, 323*, 5919. doi:10.1126/science.1167000

Liu, N., Xiong, Y., Li, S., Ren, Y., Siqi Gao, Q. H., Zhou, J., & Shui, W. (2015). New HDAC6-mediated deacetylation sites of tubulin in the mouse brain identified by quantitative mass spectrometry *Sci Rep, 5*, 16869. doi:10.1038/srep16869

Lu, M. S., & Johnston, C. A. (2013). Molecular pathways regulating mitotic spindle orientation in animal cells *Development, 140*(9), 1843-1856. doi:10.1242/dev.087627

Lüders, J., Patel, U. K., & Stearns, T. (2006). GCP-WD is a gamma-tubulin targeting factor required for centrosomal and chromatin-mediated microtubule nucleation *Nat Cell Biol, 8*(2), 137-147. doi:10.1038/ncb1349

Ludueña, R. F. (2013). A hypothesis on the origin and evolution of tubulin. *Int Rev Cell Mol Biol, 302*(41), 185. doi:10.1016/B978-0-12-407699-0.00002-9

Ludueña, R. F., & Banerjee, A. (2008). The Role of Microtubules in Cell Biology, Neurobiology, and Oncology. *Humana Press*, 123-175.

Maddox, P. S., Bloom, K. S., & Salmon, E. D. (2000). The polarity and dynamics of microtubule assembly in the budding yeast Saccharomyces cerevisiae *Nat Cell Biol, 2*(1), 36-41. doi:10.1038/71357

Magiera, M. M., Bodakuntla, S., Žiak, J., Lacomme, S., Sousa, P. M., Leboucher, S., . . . Janke, C. (2018). Excessive tubulin polyglutamylation causes neurodegeneration and perturbs neuronal transport. *EMBO J, 37*(23), e100440. doi:10.15252/embj.2018100440

Magiera, M. M., Singh, P., & Janke, C. (2018). SnapShot: Functions of Tubulin Posttranslational Modifications *Cell, 173*(6), 1552-1552e1551. doi:10.1016/j.cell.2018.05.032

Mahalingan, K., Keenan, E. K., Strickland, M., Li, Y., Liu, Y., Ball, H. L., . . . Roll-Mecak, A. (2020). Structural basis for polyglutamate chain initiation and elongation by TTLL family enzymes *Nat Struct Mol Biol, 27*(9), 802-813. doi:10.1038/s41594-020-0462-0

Maiato, H., Hergert, P. J., Moutinho-Pereira, S., Dong, Y., Vandenbeldt, K. J., Rieder, C. L., & McEwen, B. F. (2006). The ultrastructure of the kinetochore and kinetochore fiber in Drosophila somatic cells. *Chromosoma, 115*(6), 469-480. doi:10.1007/s00412-006-0076-2

Maiato, H., Khodjakov, A., & Rieder, C. L. (2005). Drosophila CLASP is required for the incorporation of microtubule subunits into fluxing kinetochore fibres. *Nat Cell Biol, 7*(1), 42-47. doi: 10.1038/ncb1207

Maney, T., Wagenbach, M., & Wordeman, L. (2001). Molecular dissection of the microtubule depolymerizing activity of mitotic centromere-associated kinesin. *J Biol Chem, 276*(37), 34753-34758. doi:10.1074/jbc.M106626200

McEwen, B. F., & Dong, Y. (2010). Contrasting models for kinetochore microtubule attachment in mammalian cells. *Cell Mol Life Sci, 67*(13), 2163-2172. doi:10.1007/s00018-010-0322-x

McGill, M., & Brinkley, B. R. (1975). Human chromosomes and centrioles as nucleating sites for the in vitro assembly of microtubules from bovine brain tubulin. *J Cell Biol., 67*(1), 189-199. doi:10.1083/jcb.67.1.189

Meunier, S., Shvedunova, M., Van Nguyen, N., Avila, L., Vernos, I., & Akhtar, A. (2015). An epigenetic regulator emerges as microtubule minus-end binding and stabilizing factor in mitosis *Nat Commun, 5*(6), 7889. doi:10.1038/ncomms8889

Meunier, S., & Vernos, I. (2011). K-fibre minus ends are stabilized by a RanGTP-dependent mechanism essential for functional spindle assembly *Nat Cell Biol, 13*(12), 1406-1414. doi:10.1038/ncb2372
Meunier, S., & Vernos, I. (2012). Microtubule assembly during mitosis - from distinct origins to distinct functions? . *J Cell Sci, 125*(12), 1805-1814. doi:10.1242/jcs.092429
Meunier, S., & Vernos, I. (2016). Acentrosomal Microtubule Assembly in Mitosis: The Where, When, and How. *Trends Cell Biol, 26*(2), 80-87. doi: 10.1016/j.tcb.2015.09.001
Mitchison, T., Evans, L., Schulze, E., & Kirschner, M. W. (1986). Sites of microtubule assembly and disassembly in the mitotic spindle *Cell, 45*(4), 515-527. doi:10.1016/0092-8674(86)90283-7
Mitchison, T., & Kirshner, M. (1984a). Dynamic instabiliy of microtubule growth. *Nature, 312*(5991), 237-242. doi:10.1038/312237a0
Mitchison, T., & Kirshner, M. (1984b). Microtubule assembly nucleated by isolated centrosomes. *Nature, 312*, 232-237. doi:10.1038/312232a0
Mitchison, T. J. (1992). Localization of an Exchangeable GTP Binding Site at the Plus End of Microtubules. *Science, 261*(5124), 1044-1047.
Mitchison, T. J. (2014). The engine of microtubule dynamics comes into focus. *Cell, 157*(5), 1008-1010. doi:10.1016/j.cell.2014.05.001
Mohri, H. (1968). Amino-acid composition of "tubulin" constituting microtubulre of sperm flagella. *Nature, 217*, 1053-1054.
Monda, J. K., Whitney, I. P., Tarasovetc, E. V., Wilson-Kubalek, E., Milligan, R. A., Grishchuk, E. L., & Cheeseman, I. M. (2017). Microtubule tip tracking by the spindle and kinetochore protein ska1 requires diverse tubulin-interacting surfaces. *Curr Biol, 27*(23), 3666-3675. doi:10.1016/j.cub.2017.10.018
Moritz, M., Braunfeld, M. B., Sedat, J. W., Alberts, B., & Agard, D. A. (1995). Microtubule nucleation by γ-tubulin-containing rings in the centrosome. *Nature, 378*(6557), 638-640. doi:10.1038/378638a0.
Morley, S. J., Qi, Y., Iovino, L., Andolfi, L., Guo, D., Kalebic, N., . . . Heppenstall, P. A. (2016). Acetylated tubulin is essential for touch sensation in mice. *eLIFE, 5*, e20813. doi:10.7554/eLife.20813
Multigner, L., Pignot-Paintrand, I., Saoudi, Y., Job, D., Plessmann, U., Rüdiger, M., & Weber, K. (1996). The A and B tubules of the outer doublets of sea urchin sperm axonemes are composed of different tubulin variants *Biochemistry, 25*(33), 10862-10871. doi:10.1021/bi961057u
Musacchio, A., & Desai, D. (2017). A Molecular View of Kinetochore Assembly and Function *Biology (Basel), 6*(1), 1-5. doi:10.3390/biology6010005
Musacchio, A., & Salmon, E. D. (2007a). The spindle-assembly checkpoint in space and time *Nat Rev Mol Cell Biol, 8*(5), 379-393. doi:10.1038/nrm2163
Musacchio, A., & Salmon, E. D. (2007b). The spindle-assembly checkpoint in space and time. *Nat Rev Mol Cell Biol, 8*(5), 379-393. doi:10.1038/nrm2163
Nam, H., Naylor, R., & van Deursen, J. M. (2016). Centrosome dynamics as a source of chromosomal instability. *Trends Cell Biol, 25*(2), 65-73. doi: 10.1016/j.tcb.2014.10.002
Neff, N. F., Thomas, J. H., Grisafi, P., & Botstein, D. (1983). Isolation of the beta-tubulin gene from yeast and demonstration of its essential function in vivo *Cell, 33*(1), 211-219. doi: 10.1016/0092-8674(83)90350-1

Nicklas, R. B. (1997). How cells get the right chromosomes. *Science, 275*(5300), 632-637. doi:10.1126/science.275.5300.632
Nicklas, R. B., & Koch, C. A. (1969). Chromosome micromanipulation. 3. Spindle fiber tension and the reorientation of mal-oriented chromosomes. *J Cell Biol, 43*(1), 40-50. doi:10.1083/jcb.43.1.40
Nicklas, R. B., & Ward, S. C. (1994). Elements of error correction in mitosis: microtubule capture, release, and tension *J Cell Biol, 126*(5), 1241-1253. doi:10.1083/jcb.126.5.1241
Nicklas, R. B., Ward, S. C., & Gorbsky, G. J. (1995). Kinetochore chemistry is sensitive to tension and may link mitotic forces to a cell cycle checkpoint. *J Cell Biol, 130*(4), 929-939. doi:10.1083/jcb.130.4.929
Nieuwenhuis, J., Adamopoulos, A., Bleijerveld, O. B., Mazouzi, A., Stickel, E., Celie, P., . . . Brummelkamp, T. R. (2017). Vasohibins encode tubulin detyrosinating activity. *Science, 358*(6369), 1453. doi:10.1126/science.aao5676.
Nixon, F. M., Gutiérrez-Caballero, C., Hood, F. E., Booth, D. G., Prior, I. A., & Royle, S. J. (2015). The mesh is a network of microtubule connectors that stabilizes individual kinetochore fibers of the mitotic spindle. *eLIFE, 4*, e07635. doi:10.7554/eLife.07635
Nogales, E. (2000). Structural Insights into Microtubule Function. *Annu. Rev. Biochem., 69*, 277–302.
Nogales, E., Whittaker, M., Milligan, R. A., & Downing, K. H. (1991). High-Resolution Model of the Microtubule. *Cell, 96*, 79-88. doi:10.1126/science.8102497
North, B. J., Marshall, B. L., Borra, M. T., Denu, J. M., & Verdin, E. (2003). The human Sir2 ortholog, SIRT2, is an NAD+-dependent tubulin deacetylase *Mol Cell, 11*(2), 437-444. doi:10.1016/s1097-2765(03)00038-8
O'Hagan, R., Silva, M., Nguyen, K. C. Q., Zhang, W., Bellotti, S., Ramadan, Y. H., . . . Barr, M. M. (2017). Glutamylation Regulates Transport, Specializes Function, and Sculpts the Structure of Cilia. *Curr Biol, 27*(22), 3430-3441. doi:10.1016/j.cub.2017.09.066
Ohkawa, N., Sugisaki, S., Tokunaga, E., Fujitani, K., Hayasaka, T., Setou, M., & Inokuchi, K. (2008). N-acetyltransferase ARD1-NAT1 regulates neuronal dendritic development *Genes Cells, 13*(11), 1171-1183. doi:10.1111/j.1365-2443.2008.01235.x
Palmer, D. K., & Margolis, R. L. (1985). Kinetochore components recognized by human autoantibodies are present on mononucleosomes *Mol Cell Biol, 5*(1), 173-186. doi:10.1128/mcb.5.1.173-186.1985
Paturle-Lafanechère, L., Eddé, B., Denoulet, P., Van Dorsselaer, A., Mazarguil, H., Le Caer, J. P., . . . Job, D. (1991). Characterization of a major brain tubulin variant which cannot be tyrosinated *Biochemistry, 30*(43), 10523-10528. doi:10.1021/bi00107a022
Pease, D. C. (1963). The ultrastructure of flagellar fibrils. *The Journal of cell biology, 18*(2), 313-326.
Pekgoz Altunkaya, G. M., F.; Demianova, Z.; Zimniak, T.; Litos, G.; Weissmann, F.; Mechtler, K.;Herzog, F.; Westermann, S. (2016). Ccan assembly configures composite binding interfaces to promote cross-linking of ndc80 complexes at the kinetochore. *Curr. Biol, 26*(17), 2370-2378. doi:10.1016/j.cub.2016.07.005
Peris, L., Thery, M., Fauré, J., Saoudi, Y., Lafanechère, L., Chilton, J. K., . . . Job, D. (2006). Tubulin tyrosination is a major factor affecting the recruitment of CAP-

Gly proteins at microtubule plus ends *J Cell Biol, 174*(6), 839-849. doi:10.1083/jcb.200512058
Peris, L., Wagenbach, M., Lafanechère, L., Brocard, J., Moore, A. T., Kozielski, F., . . . Andrieux, A. (2009). Motor-dependent microtubule disassembly driven by tubulin tyrosination *J Cell Biol, 185*(7), 1159-1166. doi:10.1083/jcb.200902142
Peters, J. (2006). The anaphase promoting complex/cyclosome: a machine designed to destroy. *Nat Rev Mol Cell Biol, 7*(9), 644-656. doi:10.1038/nrm1988
Petry, S. (2016). Mechanisms of Mitotic Spindle Assembly *Annu Rev Biochem, 2*(85), 659-683. doi:10.1146/annurev-biochem-060815-014528
Petry, S., Groen, A. C., Ishihara, K., Mitchison, T. J., & Vale, R. D. (2013). Branching microtubule nucleation in Xenopus egg extracts mediated by augmin and TPX2. *Cell, 152*(2), 768-777. doi:10.1016/j.cell.2012.12.044
Pinyol, R., Scrofani, J., & Vernos, I. (2013). The role of NEDD1 phosphorylation by Aurora A in chromosomal microtubule nucleation and spindle function *Curr Biol, 23*(2), 143-149. doi:10.1016/j.cub.2012.11.046
Porter, M. C. L. K. R. (1963). A "Microtubule" in plant cell fine structure. *J Cell Biol., 19*(1), 239–250. doi:10.1083/jcb.19.1.239
Redeker, V., Levilliers, N., Schmitter, J. M., Le Caer, J. P., Rossier, J., Adoutte, A., & Bré, M. (1994). Polyglycylation of tubulin: a posttranslational modification in axonemal microtubules *Science, 266*(5191), 1688-1691. doi:10.1126/science.7992051
Redelings, B. (2014). Erasing errors due to alignment ambiguity when estimating positive selection. *Mol Biol Evol, 31*(8), 1979-1993. doi:10.1093/molbev/msu174
Redelings, B. D. (2021). Bali-Phy version 3: Model-based co-estimation of alignment and phylogeny. *Bioinformatics*. doi:10.1093/bioinformatics/btab129
Regnard, C., Desbruyères, E., Denoulet, P., & Eddé, B. (1999). Tubulin polyglutamylase: isozymic variants and regulation during the cell cycle in HeLa cells *J Cell Sci, 112*(23), 4281-4289.
Regnard, C., Desbruyères, E., Huet, J. C., Beauvallet, C., Pernollet, J. C., & Eddé, B. (2000). Polyglutamylation of nucleosome assembly proteins. *J Biol Chem, 275*(21), 15969-15976. doi:10.1074/jbc.M000045200
Remark, R. (1852). Untersuchungen über die Entwickelung der Wirbelthiere Retrieved from https://play.google.com/books/reader?id=Kknf7ZRHzagC&pg=GBS.PA56&hl=it
Rieder, C. L., Cole, R. W., Khodjakov, A., & Sluder, G. (1995). The checkpoint delaying anaphase in response to chromosome monoorientation is mediated by an inhibitory signal produced by unattached kinetochores. *J Cell Biol, 130*(4), 941-948. doi:10.1083/jcb.130.4.941
Rieder, C. L., & Maiato, H. (2004). Stuck in division or passing through: what happens when cells cannot satisfy the spindle assembly checkpoint *Dev Cell, 7*(5), 637-651. doi:10.1016/j.devcel.2004.09.002
Rieder, C. L., & S.P., A. (1990). Kinetochores are transported poleward along a single astral microtubule during chromosome attachment to the spindle in newt lung cells *J Cell Biol, 110*(1), 81-95. doi:10.1083/jcb.110.1.81
Rogers, G. C., Rogers, S. L., Schwimmer, T. A., Ems-McClung, S. C., Walczak, C. E., Vale, R. D., . . . Sharp, D. J. (2004). Two mitotic kinesins cooperate to drive

sister chromatid separation during anaphase,. *Nature, 427*(6972), 364-370. doi:10.1038/nature02256
Rogowski, K., Juge, F., van Dijk, J., Wloga, D., Strub, J., Levilliers, N., . . . Janke, C. (2009). Evolutionary divergence of enzymatic mechanisms for posttranslational polyglycylation *Cell, 137*(6), 1076-1087. doi:10.1016/j.cell.2009.05.020
Rogowski, K., van Dijk, J., Magiera, M. M., Bosc, C., Deloulme, J., Bosson, A., . . . Janke, C. (2010). A family of protein-deglutamylating enzymes associated with neurodegeneration *Cell, 143*(4), 564-578. doi:10.1016/j.cell.2010.10.014
Roll-Mecak, A. (2020). The Tubulin Code in Microtubule Dynamics and Information Encoding. *Dev Cell, 54*(1), 7-20. doi:10.1016/j.devcel.2020.06.008
Rüdiger, M., Wehland, J., & Weber, K. (1994). The carboxy-terminal peptide of detyrosinated alpha tubulin provides a minimal system to study the substrate specificity of tubulin-tyrosine ligase *Eur J Biochem, 220*(2), 309-320. doi:10.1111/j.1432-1033.1994.tb18627.x
Sánchez-Huertas, C., & Lüders, J. (2015). The augmin connection in the geometry of microtubule networks *Curr Biol, 25*(5), R294-299. doi:10.1016/j.cub.2015.02.006
Schatz, P. J., Pillus, L., Grisafi, P., Solomon, F., & Botstein, D. (1986). Two functional alpha-tubulin genes of the yeast Saccharomyces cerevisiae encode divergent proteins. *Mol Cell Biol., 6*(11), 3711.3721. doi:10.1128/mcb.6.11.3711
Schmidt, J. C., Arthanari, H., Boeszoermenyi, A., Dashkevich, N. M., Wilson-Kubalek, E. M., Monnier, N., . . . Cheeseman, I. M. (2012). The kinetochore-bound ska1 complex tracks depolymerizing microtubules and binds to curved protofilaments. *Dev Cell, 23*(5), 968-980. doi:10.1016/j.devcel.2012.09.012
Schröder, H. C., Wehland, J., & Weber, K. (1985). Purification of brain tubulin-tyrosine ligase by biochemical and immunological methods *J Cell Biol, 100*(1), 276-281. doi:10.1083/jcb.100.1.276
Scrofani, J., Sardon, T., Meunier, S., & Vernos, I. (2015). Microtubule nucleation in mitosis by a RanGTP-dependent protein complex *Curr Biol, 25*(2), 131-140. doi:10.1016/j.cub.2014.11.025
Sdelci, S., Schütz, M., Pinyol, R., Bertran, M. T., Regué, L., Caelles, C., . . . Roig, J. (2012). Nek9 phosphorylation of NEDD1/GCP-WD contributes to Plk1 control of γ-tubulin recruitment to the mitotic centrosome *Curr Biol, 22*(16), 1516-1523. doi:10.1016/j.cub.2012.06.027
Severson, A. F., von Dassow, G., & Bowerman, B. (2020). Oocyte Meiotic Spindle Assembly and Function. *Curr Top Dev Biol, 116*, 65-98. doi:10.1016/bs.ctdb.2015.11.031
Shelby, R. D., Vafa, O., & Sullivan, K. F. (1997). Assembly of CENP-A into centromeric chromatin requires a cooperative array of nucleosomal DNA contact sites *J Cell Biol, 136*(3), 501-513. doi:10.1083/jcb.136.3.501
Shida, T., Cueva, J. G., Xu, Z., Goodman, M. B., & Nachury, M. V. (2010). The major alpha-tubulin K40 acetyltransferase alphaTAT1 promotes rapid ciliogenesis and efficient mechanosensation *Proc Natl Acad Sci U S A, 107*(50), 21517-21522. doi:10.1073/pnas.1013728107
Sirajuddin, M., Rice, L. M., & Vale, R. D. (2014). Regulation of microtubule motors by tubulin isotypes and post-translational modifications *Nat Cell Biol, 16*(4), 553-544. doi:10.1038/ncb2920

Skibbens, R. V., & Salmon, E. D. (1997). Micromanipulation of chromosomes in mitotic vertebrate tissue cells: Tension controls the state of kinetochore movement. *Exp Cell Res, 235*(2). doi:10.1006/excr.1997.3691

Slautterback, D. B. (1963). Cytoplasmic Microtubules. *J Cell Biol., 18*(2), 367-388. doi: 10.1083/jcb.18.2.367

Solinger, J. A., Paolinelli, R., Klöss, H., Scorza, F. B., Marchesi, S., Sauder, U., . . . Cassata, G. (2010). The Caenorhabditis elegans Elongator complex regulates neuronal alpha-tubulin acetylation *PLoS Genet, 6*(1), e1000820. doi:10.1371/journal.pgen.1000820

Steblyanko, Y., Rajendraprasad, G., Osswal, M., Eibes, S., Jacome, A., Geley, S., . . . Barisic, M. (2020). Microtubule poleward flux in human cells is driven by the coordinated action of four kinesins *EMBO J, 39*(23), e105432. doi:10.15252/embj.2020105432

Suchard, M. A., & Redelings, B. D. (2006). BAli-Phy: simultaneous Bayesian inference of alignment and phylogeny. *Bioinformatics, 22*(16), 2047-2048. doi:10.1093/bioinformatics/btl175

Sudakin, V., Chan, G. K., & Yen, T. J. (2001). Checkpointinhibition of the APC/C in HeLa cells is mediated by a complex of BUBR1, BUB3, CDC20, and MAD2. *J Cell Biol, 154*(5), 925-936. doi:10.1083/jcb.200102093

Suijkerbuijk, S. J. E., van Osch, M. H. J., Bos, F. L., Hanks, S., Rahman, N., & Kops, G. J. L. (2010). Molecular causes for BUBR1 dysfunction in the human cancer predisposition syndrome mosaic variegated aneuploidy. *Cancer Res., 70*(12), 4891-4900. doi:10.1158/0008-5472.CAN-09-4319

Surrey, T., Nedelec, F., Leibler, S., & Karsenti, E. (2001). Physical properties determining self-organization of motors and microtubules *Science, 292*(5519), 1167-1171. doi:10.1126/science.1059758

Tanaka, T. U. (2008). Bi-orienting chromosomes: acrobatics on the mitotic spindle. *Chromosoma, 117*(6), 521-533. doi:10.1007/s00412-008-0173-5

Tanaka, T. U., Rachidi, N., Janke, C., Pereira, G., Galova, M., Schiebel, E., . . . Nasmyth, K. (2002). Evidence that the Ipl1-Sli15 (Aurora Kinase-INCENP) Complex Promotes Chromosome Bi-orientation by Altering Kinetochore-Spindle Pole Connections. *Cell, 108*(3), 317-329. doi:10.1016/s0092-8674(02)00633-5

Tariq, A., Green, G., Jeynes, J. C., Soeller, C., & Wakefield, J. G. (2020). In vitro reconstitution of branching microtubule nucleation. *eLIFE, 9*, e49769. doi:10.7554/eLife.49769

Taylor, A. M., Shih, J., Ha, G., Gao, G. F., Zhang, X., Berger, A. C., . . . Meyerson, M. (2018). Genomic and Functional Approaches to Understanding Cancer Aneuploidy. *Cancer Cell, 33*(4), 676-689 e673. doi:10.1016/j.ccell.2018.03.007

Teixido -Travesa, N., Roig, J., & Luders, J. (2012). The where, when and how of microtubule nucleation – one ring to rule them all. *J Cell Sci 125*(29), 4445–4456. doi:10.1242/jcs.106971

Thompson, S. L., & Compton, D. A. (2008). Examining the link between chromosomal instability and aneuploidy in human cells. *J Cell Biol, 180*(4), 665-672. doi:10.1083/jcb.200712029

Thompson, S. L., & Compton, D. A. (2008). Examining the link between chromosomal instability and aneuploidy in human cells. *J Cell Biol, 180*(4), 665-672. doi:10.1083/jcb.200712029

Thompson, S. L., & Compton, D. A. (2011). Chromosome missegregation in human cells arises through specific types of kinetochore-microtubule attachment errors. *Proc Natl Acad Sci U S A, 108*(44), 17974-17978. doi:10.1073/pnas.1109720108

Tort, O., Tanco, S., Rocha, C., Bièche, I., Seixas, C., Bosc, C., . . . Janke, C. (2014). The cytosolic carboxypeptidases CCP2 and CCP3 catalyze posttranslational removal of acidic amino acids. *Mol Biol Cell, 25*(19), 3017-3027. doi:10.1091/mbc.E14-06-1072

Tran, L. D., Hino, H., Quach, H., Lim, S., Shindo, A., Mimori-Kiyosue, Y., . . . Sampath, K. (2012). Dynamic microtubules at the vegetal cortex predict the embryonic axis in zebrafish. *Development, 139*(19), 3644-3652. doi:10.1242/dev.082362

Trichet, V., Ruault, M., Roizès, G., & De Sario, A. (2000). Characterization of the human tubulin tyrosine ligase-like 1 gene (TTLL1) mapping to 22q13.1 *Genes Cells, 257*(1), 109-117. doi:10.1016/s0378-1119(00)00383-8

Valenstein, M. L., & Roll-Mecak, A. (2016). Graded Control of Microtubule Severing by Tubulin Glutamylation. *Cell, 164*(5), 911-921. doi:10.1016/j.cell.2016.01.019

van Dijk, J., Miro, J., Strub, J. M., van Dorsselaer, A., Edde, B., & Janke, C. (2008). Polyglutamylation Is a Post-translational Modification with a Broad Range of Substrates. *Journal of Biological Chemistry, 283*(7), 3915-3922. doi:10.1074/jbc.M705813200

van Dijk, J., Rogowski, K., Miro, J., Lacroix, B., Eddé, B., & Janke, C. (2007). A Targeted Multienzyme Mechanism for Selective Microtubule Polyglutamylation. *Mol Cell, 26*(3), 437-448. doi:10.1016/j.molcel.2007.04.012

VandenBeldt, K. J., Barnard, R. M., Hergert, P. J., Meng, X., Maiato, H., & McEwen, B. F. (2006). Kinetochores use a novel mechanism for coordinating the dynamics of individual microtubules *Curr Biol, 16*(12), 1217-1223. doi:10.1016/j.cub.2006.04.046

Vanneste, D., Takagi, M., Imamoto, N., & Vernos, I. (2009). The role of Hklp2 in the stabilization and maintenance of spindle bipolarity *Curr Biol, 19*(20), 1712-1717. doi:10.1016/j.cub.2009.09.019

Veld, P. J. H., Jeganathan, S., Petrovic, A., Singh, S., John, J., Krenn, V., . . . Musacchio, A. (2016). Molecular basis of outer kinetochore assembly on cenp-t. *eLIFE, 5*, e21007. doi:10.7554/eLife.21007

Verma, V., & Maresca, T. J. (2019). Direct observation of branching MT nucleation in living animal cells *J Cell Biol 218*(9), 2829-2840. doi:10.1083/jcb.201904114

Vérollet, C., Colombié, N., Daubon, T., Bourbon, H., Wright, M., & Raynaud-Messina, B. (2006). Drosophila melanogaster γ-TuRC is dispensable for targeting γ-tubulin to the centrosome and microtubule nucleation. *J Cell Biol., 172*(4), 517-528. doi:10.1083/jcb.200511071

Walczak, C. E., Vernos, I., Mitchison, T. J., Karsenti, E., & Heald, R. (1998). A model for the proposed roles of different microtubule-based motor proteins in establishing spindle bipolarity *Curr Biol, 8*(16), 903-913. doi:10.1016/s0960-9822(07)00370-3

Wandke, C., Barisic, M., Sigl, R., Rauch, V., Wolf, F., Amaro, A. C., . . . Geley, S. (2012). Human chromokinesins promote chromosome congression and spindle microtubule dynamics during mitosis. *J Cell Biol, 198*(5), 847-863. doi:10.1083/jcb.201110060

Wang, A., Zhang, Y., Wang, B., Zhao, X., Wu, F., Zhai, X., . . . Mei, S. (2018). Mutation analysis of the TUBB8 gene in primary infertile women with arrest in oocyte maturation *Gynecol Endocrinol, 34*(10), 900-904. doi:10.1080/09513590.2018.1464138

Wang, D., Villasante, A., Lewis, S. A., & Cowan, N. J. (1986). The mammalian beta-tubulin repertoire: hematopoietic expression of a novel, heterologous beta-tubulin isotype. *J Cell Biol., 103*(5), 1903-1910. doi:10.1083/jcb.103.5.1903

Wang, Q., Crevenna, A. H., Kunze, I., & Mizuno, N. (2014). Structural basis for the extended CAP-Gly domains of p150(glued) binding to microtubules and the implication for tubulin dynamics *Proc Natl Acad Sci U S A, 111*(31), 11347-11352. doi:10.1073/pnas.1403135111

Wei, R. R., Schnell, J. R., Larsen, N. A., Sorger, P. K., Chou, J. J., & Harrison, S. C. (2006). Structure of a central component of the yeast kinetochore: the Spc24p/Spc25p globular domain. *Structure, 14*(6), 1003-1009. doi:10.1016/j.str.2006.04.007

Wei, R. R., Sorger, P. K., & Harrison, S. C. (2005). Molecular organization of the Ndc80 complex, an essential kinetochore component *Proc Natl Acad Sci U S A, 102*(15), 5363-5367. doi:10.1073/pnas.0501168102

Weingarten, M. D., Lockwood, A. H., Hwo, S., & Kirschner, M. W. (1975). A Protein Factor Essential for Microtubule Assembly. *Proc. Nat. Acad. Sci., 72*(5), 1858-1862. doi:10.1073/pnas.72.5.1858

Wen, R., Xiao, J., Zhang, Y., Yang, M., Lin, Y., & Tang, J. (2016). Identification of a novel transcript isoform of the TTLL12 gene in human cancers. *Oncol Rep, 36*(6), 3172-3180. doi:10.3892/or.2016.5135

Wilson, E. B. (1896). The cell development and inheritance

Wilson, E. B. (1925). The cell development and heredity.

Winey, M., Mamay, C. L., O'Toole, E. T., Mastronarde, D. N., Giddings, T. H., McDonald, K. L., & McIntosh, J. R. (1995). Three-dimensional ultrastructural analysis of the Saccharomyces cerevisiae mitotic spindle *J Cell Biol, 129*(6), 1601-1615. doi:10.1083/jcb.129.6.1601

Wittmann, T., Wilm, M., Karsenti, E., & Vernos, I. (2000). Tpx2, a Novel Xenopus Map Involved in Spindle Pole Organization. *J Cell Biol, 149*(7), 1405-1418. doi:10.1083/jcb.149.7.1405

Wojcik, E., Basto, R., Serr, M., Scaërou, F., Karess, R., & Hays, T. (2001). Kinetochore dynein: its dynamics and role in the transport of the Rough deal checkpoint protein. *Nat Cell Biol, 3*(11), 1001-1007. doi:10.1038/ncb1101-1001

Wollman, R., Cytrynbaum, E. N., Jones, J. T., Meyer, T., Scholey, J. M., & Mogilner, A. (2005). Efficient chromosome capture requires a bias in the 'search-and-capture' process during mitotic-spindle assembly *Curr Biol, 15*(9), 828-832. doi:10.1016/j.cub.2005.03.019

Wordeman, L., & Mitchison, T. J. (1995). Identification and partial characterization of mitotic centromere-associated kinesin, a kinesin-related protein that associates with centromeres during mitosis. *J Cell Biol, 128*(1-2), 95-104. doi:10.1083/jcb.128.1.95

Xu, Z., Schaedel, L., Portran, D., Aguilar, A., Gaillard, J., Marinkovich, M. P., . . . Nachury, M. V. (2017). Microtubules acquire resistance from mechanical breakage through intralumenal acetylation. *Science, 356*(6335), 328-332. doi:10.1126/science.aai8764

Yang, Z., Tulu, U. S., Wadsworth, P., & Rieder, C. L. (2007). Kinetochore dynein is required for chromosome motion and congression independent of the spindle checkpoint *Curr Biol, 17*(11), 973-980. doi:10.1016/j.cub.2007.04.056

Yao, X., Anderson, K. L., & Cleveland, D. W. (1997). The microtubule-dependent motor centromere-associated protein E(CENP-E) is an integral component of kinetochore corona fibers that link centromeres to spindle microtubules. *J Cell Biol, 139*(2), 435-447. doi:10.1083/jcb.139.2.435

Yu, K., Zhong, N., Xiao, Y., & She, Z. (2019). Mechanisms of kinesin-7 CENP-E in kinetochore-microtubule capture and chromosome alignment during cell division. *Biol Cell, 111*(6), 143-160. doi:10.1111/boc.201800082

Zasadil, L. M., Britigan, E. M., & Weaver, B. A. (2013). 2n or not 2n: Aneuploidy, polyploidy and chromosomal instability in primary and tumor cells. *Semin Cell Dev Biol, 24*(4), 370-379. doi:10.1016/j.semcdb.2013.02.001

Zaytsev, A. V., Mick, J. E., Maslennikov, E., Nikashin, B., DeLuca, J. G., & Grishchuk, E. L. (2015). Multisite phosphorylation of the NDC80 complex gradually tunes its microtubule-binding affinity *Mol Biol Cell, 26*(10), 1829-1844. doi:10.1091/mbc.E14-11-1539

Zhai, Y., Kronebusch, P. J., & Borisy, G. G. (1995). Kinetochore microtubule dynamics and the metaphase-anaphase transition. *J Cell Biol, 131*(3), 721-734. doi:10.1083/jcb.131.3.721

Zhai, Y., Kronebusch, P. J., Simon, P. M., & Borisy, G. G. Microtubule Dynamics at the G2/M Transition: Abrupt Breakdown of Cytoplasmic Microtubules at Nuclear Envelope Breakdown and Implications for Spindle Morphogenesis. *J Cell Biol, 135*(1), 201-214. doi:10.1083/jcb.135.1.201

Zhu, H., Coppinger, J. A., Jang, C., Yates, J. R., & Fang, G. (2008). FAM29A promotes microtubule amplification via recruitment of the NEDD1-gamma-tubulin complex to the mitotic spindle *J Cell Biol, 283*(5), 835-848. doi: 10.1083/jcb.200807046

Annex

8. Annex

Figure 20C. MT polyE levels (a.u.)

		n	mean	SD	test
N = 5	Control	105	0,821	0,192	t.test
	siTTLL11	50	0,521	0,145	

Figure 21A. MT GT335 levels (a.u.)

			n	mean	SD	test
N = 2	mitosis	Control	35	1,701	0,306	Two-way ANOVA
		siTTLL11	38	1,580	0,277	
	interphase	Control	27	1,885	0,138	
		siTTLL11	33	1,818	0,113	

Figure 21B. MT PolyE levels (a.u.)

			n	mean	SD	test
N = 2	mitosis	Control	56	0,371	0,104	Two-way ANOVA
		siTTLL11	54	0,305	0,082	
	interphase	Control	14	0,185	0,052	
		siTTLL11	14	0,198	0,036	

Figure 22. MT PolyE levels (a.u.)

		n	mean	SD	test
N = 2	Control	56	0,371	0,104	Two-way ANOVA
	siTTLL11	54	0,305	0,082	
	siNuf2	48	0,193	0,042	
	siTTLL11/ hKLP2	22	0,226	0,043	

Figure 23B. Mitotic progression live imaging (min)

		n	mean	SD	test
N = 3	Control	66	48,59	29,77	t.test
	siTTLL11	46	54,33	28,34	

Figure 23C. Mitotic index (%)

		n	mean	SD	test
N = 3	Control	>1000	4,8	0,452	t.test
	siTTLL11	>1000	4,58	0,237	

Figure 13A. Anaphase lagging chromosomes

		n	mean	SD	test
N = 3	Control	>117	8,6	2,21	χ^2 test
	siTTLL11	>105	25,53	5,94	

Figure 24D. Zebrafish embryos phenotype analysis at 36 hpf (%)

		n	Mean None (%)	Mean Mild (%)	Mean Severe (%)
N = 2	Scramble	>31	100	0	0
	MO-1	>20	14,3	28,6	57,1
	MO-1+WT	>30	36,4	45,5	18,2
	MO-1+E466G	>20	14,3	33.3	52,4

Figure 24D. Zebrafish embryos phenotype analysis at 36 hpf (raw count)

		Control	MO-1	MO-1 + WT	MO-1 + E466G	test
N = 3	None	15	8	20	7	
	Mild	0	20	26	20	χ^2 test
	Severe	0	34	9	29	

Figure 24E. Zebrafish embryo anaphase cell with lagging chromosomes (%)

		n	Normal	Lagging
N = 3	Control	52	51	1
	siTTLL11	61	26	61

Figure 24F. Embryos showing at least one anaphase lagging chromosomes event (%)

		n	Normal	Lagging
N = 3	Control	18	17	1
	siTTLL11	18	2	16

Figure 25. co-injection of MO-1 and WT *ttl11* rescue the lagging chromosome phenotype in zebrafish embryos (raw count)

		Control	MO-1	MO-1 + WT	MO-1 + E466G	test
N = 3	Normal	38	22	34	17	χ^2 test
	Lagging	3	24	5	14	

Figure 30A. STLC mitotic progression live imaging (min)

		n	mean	SD	test
N = 3	Control	46	191,59	51,70	t.test
	siTTLL11	88	195,71	28,34	

Figure 30B. Length (μm)

		n	mean	SD	test
N = 3	Control	56	9,235	0,977	t.test
	siTTLL11	47	10,716	0,766	

Figure 30B. Width (μm)

		n	mean	SD	test
N = 3	Contol	48	7,928	0,546	t.test
	siTTLL11	48	8,547	0,834	

Figure 30B. Area (μm^2)

		n	mean	SD	test
N = 3	Contol	53	63,165	10,372	t.test
	siTTLL11	48	72,561	12,635	

Figure 30C. K-fibre stability cumulative bar plot (%)

		Time (min)	n	I (%)	II (%)	III (%)	IV (%)	test
	Control	0	40	100	0	0	0	χ^2
	Control	5	29	41,00	53,9	5,1	0	test
N = 3	Control	10	43	9,3	41,9	41,9	7	
	siTTLL11	0	40	100	0	0	0	
	siTTLL11	5	57	18,9	21,1	0	0	
	siTTLL11	10	59	18,6	67,8	11,9	1,7	

Figure 30D. Interkinetochore distance (μm)

		n	mean	SD	test
N = 3	Control	71	1,155	0,245	t.test
	siTTLL11	81	0,96	0,263	

Figure 30E. Spindle flux (μm/min)

		n	mean	SD	test
N = 3	Control	19	0,596	0,116	t.test
	siTTLL11	16	0,424	0,114	

Figure 28A. TTLL11 differential expression in tumors (log_2(Norm.Count+1))

cancer_type	sample_type	n	mean	SD
LUSC	Solid Tissue Normal	51	6,375	0,311
LUSC	Primary Tumor	502	5,349	0,713
UCEC	Solid Tissue Normal	34	6,513	0,441

UCEC	Primary Tumor	532	5,672	0,701
BRCA	Solid Tissue Normal	114	6,580	0,356
BRCA	Primary Tumor	1097	5,816	0,555
STAD	Solid Tissue Normal	35	6,569	0,969
STAD	Primary Tumor	415	5,813	0,789
LUAD	Solid Tissue Normal	59	6,326	0,327
LUAD	Primary Tumor	515	5,745	0,751
KIRP	Solid Tissue Normal	32	6,079	0,304
KIRP	Primary Tumor	290	5,709	0,549
THCA	Solid Tissue Normal	59	6,005	0,278
THCA	Primary Tumor	505	5,714	0,427
KICH	Solid Tissue Normal	25	6,238	0,352
KICH	Primary Tumor	66	5,825	0,551
COAD	Solid Tissue Normal	41	6,365	0,633
COAD	Primary Tumor	452	5,902	0,491
LIHC	Solid Tissue Normal	50	6,221	0,443
LIHC	Primary Tumor	371	5,997	0,693
HNSC	Solid Tissue Normal	44	6,739	0,629
HNSC	Primary Tumor	520	6,339	0,953
PRAD	Solid Tissue Normal	52	6,468	0,448
PRAD	Primary Tumor	497	6,212	0,394
KIRC	Solid Tissue Normal	72	6,084	0,283
KIRC	Primary Tumor	533	5,863	0,566

Abbreviation legend: https://gdc.cancer.gov/node/677

Table 1. RT-qPCR primer sequences

target	sense	sequence
TTLL11	Fw	5’—ACTTCTACCCTCGCTCATGG—3’
	Rv	5’—CCTGACAACCACCATCAGGTT—3’
TTLL13	Fw	5’—ACCAACCCCTCTAACTCTTC—3’
	Rv	5’—TTTCCGCCTTCTCTTCCTC—3’
Actin	Fw	5’—CGAGAAGATGACCCAGATCATG—3’
	Rv	5’—CCACAGGACTCCATGCCCAGG—3’
ttll11	Fw	5’—GTGGACATCAAGAAGGTCTG—3’
	Rv	5’—AAAGTCTAGGACCCGAAAC—3’

Antibodies

antibody	reference	company	target
DM1A	T6199	Sigma-Aldrich	α-tubulin

β-tubulin	ab6046	Abcam	**β**-tubulin
polyE	Home-made	Home made	≥ 3 glutamates
GT335	804-885-C100	Enzo life science	Monoglutamylated tubulin
CREST	15-235	Antibodies Incorporated	Centromeric proteins
Hec1	GTX70268	Genetex	Hec1 protein
p150	610474	BD Bioscience	Dynactin subunit
Eg5	61186	BD Bioscience	KIF11/Eg5
TPX2	home-made	home-made	TPX2
KATNB1	Proteintech		Katanin
γ -tubulin	Sigma	T6557	γ -tubulin
Hklp2	home-made	home-made	KIF15/Hklp2